THESIS FOR THE DEGREE OF LICENTITATE OF ENGINEERING

Maximizing the Integration of Wind Power in Distribution Systems

SHEMSEDIN NURSEBO

Department of Energy and Environment
Division of Electric power engineering
CHALMERS UNIVERSITY OF TECHNOLOGY
Göteborg, Sweden, 2013

Maximizing the Integration of Wind Power in Distribution Systems
SHEMSEDIN NURSEBO

Department of Energy and Environment
Division of Electric Power Engineering
SE-412 96 Göteborg
Sweden
Telephone +46(0)31-772 1000

Chalmers Bibliotek, Reproservice
Göteborg, Sweden 2013

To the One who gave me life!

Maximizing the Integration of Wind Power in Distribution Systems

SHEMSEDIN NURSEBO
Department of Energy and Environment
Chalmers University of Technology

Abstract

The global installed capacity of wind power has shown a significant growth, from just 24 GW in 2001 to 283 GW in 2012. This trend is expected to continue for some years to come. Hence a significant amount of wind power needs to be connected to the electric power system. Usually larger wind farms are connected to transmission systems while smaller wind farms are preferably connected to distribution systems. Such preference arises from comparatively lower connection costs associated with installing wind power in lower voltage networks. But the introduction of wind power into a distribution system poses a number of power quality and reliability concerns such as voltage flicker and harmonics, overvoltage and thermal overloading, and increased fault level. Moreover due to highly fluctuating nature of wind power, some distribution system operators (DSOs) are also concerned about an increase on the frequency of tap changes (FTC) due to the introduction of wind power. Should there be an increase in FTC, in a power system which is already vulnerable to wear and tear due to aging, the DSO may limit the integration of wind power to its network to avoid increased maintenance costs or unexpected tap changer failures. Thus, the thesis discusses these integration issues of wind power and identify the limiting factors. Once identified, the thesis proposes mitigation solutions so as to maximize the hosting capacity of a distribution system. This facilitates the introduction of wind power to the power system in a cost-effective manner.

The investigation of the effect of wind power on the FTC shows that the change on the FTC in a distribution system connected to relatively strong external grid (with $X/R \geq 5$) is negligible up to a significant level of wind power penetration. But in a distribution system connected to a relatively weak external grid, a significant increase in the FTC has been observed as wind power penetration increases. Hence a further investigation is carried out to limit the FTC by using reactive power from local wind turbines. The results have shown that the methodology is very effective in reducing the FTC.

Furthermore, the thesis identifies voltage rise and thermal overloading as the two main limiting factors of wind power integration into distribution systems. Thus, active management strategies (AMSs)–such as wind energy curtailment, reactive power compensation, and coordinated on load tap changer (OLTC) voltage control– have been investigated in the thesis to increase the wind power hosting capacity of distribution systems. To facilitate the investigation, an optimization model incorporating these AMSs is developed. The output of the model is the optimal wind power hosting capacity of the distribution system which will maximize the profit gained by the DSO and the wind farm owner (WFO). The result of the analysis shows that by using AMSs the wind power hosting capacity of distribution system can be increased up to twice the capacity that would have been installed without AMSs.

Index Terms: distribution system, integration issues of wind power, frequency of tap change, active management strategies, cost benefit analysis.

Acknowledgements

I would like to take this opportunity to thank my supervisor Dr. Peiyuan Chen for his consistent assistance and help during the course of the project, for his detailed revision of the present work, and for his friendly approach. I would like also to thank my supervisor and examiner Prof. Ola Carlson for allowing me to participate in this project, for his valuable inputs during the course of the project, and for facilitating the course of the project. Thanks to Prof. Lina Bertling Tjernberg for taking part in revision of most of the work. My gratitude goes to Prof. Torbjörn Thiringer for his willingness to help and for provision of useful data on flicker and harmonics.

This project has been funded by Chalmers Energy Initiative (CEI) and the financial support is highly appreciated.

Network data and measurement data from Falbygden Energi is extensively used in this thesis. In this regard, I would like to thank Lars Ohlsson for making these data available, for his valuable inputs from the utility perspectives, and for his quick response to my e-mails.

During the course of the project my wife has given me the strength I need with endless love. Thank you for your patience and support. Thank you my parents for the sacrifice you pay to make me who I am today. Praise be to the Almighty for His countless blessings He bestowed on me.

Last, but not least, I would like to thank my colleagues at the division electric power engineering for making my stay at Chalmers fun and enjoyable. Special thanks to Khalid, Tarik, Mebtu, my roommate Georgios for their friendly help whenever needed.

Shemsedin,
Göteborg,
Nov, 2013

Contents

List of Acronyms

AMS	Active management strategy
CF	Capacity factor
DFIG	Double fed induction generator
DG	Distributed generation
DR	Discount rate
DSO	Distribution system operator
FTC	Frequency of tap changes
OLTC	On load tap changer
OLTC	On-load tap changer
OPF	Optimal power flow
PCC	Point of common coupling
PF	Power factor
RPC	Reactive power compensation
SCIG	Squirrel cage induction generator
STATCOM	Static synchronous compensator
SVC	Static VAR compensator
THD	Total harmonic distortion
WEC	Wind energy curtailment
WFO	Wind farm owner

1

Introduction

The global installed wind power capacity has shown a significant growth from just 24 GW in 2001 to 283 GW in 2012 [1]. This growth is expected to continue for some years to come [2]. The growth is mainly attributed to government policies to increase the share of energy consumption from renewable resources. By doing so governments are trying to decrease the emission of greenhouse gases to the atmosphere and the dependence on using coal and imported petroleum.

This substantial amount of wind power needs to be connected to the power system for supplying its electricity to potential consumers. But wind power plants have various characteristics which make their integration different from conventional power plants. On one hand, in contrast to conventional power plants, the size of wind power plants varies from kW range single wind turbine to hundreds of MW wind farms. Hence wind power plants are connected to the grid at different voltage levels. On the other hand, during the normal operation of conventional power plants the required power can be generated at any time, given that the power demand is within the technical constraints of the plant. Hence the power output is controllable and predictable. However, the power output from wind power plants depends on the wind condition of the area, and in addition, it fluctuates. Moreover, conventional sources use mainly synchronous generators to produce electrical energy. However wind power plants use different types of generator systems such as induction generators, double fed induction generators, and induction or synchronous generator with full power converters. Each of these generator systems pose different opportunities and challenges to the grid.

While most large wind farms are connected to high voltage transmission systems, medium sized farms are preferably connected to lower voltage distribution systems. This preference stems from comparatively lower connection costs associated with installing wind farms/turbines in lower voltage systems [3]. Thus, there is a need to effectively exploit the wind power hosting capacity of distribution systems. However medium voltage distribution systems have lower grid strength than their high voltage counter parts. Hence they are more vulnerable to the power quality and reliability issues introduced by wind power. Depending on the wind turbine technology, these issues of wind power include voltage flicker, harmonics, overvoltage, overloading, increased short circuit power level, and protection malfunctioning. Some distribution system operators (DSOs) are also concerned about the effect of wind power on increasing the frequency of tap changes (FTC) of a substation transformer.

Therefore in this thesis, these different integration issues of wind power are investigated. Special attention is given to the effect of wind power on overvoltage, overloading, and increasing the FTC of substation transformers. The role of active management strategies (AMSs) in mitigating these effects of wind power has been investigated and demonstrated using case studies. This chapter provides the background, aim, contribution and structure of the thesis. The chapter concludes by providing the list of papers published during the progress of the thesis.

1.1 Overview of previous works

Presently, it is widely accepted that the most common limiting factors of wind power integration to distribution system are the voltage rise problem and overloading of the system components [3]. Both of them are more likely to occur under low system loading condition and high wind power generation. Hence DSOs use this worst system condition to evaluate the possibility of connecting a given capacity of wind power. This works fine under passively operated distribution systems. But it severely limits the hosting capacity of distribution systems, which will intern hinder the penetration of wind power to the power system. Thus, various AMSs have been proposed to increase the hosting capacity of distribution systems. These AMSs include wind energy curtailment (WEC), reactive power compensation (RPC), coordinated on load tap changer (OLTC) voltage control (C-OLTC) [3–9].

However, there is still a limit to the amount of wind power that can be installed using AMSs. For example, the hosting capacity of the distribution system can be increased by curtailing part of the wind power during system overload or overvoltage. But WEC causes loss in revenue for the wind farm owner (WFO) and cannot be used indefinitely. Similarly, RPC can be used to increase the hosting capacity of a distribution system by avoiding overvoltage which would otherwise happen due to wind power. However, if used excessively, RPC may lead to unacceptable power losses in the system. Thus, there is a limit on the amount of wind power that can be installed using AMSs. In the literature reviewed, for example, in case of WEC, this is done either by limiting the amount of curtailed energy [4,9,10] or by constraining the capacity of wind power [3,5–7]. This approach, however, does not ensure the optimal use of the AMSs as the limit of energy curtailed set at each case is chosen arbitrarily and not based on the cost benefit analysis. Therefore, the increase in hosting capacity using these active management strategies requires further investigation.

Moreover, in addition to the main limiting factors, other effects of wind power (such as flicker, harmonics) need to be examined if and when they can be a limiting factor for the wind power integration in distribution systems. Special attention is given to the effect of wind power on the FTC of transformers as such an analysis is rarely found in literature.

1.2 Objective of the thesis and the main contributions

The overall aim of this thesis is to maximize the wind power hosting capacity of distribution systems in a cost-effective manner. To this end, different integration issues of wind power are examined as limiting factors for wind power integration. Furthermore, different AMSs are investigated

to increase the hosting capacity of distribution systems. This is accompanied by the development of a model based on cost benefit analysis to determine the optimal usage level of AMSs, specially of WEC, and the maximum hosting capacity of distribution systems.

To the best knowledge of the author the following points are the contributions of the thesis.

- **The determination of the effect of wind power on the frequency of tap changes** with respect to varying grid condition accompanied by analyzing the use of RPC from wind turbines for reducing the FTC (Chapter 3).
- **The proposed simple method of siting wind power** to maximize the hosting capacity of a given distribution system (Chapter 4).
- **The development of a new optimization model based on cost benefit analysis** for determining the optimal usage level of AMSs and optimal hosting capacity of a given distribution system. (Chapter 5).

1.3 Thesis structure

With the thesis introduction already given in this chapter i.e. Chapter 1, the rest of the thesis is structured as follows:

Chapter 2 provides the basics of wind power integration in a distribution system which includes the discussion of the nature of the wind power and its effect on power quality and reliability of the distribution system.
In **Chapter 3** the effect of wind power on the FTC of a substation transformer is investigated. The chapter also analyses the use of RPC from the wind turbines to decrease the FTC of substation transformer.
Chapter 4 proposes a simple approach of sitting wind power in order to maximize the hosting capacity of distribution systems.
In **Chapter 5** develops a mathematical model based on cost benefit analysis to optimize the hosting capacity of distribution systems.
Finally the conclusions of the thesis and future works are presented in **Chapter 6**.

1.4 List of publications

The following papers are published during the course of this thesis:

I. S. N. Salih, P. Chen, and O. Carlson, “Maximizing Wind Power Integration in Distribution System,” in 10th International Workshop on Large-Scale Integration of Wind Power into Power Systems as well as on Transmission Networks for Offshore Wind Power Plants, Aarhus, Oct. 2011.

II. S. N. Salih, P. Chen, and O. Carlson, “The effect of wind power integration on the frequency of tap changes of a substation transformer,” Power Systems, IEEE Transactions on , vol.28, no.4, pp.4320,4327, Nov. 2013.

III. S. N. Salih, P. Chen, O. Carlson, L. Bertling Tjernberg, "Optimizing wind power hosting capacity of a distribution system using costs benefit analysis," IEEE Transactions on Power delivery, Aug. 2013, under second revise and resubmit phase.

2

Wind power and its impact on a distribution system

The introduction of wind power to an electrical distribution system poses different types of power quality and reliability issues. Depending on the location and technology of the wind turbine and the characteristics of the distribution system, these integration issues of wind power include overloading of system components, over voltage, malfunction of protection system, voltage flickers and harmonics, etc. Thus this chapter is devoted to the discussion of these integration issues of wind power. However, the discussion of the characteristic of the wind power itself is vital to the understanding of the power quality and reliability issues that arise due to the introduction of wind power. Hence the chapter starts with the discussion of the characteristics of wind power in terms of the nature of the source of energy, i.e. the wind, and the generator system that converts the kinetic energy extracted from the wind into electrical energy. Then the different integration issues of wind power are discussed in terms of how they are quantified and assessed, how their effects differ depending on the turbine generator technology, etc.

2.1 Stochastic nature of wind power

The stochastic nature of wind power stems from mainly the stochasticity of the wind. However, understanding the characteristic of the wind turbines is also vital to understand the effect of wind power on the grid. Hence, this section provides the discussion of the wind and the wind turbine.

2.1.1 The wind

Wind fluctuates both temporally and spatially. The temporal fluctuation ranges from a time scale of less than one second to several days. In this respect three peaks are identified: turbulent peak, diurnal peak, and synoptic peak [11]. The turbulent peak is caused mainly by wind gusts in the sub-seconds to minute range. The diurnal peak is the result of daily wind speed variation caused by such factors as land breeze and sea breeze, which happens due to temperature differences between land and sea. On most of the globe this peak occurs in the early afternoon [12]. The synoptic peak

is the result of changing weather patterns, which typically vary daily to weekly but includes also seasonal cycles [11]. On this regard, particularly in Europe, the wind speed tends to be higher in winter than in summer [13]. This is ideal because the electricity consumption has also a similar seasonal pattern in this region.

From a wind turbine's point of view, the diurnal, synoptic fluctuations of the wind are used together with the mean wind speed to predict the energy yield for a site. The knowledge about turbulence and gustiness is required, first of all, for the load calculation of the wind turbine [14]. From the power system's point of view, the diurnal and the synoptic peaks mainly affect the operational aspect of the power system. The short term variation, and hence the turbulent peak, is the one that is given greater attention in terms of power quality, though its effect depends on the technology of the wind turbine connected to the system.

The spatial variations range from some millimeters to several kilometers [14]. The knowledge of these variations and the correlation between different sites is vital in the planning and operation of the power system. In this regard, a study carried out using two-year wind data with a three-hour resolution obtained from 142 synoptic stations in Sweden shows that the distance at which the correlation between wind speeds from two location drops to approximately 0.37 ranges from 38 to 530 km [15]. Since the area covered by a typical radial distribution system is not that large, the study implies that wind power in distribution systems can have a high level of correlation. In fact, we have observed a correlation that ranges from 0.82 to 0.95 among an hourly time series wind power data of one year. The data are obtained from 10 sites in a distribution system where there is a maximum of distance of around 10 km among the sites. Hence in a distribution system of such size full correlation can be assumed between wind turbine sites for planning studies.

2.1.1.1 Probability distribution of wind speed

For wind power planning projects, the knowledge of the long term wind speed distribution of the area being studied is given the utmost importance to assess the expected yield and the profitability of the project. Such data for a given area are usually represented in a concise mathematical description, i.e. the Weibull distribution function (2.1). Data representation using Weibull distribution uses two parameters only: the shape factor and the scaling factor. Thus, the representation of wind data using the Weibull distribution is quite handy and facilitates data sharing.

$$f(v) = \frac{k}{A}\left(\frac{v}{A}\right)^{k-1} \exp\left(-\left(\frac{v}{A}\right)^{k}\right) \tag{2.1}$$

The scaling factor A is a measure for the characteristic wind speed of the considered time series [14] and is given by

$$A = \frac{\bar{v}}{\Gamma\left(1+\frac{1}{k}\right)} \tag{2.2}$$

where $\bar{v}$ is the long term, such as annual, mean speed of the area, and Γ is the gamma function. The shape factor k describes the curve shape. It is in the range between 1 and 4. If there are small fluctuations around the mean wind speed, the value of k is high whereas large fluctuations give a smaller shape factor k (see Fig. 2.1). In general, the reference energy yield given by wind turbine manufacturers in the data sheets is calculated based on a Weibull distribution with k=2, i.e. a Rayleigh distribution function [14].

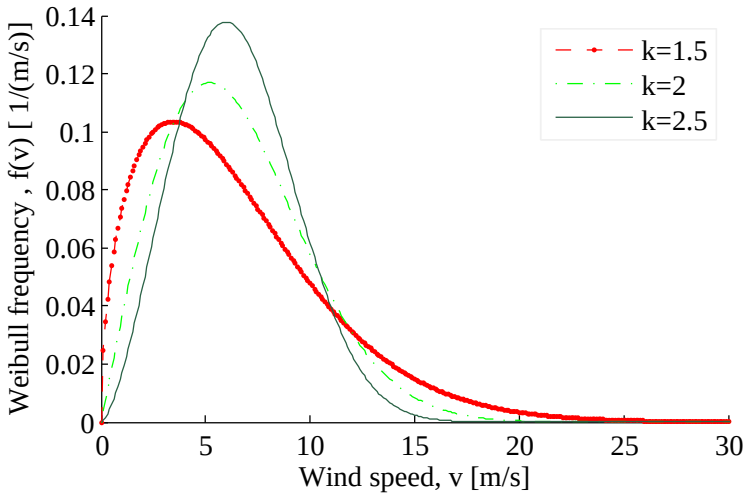

Figure 2.1: The Weibull distribution representation of wind with average speed of 6.5 m/s and a varying shape factor

On the other hand, for analyzing mechanical loads on the wind turbine and, in turn, for assessing the effect of wind power on the grid, knowledge of the short variations occuring in a given area is necessary. To this end, the short term variation is represented through the average value of the wind speed in the considered time (mostly 10 min) and the turbulence intensity [14]. Turbulence intensity is the ratio of the standard deviation of the wind speed to the average wind speed. Roughly considered, the turbulent fluctuations have a Gaussian distribution around the mean wind speed with its standard deviation. The turbulence intensity varies in a wide range, from 0.05 to 0.40 [14].

2.1.1.2 Wind energy yield determination

In wind power planning studies it is vital to know the energy available from a wind turbine. To this end, the power output of a wind turbine at a given time depends on the power curve of the wind turbine and the wind speed. Fig. 2.2 shows the power curve of a typical fixed speed and variable speed wind turbine. Below the cut in speed, since the wind is too low for useful energy production, the wind turbine is shut down. Then, once operating, the power output increases following a broadly cubic relationship with wind speed (although modified by the variations in power coefficient C_P) until rated wind speed is reached. Above the rated wind speed, the rotor is arranged to limit the mechanical power extracted from the wind [16]. Above the cut-out wind speed, the turbine is shut down to avoid mechanical damage on the wind turbine.

Based on the power curve P_{WT} of the wind turbine and the probability distribution the wind speed at a given site $f(v)$, the total energy yield of the wind turbine, E_{TWT}, can be calculated using

$$E_{\mathrm{TWT}} = T \int_0^{\infty} f(v) P_{\mathrm{WT}}(v) dv \tag{2.3}$$

where T is the time period of interest, e.g. a year. The energy yield is usually expressed in terms of the the capacity factor (C^F) of the wind turbine at that particular site, which is calculated using

$$C^F = \frac{E_{\mathrm{TWT}}}{8760 P_{rat}} \tag{2.4}$$

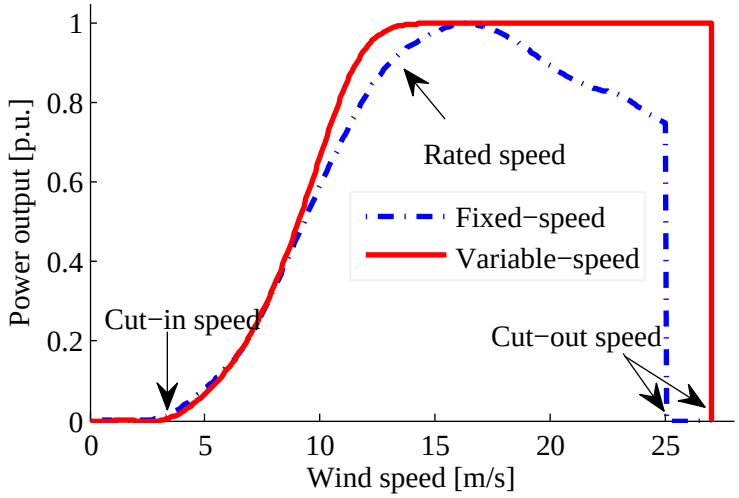

Figure 2.2: power curves of a typical fixed and variable speed wind turbines

where P_{rat} is the rated power of the wind turbine and 8760 is the number of hours per year. In practice this capacity factor lies in the range about 0.20 to 0.40 [11]. It is sometimes convenient to represent the capacity factor as the utilization time t_{util} in hours per year, calculated as

$$t_{util} = 8760C^F \tag{2.5}$$

2.1.2 The wind turbine

A wind turbine is composed of various components: the turbine blades, the tower, the generator system, etc. However, our aim in this thesis is to investigate the impact of wind power on power quality and reliability of an electrical distribution system. Thus, it is of interest to study the characteristic of the power output from the wind turbine which is governed by the characteristic of the generator system. In this respect, today's commercial wind turbines can be classified into four major groups depending on their ability to control the rotational speed, hence the power output, of the wind turbine [11].

2.1.2.1 Type A: Fixed speed wind turbines

Wind turbines equipped with squirrel-cage induction generators (SCIGs) are generally known as fixed speed wind turbines since these wind turbines work at almost constant speed, with slip order of 2% at rated power [11]. A typical fixed wind speed turbine have the configuration given in Fig. 2.3. Since there is a large inrush current during starting the induction generator, which can be as high as 6 to 8 times the current at rated operation [14], these wind turbines are equipped with soft-starters to limit the inrush current and bring the drive train slowly to the operational speed [16]. These wind turbines also consume a substantial amount of reactive power during idling as well as operation, as long as they are connected to the grid; the higher the power output is, the higher is the reactive power consumption as shown in Fig. 2.4. Consequently, these wind turbines are equipped with capacitor banks to provide a reactive support. However, these capacitor banks only shift the reactive power consumption curve downward.

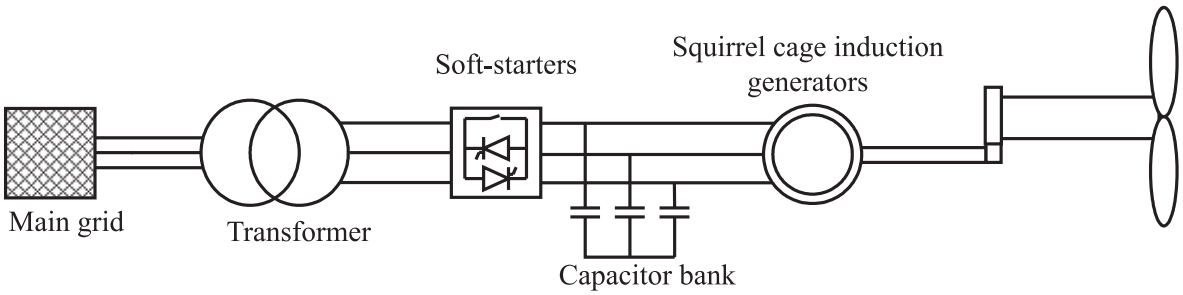

Figure 2.3: Schematic of fixed speed wind turbine

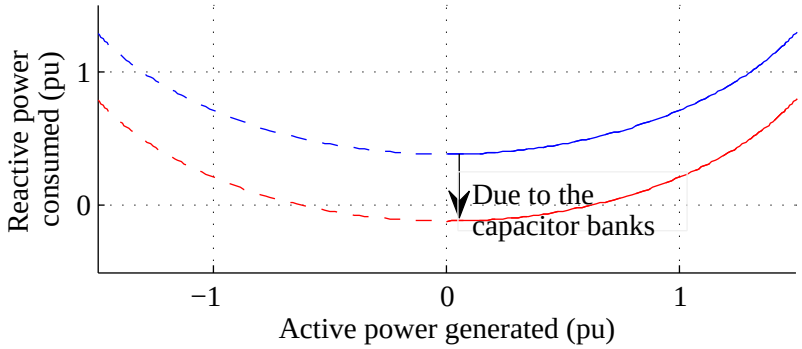

Figure 2.4: PQ curve of a typical fixed speed wind turbine

Fixed speed wind turbines constitute most of the early generation utility scale wind turbines. In the year 2000, these wind turbines still represented 39 % of the total installed wind turbines in the world [17]. The main reason for the use of SCIGs is the damping they provide for the drive train. The damping is provided by the difference in speed between the rotor and the stator magneto motive force (MMF), i.e. the slip speed. Additional benefits include the simplicity and robustness of their construction and the lack of requirement for synchronizing [18]. However, regardless of the power control principle (active or stall), the wind fluctuation are converted to mechanical fluctuations and consequently into electrical power fluctuation. The electrical power fluctuation can yield voltage fluctuation and flicker emission in weak grids while the mechanical fluctuation increases the stress on the drive train.

2.1.2.2 Type B: Limited variable speed wind turbines

One of the disadvantages of fixed wind speed turbines is that during wind gusts and high wind speeds, the drive train is exposed to high mechanical stresses. If a larger slip is allowed temporarily, the drive train will be relieved. Moreover during high wind speeds, a smoother increase in power output is possible. This is done by varying the resistance of the rotor circuit. Such control of rotor circuit resistance is possible in wound rotor induction generators (WRIG) as they allow access to the rotor winding via slip rings and brushes. By connecting electronically controlled variable resistance to the terminals of the rotor winding it is possible to vary rotor circuit resistance. Using this approach a brief increase in rotational speed up to 20% has been achieved [14]. At normal wind speeds, the additional variable resistor is shorted out for maximum efficiency. During strong wind the variable resistors are manipulated to get the required torque. Hence during wind gusts the

additional wind power is dissipated in the resistors, which needs additional cooling consideration. Whenever necessary, pitching can be combined with varying the rotor circuit resistance to get an optimum performance. To this end, varying the rotor circuit resistance is convenient whenever fast response is required while pitching can be used to reduce the power extracted from the wind rather than dissipating it in the resistors. Apart from this improved power controllability described, the characteristic of Type B wind turbine can be considered similar to Type A wind turbines.

2.1.2.3 Type C: Double fed induction generators

Though Type B wind turbines have improved some of the drawbacks of their Type A counterparts, they have their own shortcomings. One of this is the fact that the speed variability achieved is at the expense of increased power loss in the rotor circuit. Besides, the achieved variability in speed is not sufficient enough to ensure maximum energy extraction under varying wind speed condition. The next generation of wind turbines with improved performance are Type C, i.e. double fed induction generator (DFIG), wind turbines.

Fig. 2.5 presents the schematic diagram of this type of wind turbine. The rotor windings, that are accessible through slip rings, are connected back to the grid through a back to back AC/DC/AC power converter. This converter circuit, through injecting a controllable voltage at the rotor frequency, realizes a variable speed operation of the wind turbine [19]. Moreover, the energy that

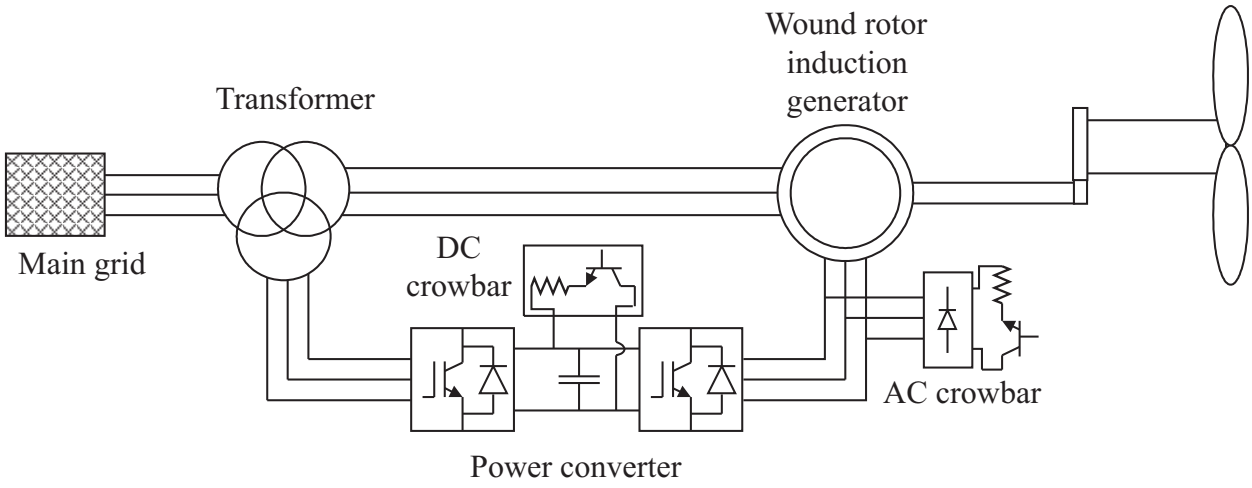

Figure 2.5: Schematic diagram of DFIG wind turbines [20]

used to be dissipated in the external resistors in Type B wind turbines is now fed back to the grid through machine-side converter. The power converters can also be used for smooth connection of the wind turbines to the grid as well as to provide the required reactive power compensation. During faults, the crowbar switches the rotor circuit to an external resistor to protect the machine-side converter from excessive current [21]. Similarly, the DC-link crowbar activates to protect the DC-link capacitor from overvoltage [20, 22].

The extent of speed variability achieved and the amount of wind power absorbed or delivered by the rotor depend on the size of the power converter used. Considering also the economic aspect of the converter, it is usually sized to be around 30% of the rated power of the wind turbine. And the usual speed range of operation of these wind turbines is between -40% to $+30\%$ of the

synchronous speed [11].

The reactive power capability of a DFIG wind depends on the stator current limit, the rotor current limit, and the rotor voltage. In general, the rotor current limits the reactive power production capacity of the machine while the stator current limits reactive power absorption capacity. The rotor voltage becomes a limiting factor only at high slips [23]. The grid side converter can provide additional reactive power support when it is not fully used for active power transfer. A typical reactive power curve a DFIG wind turbine is shown in Fig. 2.6 (adapted from [23, 24]). This is assuming that the wind turbine is always connected to the grid. However, at zero power output, the wind turbine is switched off. Hence reactive power support would only be available from the grid side converter. The magnitude of this reactive support will then depend on the ratings of the converter [24].

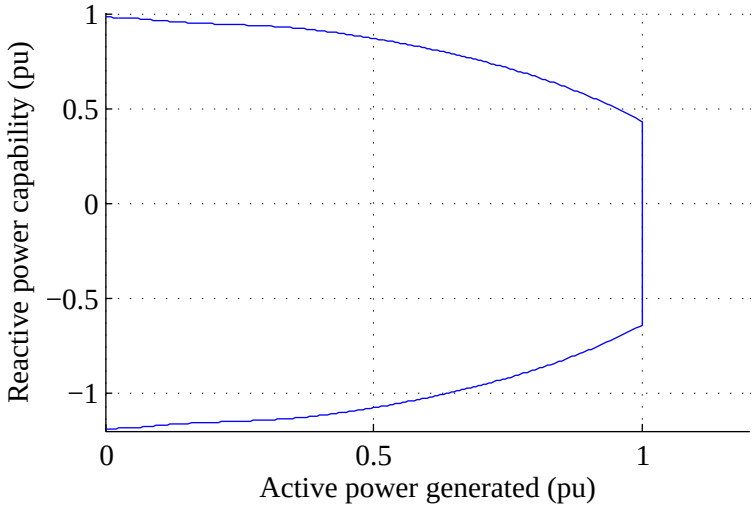

Figure 2.6: A reactive power capability diagram of a typical DFIG wind turbine

2.1.2.4 Type D: Full power converter wind turbines

In this wind turbine type the converter is rated to handle the full capacity of the wind turbine. That is, it completely decouples the wind turbine generator from the grid, giving the opportunity to vary the frequency of the generator as required. This also makes it possible to employ different types of generators such as induction, wound rotor synchronous, and permanent magnet synchronous generators [25]. The schematic diagram of a full power converter wind turbine is shown in Fig. 2.7.

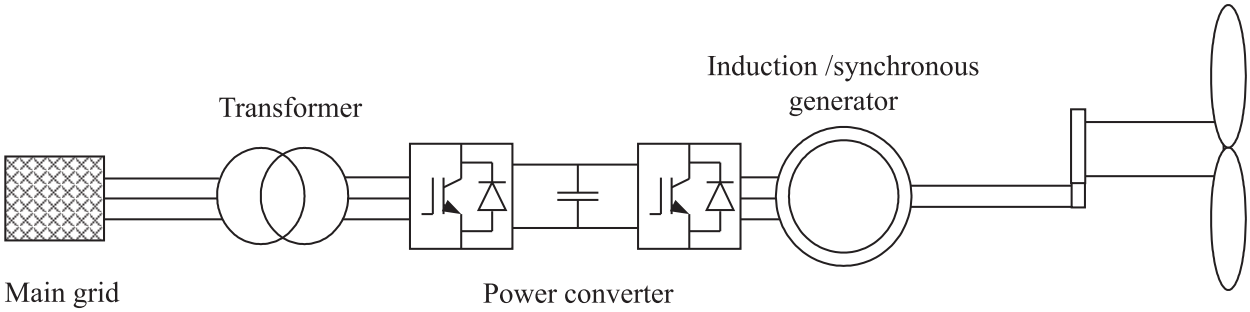

Figure 2.7: Schematic diagram of full power converters

These wind turbines can provide a wider range of speed variability than the DFIG wind turbines. The converter is used for smooth connection of the wind turbine as well as for providing the required reactive power support [11].

The reactive power capability of these wind turbines depends on the current rating as well as the voltage of the grid side converter. These ratings are chosen to meet grid code requirements in terms of providing specific level of reactive power support at varying conditions of system voltage and frequency [26]. For example, Fig. 2.8 shows the reactive power capability curve of a full power converter wind turbine with design power factors (pf_d) of 1 and 0.95 at grid voltages (V_g) of 1.0 and 1.05 pu. Similar to the case of DFIG wind turbines, they can provide larger reactive support at absorption compared to production. However, if the converter voltage is selected such that the converter voltage limitation is avoided, then Type D wind turbines can provide similar level of reactive support at both absorption and production [26].

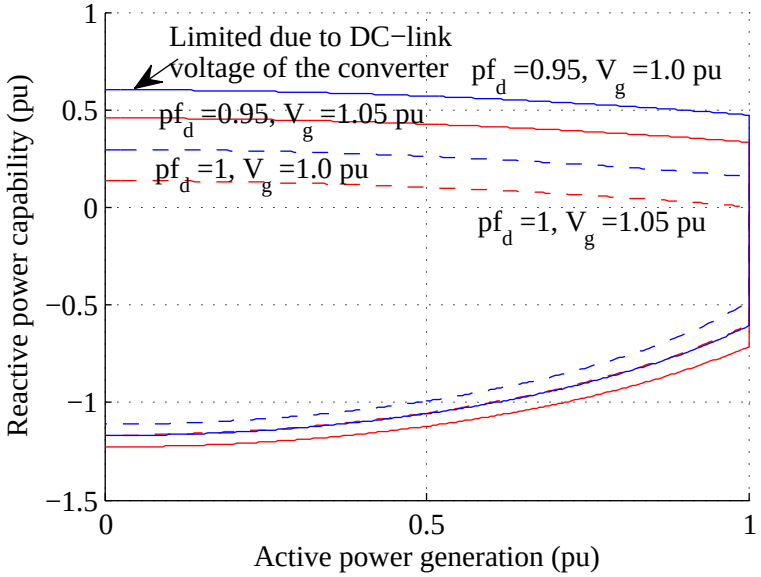

Figure 2.8: Reactive power capability a typical full power converter wind turbine

2.2 Impact of wind power on a distribution system

This sections provides the discussion of the different impacts of wind power on a distribution system.

2.2.1 Overvoltage

2.2.1.1 Voltage regulation in a distribution system

In an electrical distribution system there are one or more transformers through which electricity is supplied to the consumers in the network. The purpose of these transformers is to step down the voltage from transmission or sub-transmission systems. These transformers are also equipped with

on-load tap changers (OLTC) that regulate the voltage at the secondary side of the transformer so as to keep the voltage in the distribution system within, for example, ±10% of the nominal voltage. These range is not continuous, it is divided into steps of, for example, 1.67% so that each change represents a specific voltage increment. Moreover, tap changers have adjustable deadbands and time delays. The deadband is the voltage range around the reference value within which the tap changer does not take action. The time delay is the duration during which the voltage should be outside this deadband before the tap changer takes action.

The tap changers can accomplish the voltage regulation in two ways [27]. One way is through maintaining the voltage at the secondary side of the transformer at a given deadband around a constant voltage set point. In the second alternative, the voltage set-point is augmented with line drop compensation, i.e. the voltage set-point changes depending on the voltage drop on the user-adjusted internal impedance. This internal impedance is chosen to give the required voltage boost from low to high loading condition.

Though many regulators have a bidirectional capability, to give the required boost depending on the direction of the power flow, the change in power factor of the load complicates the application of the method. Many regulators are, thus, set up without line drop compensation. It is obviously easier and less prone to mistakes, but at the expense of losing some significant capability [27].

2.2.1.2 Wind turbines contribution to overvoltage

Whichever is used, the above voltage regulation approaches have been utilized and was found effective in passively operated distribution systems for many years. But due to the introduction of wind power, or any distributed generation for that matter, voltage regulation has become a challenge. Wind power introduces a reverse power to the external grid. With the voltage at the transformer being held almost constant, this results in a higher voltage at the point of common connection (PCC) compared to that at the substation. Depending on the amount of reverse power flow, the voltage at the PCC could be above the allowed voltage level in the distribution system.

Consider a simple network with wind power shown in Fig. 2.9. The cable between the reference

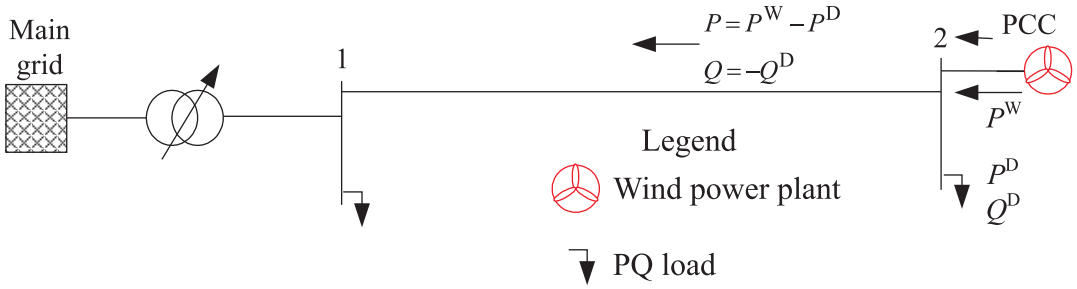

Figure 2.9: A simple distribution system with wind power

node 1 and the PCC can be represented by the π-model of a transmission line (see Fig 2.10). Given a constant voltage V_1 at node 1, the voltage V_2 at node 2 in p.u. is given by

$$V_2 = V_1 - I \times Z \tag{2.6}$$

where

$$I = \frac{-P + iQ_n}{V_2^*} \tag{2.7}$$

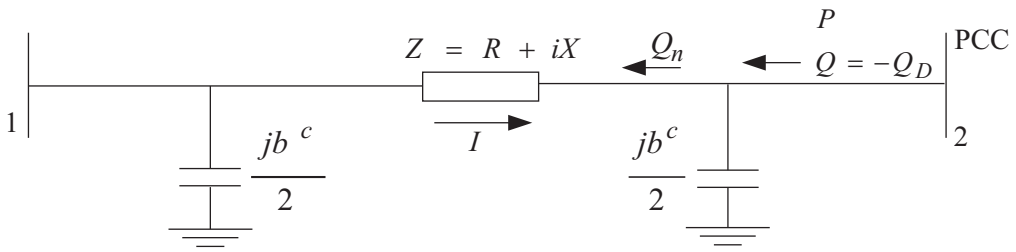

Figure 2.10: A π-model of power line between two buses

and

$$Q_n = Q + \frac{b^c}{2}|V_2|^2 \tag{2.8}$$

Hence

$$V_2 = V_1 + \frac{P - iQ_n}{V_2^*} \times (R + iX) \tag{2.9}$$

Unless there is a high reactive power consumption compared to active power generation and the cable have considerable resistance, the angle between V_1 and V_2 is usually small and the magnitude of V_2 is usually close to 1 pu. Hence it follows that:

$$|V_2| - |V_1| \approx PR + Q_n X \tag{2.10}$$

Since the length of the cable between any two buses in distribution networks can be considered electrically short, the capacitance part can also be neglected. Hence for most practical cases of a short line

$$\Delta|V| \approx PR + QX \tag{2.11}$$

where $\Delta|V| = |V_2| - |V_1|$. From (2.11), one can see that the higher the value of P, the larger the increase in voltage level at bus 2 (PCC) will be. Thus, depending on the power output from the wind farm and the network impedance between the wind farm and the substation, this can cause an overvoltage in the network.

Fig. 2.11a shows the voltage at the PCC for different cable types (given in Table 2.1) and for varying level of wind power. The error introduced in calculating the voltage by using (2.11) is shown in Fig. 2.11b. The calculation is done assuming the distance between the PCC and the substation is 5km.

It can be clearly seen from Fig. 2.11a that the voltage level increases parallel to the increase in the wind power injection. Moreover, the amount of wind power that can be installed without violating the $\pm 5\%$, also known as the wind power hosting capacity of the network, decreases with the increase in per km resistance of the cable. This is evident from (2.11), since the power output from the wind turbine is mainly composed of active power, the voltage rise is approximately proportional to the resistance of the cable. Moreover, given that the capacity of the wind power is within the hosting capacity of the network, Fig. 2.11b shows that the error introduced by using the approximate formula is less than 1%.

Though $\pm 5\%$ voltage limit has been used in Fig. 2.11a, the Swedish AMP standard specifies the limit at the PCC with the first customer to be within $\pm 2.5\%$ while $\pm 5\%$ requirement is fulfilled at the terminal of the wind power installation [28]. Thus, with the AMP standard voltage limits in

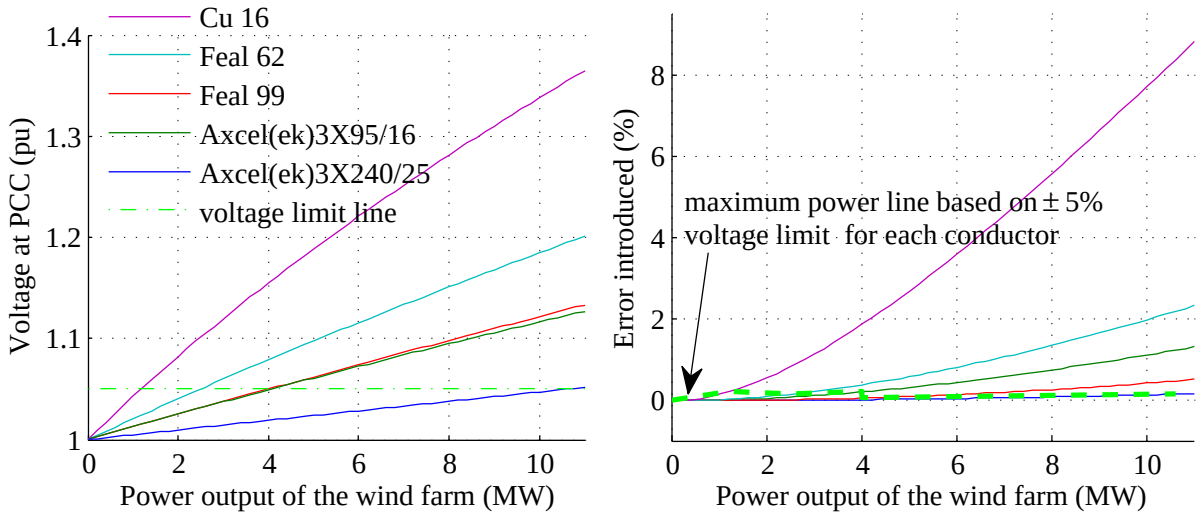

(a) Voltage level at PCC

(b) Error introduced due to (2.11)

Figure 2.11: Voltage rise effect of wind power

Table 2.1: Cable types and their characteristic

Type	Conductor	Resistance r (Ω/km)	Reactance x (Ω/km)	Shunt reactance $b_c/2$ (S/km)	X/R	Current rating (A)
Underground cable	AXCEL(EK) 3X240/25	0.125	0.085	6.28E-05	0.679	360
	AXCEL(EK) 3X95/16	0.320	0.094	4.40E-05	0.295	215
Overhead line	FEAL 99	0.336	0.354	1.88E-06	1.053	435
	FEAL 62	0.535	0.369	1.88E-06	0.689	305
	Cu 16	1.100	0.385	1.88E-06	0.350	-

place, the hosting capacity of the network in Fig. 2.9 will be lower than those implied by Fig. 2.11a. On the other hand, according to the European Norm EN 50160, the voltage in LV and MV networks be with in ± 10 for 95% of the time in a week as measured by 10 minute average of the rms voltage [29]. One argument against the use of such large voltage variation at PCC is that should there be any increase in voltage downstream of the PCC, it can result in an overvoltage. However a better understanding of the system condition may allow a voltage rise higher than those specified by the AMP manual.

2.2.2 Overloading

The components of a distribution system, such as cables and transformers, can continuously carry only up to a given current level. This limit is based on their thermal rating. The introduction of wind power can have both positive and negative effect on the loading level of distribution system components. If the capacity of the wind power is relatively low compared to the load in the system,

it can reduce the power flow through network thereby relieving the thermal stress on the system components. It may also decrease the system loss. On the other hand, if the installed wind power in the distribution system is relatively high there will be a substantial reverse power flow. This reverse power flow can also be higher than the forward power flow that used to flow through the system before the introduction of wind power. This of course will increase both the thermal stress in the network components and the system loss. Under special cases, this reverse power flow can even exceed the thermal rating of the network components, resulting in an overloading situation.

For example, Table. 2.2 provides the maximum current flows though the cables for the case considered in Fig. 2.11. It can be seen that for the case of AXCEL(EK) 3X240/25 cable, the thermal limit is violated. Hence, even though the voltage limit allows the installation of almost 11 MW wind power capacity, the thermal limit imposes a considerable reduction on the allowed level of wind power capacity.

Table 2.2: The maximum current flows though the conductors for the case considered in Fig. 2.11

Conductor	Current rating (A)	Maximum wind power capacity based on voltage limit (MW)	Maximum current flow through the cable (A)
AXCEL(EK) 3X240/25	360	10.6	556
AXCEL(EK) 3X95/16	215	4.0	210
FE-AL 99	435	4.0	210
FE-AL 62	305	2.4	126
Cu 16	-	1.0	52

2.2.3 Voltage Flickers

Voltage flickers are the rapid fluctuation of voltage which may cause a perceptible light flicker depending on the magnitude and frequency of the fluctuation. Large voltage flickers can also cause malfunctioning of sensitive equipment. Hence a measurement system was developed by IEC [30] to quantify and put a limit on the allowed level of these disturbances. Based on this standard two quantities are identified for flicker measurement: the short term flicker severity factor P_{st} and the long term flicker severity factor P_{lt}. The former is based on measurements over 10 minute period while the latter is based on 2 hour measurements [31]. Using this flicker emission quantification, flicker emission limits are imposed on each installation to ensure that the cumulative effect of the emissions at various voltages will not be disturbing to the customers located on the low voltage side. The Swedish AMP manual specifies these limits as $E_{\mathrm{Pst},i} = 0.35$ and $E_{\mathrm{Plt},i} = 0.25$ for short term and long term emission levels, respectively. The IEC standard provides a strategy of allocating these emission limits accounting for the capacity of the installation compared to the total system capacity (provided in Appendix A).

Wind turbines introduce two types of flicker: flicker emission during continuous operation and flicker emission during switching operation. The flicker emission during continuous operation is caused by wind turbulence, the wind gradient and tower shadow effect, and the mechanical properties of the wind turbine [11, 32]. The voltage flicker that occur due to switching operation are induced by a change in power production due to start up and shut down of the wind turbines. More-

over switching between generators or generator windings causes switching voltage flicker [11].

In general, the flicker emission from variable speed wind turbines can be considered fairly low during both continuous and switching operation, whereas the flicker emission from fixed speed wind turbines depends on the control mechanism: stall or pitch [11]. The flicker emission from stall controlled wind turbines is average during continuous operation. However, due to limited controllability of the torque input of the turbine, the flicker emission is high during switching operation. With better controllable turbine torque input, the flicker emission from pitch controlled wind turbines during switching operation can be considered average. However, due to limited bandwidth of the the pitching system, their flicker emission during continuous operation is high [33].

Moreover, flicker emission from wind turbines depend on the short circuit capacity of the network relative to the capacity of the wind turbines, measured by short circuit ratio (SCR), the angle of the Thevenin impedance of the grid seen from the point of connection of the wind turbine, and the average wind speed. Hence wind turbine manufacturers supply different coefficients which can be used to assess the level of flicker emission from the turbine under continuous as well as switching operation. Using these flicker emission coefficients and the grid characteristic at the point of connection, the flicker emission from a given wind turbine installation can be determined.

2.2.3.1 Flicker emission during continuous operation

Flicker emission from a wind turbine under continuous operation is characterized by a flicker coefficient $c(\psi_k, v_a)$ which is specified for different average wind speeds v_a and impedance angles ψ_k. Based on the average wind speed at a particular site and the impedance angle of the grid, the flicker emission from the wind turbine is calculated using

$$P_{st} = P_{lt} = c(\psi_k, v_a)\frac{S_n}{S_k} \tag{2.12}$$

where S_n is the rated apparent power of the wind turbine and S_k is the short circuit level of the distribution system at the point of connection.

In case a number of wind turbines are connected at the point of common connection, according to IEC standard [34], their resultant flicker emission ($P_{st\Sigma}$ and $P_{lt\Sigma}$) can be calculated using

$$P_{st\Sigma} = P_{lt\Sigma} = \sqrt{\sum_{i=1}^{N_{wt}} \left(c_i(\psi_k, v_a)\frac{S_{n,i}}{S_k} \right)^2} \tag{2.13}$$

2.2.3.2 Flicker emission during switching operation

For a given wind turbine, two factors are stated to characterize the wind turbine during switching operation: voltage change factor $k_u(\psi_k)$ and flicker step factor $k_f(\psi_k)$ [34]. Similar to the flicker coefficients, these factors are functions of the grid impedance angle ψ_k.

A voltage change occurs at the PCC due to switching operation of a wind turbine installation. The magnitude of this voltage change in percent is given as [34]

$$\Delta V = k_u(\psi_k)\frac{S_n}{S_k} \cdot 100 \tag{2.14}$$

The AMP guideline requires that this voltage change be below 4% of the nominal voltage [28].

The flicker emission during switching operation can be calculated using:

$$P_{st} = 18 \times N_{10m}^{0.31} \times k_f(\psi_k)\frac{S_n}{S_k} \tag{2.15}$$

$$P_{lt} = 8 \times N_{120m}^{0.31} \times k_f(\psi_k)\frac{S_n}{S_k} \tag{2.16}$$

where N_{10m} and N_{120m} are the maximal number of switching operations that may occur during 10 minute and two hour period, respectively.

In case a number of wind turbines are connected to the PCC, the total flicker emission due to switching operation can be estimated using [34]:

$$P_{st\Sigma} = \frac{18}{S_k} \times \left(\sum_{i=1}^{N_{wt}} N_{10m,i} \times \left(k_f(\psi_k)\frac{S_n}{S_k}\right)^{3.2}\right)^{0.31} \tag{2.17}$$

$$P_{lt\Sigma} = \frac{8}{S_k} \times \left(\sum_{i=1}^{N_{wt}} N_{120m,i} \times \left(k_f(\psi_k)\frac{S_n}{S_k}\right)^{3.2}\right)^{0.31} \tag{2.18}$$

2.2.4 Harmonics

Harmonics are produced by nonlinear loads such as power electronic devices, rectifiers and inverters. They can cause overheating and equipment failure, faulty operation of protection devices, nuisance tripping of sensitive devices and interference with communication circuits [11]. Hence standards specify the harmonic emission limits which will ensure normal operation of the power system. Table 2.3 presents the harmonic voltage emission limits at low and medium voltage networks specified by the IEC standard [35, 36]. The Swedish AMP standard also specifies similar limits [28]. From these general emission limits, localized emission limits are imposed on each disturbing installation based on its capacity compared to the total system capacity. The details of the allocation of localized emission limits are provided in Appendix B.

Depending on the technology of the generator system, wind turbines emit different levels of harmonic currents to the grid. In general fixed wind speed turbines do not cause significant harmonic[1] or interharmonic[2] disturbances. Hence the specification of harmonics and inter harmonics are not required by IEC 614000-21 [11]. However, for variable speed wind turbines equipped with power electronic converters, the emission of current harmonics (up to 50 times the supply frequency), interharmonics (up to 2kHz) and higher frequency[3] components have to be specified in percent of the rated current for the operation of the wind turbine at the power bins 10, 20,.., 100% [34].

[1] Harmonics are components with frequencies that are multiple of the supply frequency

[2] Interharmonic disturbances have frequencies that are located between harmonics of the supply frequency

[3] having frequencies between 2kHz and 9kHz

Table 2.3: Compatibility levels for individual harmonic voltages in low and medium voltage networks (percent of fundamental component) [35, 36]

Odd harmonics non-multiples of 3		Odd harmonics multiples of 3		Even harmonics	
Harmonic order h	Harmonic voltage %	Harmonic order h	Harmonic voltage %	Harmonic order h	Harmonic voltage %
5	6	3	5	2	2
7	5	9	1.5	4	1
11	3.5	15	0.4	6	0.5
13	3	21	0.3	8	0.5
$17 \leq h \leq 49$	$2.27 \cdot \frac{17}{h} - 0.27$	$21 < h \leq 45$	0.2	$10 \leq h \leq 50$	$0.25 \cdot \frac{10}{h} + 0.25$
The compatibility level for total harmonic distortion (THD) is 8%					

Harmonics with magnitudes below 0.1% of the nominal current may not be reported according to the IEC 61400-21 standard.

In case a number of wind turbines are connected to the same PCC, the h^{th} order harmonic current distortion $I_{h\Sigma}$ at the PCC can be calculated using [36]

$$I_{h\Sigma} = \sqrt[\beta]{\sum_{i=1}^{N_{wt}} \left(\frac{I_{h,i}}{n_i} \right)^{\beta}} \tag{2.19}$$

where

$I_{h,i}$ the h^{th} order harmonic distortion of the i^{th} wind turbine
n_i the tap ratio of the transformer connected to the i^{th} wind turbine
β a constant value to be selected from Table. 2.4.

harmonic order	β
$h < 5$	1.0
$5 \leq h \leq 10$	1.4
$h > 10$	2.0

Table 2.4: Values of β according to IEC 61000-3-6

Moreover, the total harmonic distortion (THD) can be calculated using [34]

$$THD = \frac{\sqrt{\sum_{h=2}^{50} I_h^2}}{I_n} \times 100 \tag{2.20}$$

The harmonic emission limits presented in Table 2.3 are specified in terms of voltage harmonics while current harmonic emissions are specified for wind turbines. Thus, according to the Swedish AMP guideline, the voltage harmonic limits found in Table 2.3 can be converted to current harmonic emission limits using

$$i_h = \frac{u_h U^2}{Z_h S_{\max}} \tag{2.21}$$

where u_h is the voltage harmonic limit, i_h is the corresponding current harmonic limit, U is the nominal voltage of the system, $S_{\max}$ is the maximum apparent power of the wind turbine, and Z_h is the network harmonic impedance in Ohm and is given by

$$Z_h \cong h(X_k + X_l) \tag{2.22}$$

where X_k is the short circuit reactance of the transformer[1], X_l is the reactance of the line for the fundamental frequency, and h is the order of the harmonics.

The analysis of the actual harmonic impedance of a system can be more complex than what is presented by the AMP standard [36–40]. Hence the harmonic impedance calculation presented here can only be used as a rough approximation of the actual harmonic impedance.

2.2.5 Effect of Wind Power on the Protection System

A given distribution system is designed to handle a certain level of short circuit current. This short circuit current is often thought to come from the upstream network. But due to the installation of wind powers, or DGs in general, there is an extra contribution of short circuit current from these sources (see Fig 2.12). In distribution networks where short circuit level is already around the design limit of the switchgear, the additional short circuit current, in the worst case, can affect the fault current handling capacity of the switchgear. This may lead to malfunctioning or even destruction of the switchgear. Here we identify two components of the short circuit current and the corresponding ratings of the switchgear to assess the effect of wind power on the fault handling capability of the switchgear [41, 42]:

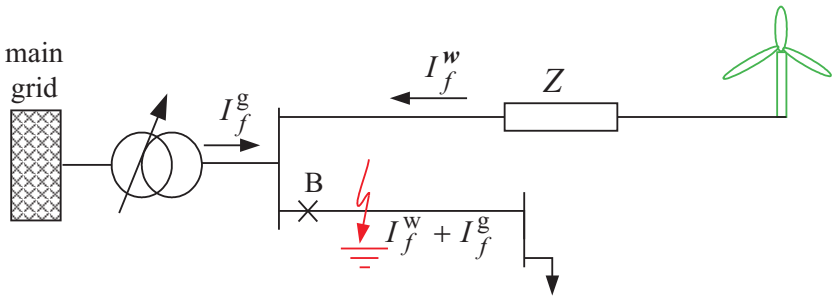

Figure 2.12: Typical equivalent circuit of a faulted radial distribution network

1. The initial symmetrical short circuit current I_k'' is the r.m.s value of the symmetrical a.c. component of the short circuit current at the instant the short circuit occurs (see Fig. 2.13). This current value should be below the rated short-time withstand current (also known as the rated short-circuit breaking current in circuit breakers) of the switchgear to insure that the switchgear is able to withstand the heat generated due to the short circuit current.

2. The peak short circuit current I_p is the maximum possible instantaneous value of the short circuit current. The rated peak withstand current (which is the same as the rated short circuit making current in circuit breakers) of the switchgear should be above this value. This will

[1] network transformer not wind turbine transformer

insure that the switchgear has the capability to withstand the electromechanical forces due to the the peak short circuit current. Usually the rated peak withstand current is 2.5 times the rated short time withstand current in 50 Hz system while it is 2.6 times in 60 Hz system [41].

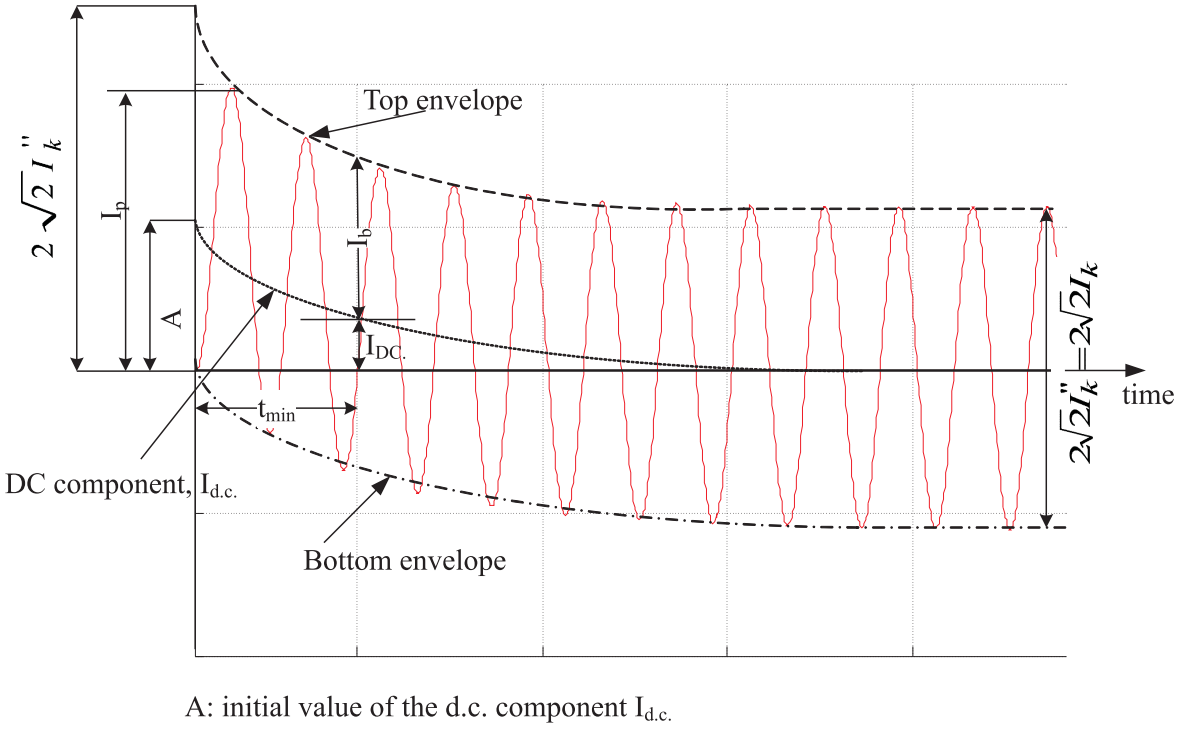

Figure 2.13: Short circuit current from far-from-generator fault [42]

In addition to increasing fault current, the introduction of wind power may also contribute to the reduction in fault current with overall impact of jeopardizing the protection coordination of the system. But such situation does not limit the integration of wind power as it only needs a change in the settings of the affected relays.

Furthermore, the fault current contribution from wind turbines is not uniform; it varies depending on the technology of the wind turbine generator system. Thus, the following subsections provide the discussion of the fault current contribution from different wind turbine types. Since, for most cases, the three phase to ground fault is the most severe fault, the discussions are limited to the fault current contribution of each wind turbine type under this fault condition.

2.2.5.1 Type A - Squirrel Cage induction generators

SCIGs are able to contribute significant fault current. In the worst case, the short circuit current contribution can be as high as 8 pu [43], but generally higher than 3 pu [44]. More detailed analysis of the short circuit current contribution can be done using simulation but it is not convenient. A simplified analysis of a short circuit current can be done using the IEC approach.

The IEC standard 60909 does not include the discussion of short circuit calculation from asynchronous generator, however it does include the discussion from asynchronous motors. Hence

Reference [45] proposes treating asynchronous generators like motors during short circuit current calculation. Accordingly, the asynchronous generators can be represented by $Z_G = R_G + iX_G$ where

$$Z_G = \frac{1}{I_{LR}/I_{rG}} \frac{U_{rG}^2}{S_{rG}} \tag{2.23}$$

and I_{LR}/I_{rG} is the ratio of the locked rotor current to the rated current of the generator, U_{rG} and S_{rG} are the rated voltage and apparent power of the generator, moreover

$$X_G = \frac{Z_G}{\sqrt{1+(R_G/X_G)^2}} \tag{2.24}$$

Typical values of $R_M/X_M = R_G/X_G$ are given in [42] depending on the voltage level and the power rating of the motors.

Moreover, based on this treatment of asynchronous generators like asynchronous generators, the peak short circuit current value i_p, according to [42], is given by

$$i_p = \kappa\sqrt{2}I_k'' \tag{2.25}$$

where κ is given in (C.9).

2.2.5.2 Type B - Wound-rotor induction generator with variable external resistance

As highlighted in Section 2.1.2, these are, in practice, SCIG with variable rotor resistances. Hence when the external circuit is shorted (i.e. when operating below the rated slip), the short circuit current is similar to that of SCIG. However operation above the rated slip requires an increase in the rotor resistance. Thus the short circuit contribution under this situation will be lower [46]. However, in general, treatment of these generators like SCIGs will result in a more conservative fault current contribution.

2.2.5.3 Type C-Double fed induction generators

The circuit set up of a DFIG system is shown in Fig. 2.5. During a fault the crowbar is switched in and the rotor side converter is blocked. This crowbar resistance can be as high as 20 times the value of the generator rotor resistance. Hence, with respect to fault current contribution, DFIGs can roughly be treated as SCIGs with higher rotor resistance [45, 47, 48]. Simulation results have shown the short circuit current to vary between 3 pu to 10 pu [44,46–48] depending on the machine parameters, which is similar to the case of SCIGs. Using the similarity with SCIGs in response to faults, an approximate equation for the peak current is derived in [47] which is given as

$$i_{\max} \approx \frac{1.8 c_{\max} U_{ph}}{\sqrt{X'^2 + R_{cb}^2}} \tag{2.26}$$

where R_{cb} is the crowbar resistance and $c_{\max}$ is added here to account for the worst case of phase voltage (see table C.1). The voltage U_{ph} is the per phase value of the nominal voltage. X' is given by

$$X' = X_1 + \frac{X_2' X_m}{X_2' + X_m} + X_{ext} \tag{2.27}$$

where X_1 is the leakage reactance of the stator, $X_2^{'}$ is the leakage reactance of the rotor referred to the stator, and X_{ext} is the reactance of the external network between the wind turbine and the fault point.

Nevertheless, the treatment of DFIGs as SCIGs with higher rotor resistance suffers error due to the simplifying assumptions used when deriving the short circuit current for SCIGs (which are no longer valid in DFIGs) [49]. Though some adjustments are made to account for these error sources, the peak three phase short circuit current calculated using (2.26) can have an error up to 15% compared to simulation results [47]. This is good enough for some rough calculations; however, it is not sufficient to study fault response of the DFIG in demanding situations. Hence an alternative analytical expression is derived in [49–51] which has a drawback of being too long to easily grasp.

2.2.5.4 Type D- full power converter wind turbine generators

The IEC standard [42] treats static converters, which have similar operational characteristic to the Type D wind turbines, like asynchronous motors/generators with $I_{LR}/I_{rG} = 3$ and $R_G/X_G = 0.1$. In doing so, the IEC standard assumes that these machines contribute to a fault up to 3 times of their rated current. However, the available information on the subject indicates that the current output from Type D wind turbines is limited by the overcurrent capability of the converter system. The converter is usually designed to have an overload capability of a little above, around 10% [46], of the rating of the wind turbine. Moreover, based on simulation results from [46], no DC component is seen. Hence the peak value of the initial fault current can only have a maximum value of

$$i_p = \sqrt{2}kI_r \tag{2.28}$$

where k is the percent of the rating of the converter relative to the rated current I_r of the wind turbine.

A calculation exercise on fault current calculation involving different technologies of wind turbines is provided in Appendix C.2.

2.3 Summary

This chapter discusses the stochastic nature of wind power and the impact of wind power integration in medium voltage distribution systems. Wind power has a stochastic nature with uncontrollable power output and a high level of correlation between wind parks at distribution system level. The long term wind speed distribution at a particular location can be roughly represented using a simple and concise mathematical expression, i.e. the Weibull distribution. For wind power planning studies this data can be used along with the power curve of a wind turbine to assess the expected energy yield of a given wind power installation.

The introduction of wind power in a given distribution system poses a number of known power quality and reliability concerns. Overvoltage and overloading can occur more or less independent of the generator technology. However, other impacts of wind power–such as flicker and harmonic

emission, increased fault level–depend on the technology of the generator system of the wind turbine. Flicker emission, for example, is higher in fixed speed wind turbines while voltage harmonics are introduced mainly due to variable speed wind turbines. The fault current contribution is highest with Type A wind turbines while significant fault currents are also injected by Type B and C wind turbines. Type D wind turbines, on the other hand, have a low level of fault current contribution as determined by the overcurrent capability of the converter system.

Flicker emission is directly related to the stochastic nature of wind power and harmonics is indirectly related to it since power electronic converters are used to avoid the negative impact of the stochastic nature. The other integration issues can arise due to any type of DG and are not specific to DGs with intermittent output.

3

Effect of wind power on frequency of tap changes

This chapter is devoted to the investigation of the issue of wind power related to the increase in the frequency of tap changes (FTC). The chapter starts by providing a background to the issue. This is followed by a formulation of a mathematical model that can be used in assessing the effect of wind power on the FTC. In the end, the results of a case study based on measured load, wind, and network data is provided.

3.1 Introduction

Substation transformers are the most critical components of a distribution system. Since they are capital intensive, only a small number of transformers supply power to a large number of customers in a distribution system. Hence high availability of these components is given the utmost importance by any DSO.

The failure of a transformer, besides jeopardizing the reliability of the distribution system, will expose the DSO to a huge amount of cost. The causes of transformer failure are numerous [52–57]. However the majority of transformer failures can be traced back to a faulty tap changer [55–58]. Hence, in terms of the reliability of the transformer, tap changers can be considered as the critical part of the transformer. This is evident from the extensive literature that is devoted for condition monitoring and maintenance of tap changers [57–63].

The main reasons for the failure of tap changers are the erosion of the diverters contact due to switching arcs, the wear and tear of the mechanical components such as the energy accumulator springs, carbon formation in the diverter oil caused by arcing, and breakdown of the insulating materials due to accumulation of sludge. Among these, the first three are directly related to the number of tap operations that occur in tap changers. Especially the wear in the diverter contacts depends not only on the number of tap changes but also on the transformer loading during the tap change [63].

With the increased introduction of wind power in distribution systems, some DSOs are concerned about its possible effect on the wear and tear of the tap changers. This concern mainly arises from

a fluctuating nature of wind power as well as the possible increase in the power flow through the transformer. The fluctuating power output from the wind turbines can introduce high power flow fluctuation through the transformer. This may ultimately lead to an increase in frequency of tap changes (FTC). If this is the case, considering the power system is already vulnerable to wear and tear due to aging, the DSO may limit the integration of wind power to its network to avoid potential increase in maintenance costs or unexpected tap changer failures. Hence, such concerns may hinder the integration of renewable energy sources at a time governments are working to increase the share of these energy sources.

However the investigation of the effect of wind power integration on the FTC is given only a minor attention. To the author's knowledge, published works that even mention the issue of FTC in relation to wind power integration are limited to [64–67]. In this chapter, a detailed analysis of the effect of wind power integration on the FTC is carried out. Moreover, most variable speed wind turbines have the capability to provide a considerable amount of controllable reactive power support. Thus, a further investigation is carried out to use this readily available reactive power from the wind turbines to decrease the FTC. Such investigation is valuable because, as mentioned above, tap changers are exposed to wear depending on the number of operation they have undergone. Moreover reactive power can provide a better voltage regulation at secondary side of the transformer since, unlike tap changer, it almost have no a time delay in operation.

3.2 Problem Formulation

This section has two subsections. The first subsection formulates the mathematical model that can be used to determine the number of tap changes in a given distribution. The next subsection develops the model further to incorporate reactive power compensation (RPC) as a means to reduce the FTC.

3.2.1 Model set up for analyzing the effect of wind power on frequency of tap changes

To analyze the effect of wind power on the FTC, one has to determine the FTC with and without wind power. Thus, a mathematical model is needed to determine the FTC in each case. Such a model can be used to carry out a series of load flow calculations using the network, load and wind power data as inputs. The main aim of these load flow calculations is to determine the tap position at each time step satisfying the different equality and inequality constraints.

During a load flow calculation at time step t, the difference between the tap ratio at time t, $n_{k,j,t}$, and $t-1$, $n_{k,j,t-1}$ needs to be as small as possible while keeping the voltage within a given range(see Fig. 3.1). Let this difference be the tap step taken at time t i.e. $W_{k,j,t}$, which can assume positive or negative value. Thus the load flow calculation at each time step, t, can be formulated as an optimization problem with the objective function to minimize the number of tap changes at each time step t:

$$\min_{W} O_t := \sum_{k}\sum_{j} W_{k,j,t}^2 \tag{3.1}$$

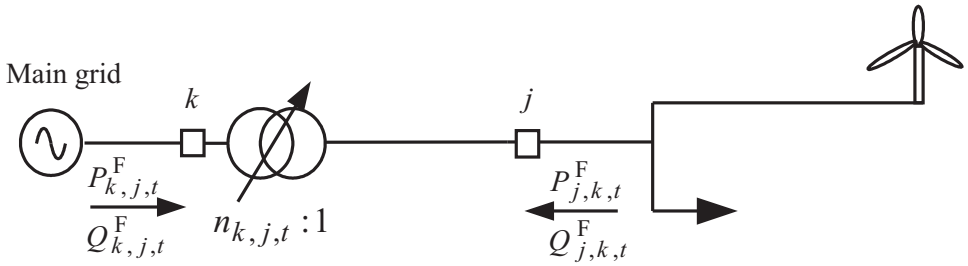

Figure 3.1: A simple distribution network with wind power and load connected.

where

$k \in K$
K set of all buses excluding the buses connected to the non tap side of the transformer
$j \in J$
J set of all buses excluding the buses connected to the tap side of a transformer.

Subject to equality and inequality constraints described as follows.

3.2.1.1 The inequality constraints

The inequality constraints include:

- The limit on secondary side voltage of the transformer,

$$V_k^{\min} \leq V_{k,t} \leq V_k^{\max} \tag{3.2}$$

where

$V_{k,t}$ voltage magnitude at node k and time t
$V_k^{\min}$ the lower voltage limit of the tap changer
$V_k^{\max}$ the upper voltage limit of the tap changer

- The limit on the available range of tap ratio,

$$n_{k,j}^{\min} \leq n_{k,j,t} \leq n_{k,j}^{\max} \tag{3.3}$$

where $n_{k,j}^{\min}$ and $n_{k,j}^{\max}$ are the maximum and minimum tap ratios that the tap changer can attain.

- The limit on the available active and reactive power of generators at each node in the network,

$$\begin{aligned} P_{i,t}^{\min} &\leq P_{i,t} \leq P_{i,t}^{\max} \\ Q_{i,t}^{\min} &\leq Q_{i,t} \leq Q_{i,t}^{\max} \end{aligned} \tag{3.4}$$

where

$P_{i,t}$ active power produced at bus i and time t
$P_{i,t}^{\max}$ maximum value of active power production at bus i and time t
$P_{i,t}^{\min}$ minimum value of active power production at bus i and time t
$Q_{i,t}$ reactive power produced at bus i and time t
$Q_{i,t}^{\max}$ maximum available values of reactive power at bus i and time t
$Q_{i,t}^{\min}$ minimum available values of reactive power at bus i and time t
$i \in I$
I a set containing all buses in the network

In the case study, it is only at the slack bus (infinite grid) that the active and reactive power is produced. Hence $P_{j,t}$ and $Q_{j,t}$ is limited to zero at all buses except the slack bus. Wind power generation is included into the load flow equations as a negative load with unity power factor.

3.2.1.2 Equality constraints

The equality constraints consist of:

- The load flow equations,

$$\begin{aligned} P_{i,t} - P^{\mathrm{D}}_{i,t} &= \sum_{u} Y_{i,u} V_{i,t} V_{u,t} \cos(\theta_{i,u} + \delta_{u,t} - \delta_{i,t}) \\ Q_{i,t} - Q^{\mathrm{D}}_{i,t} &= -\sum_{u} Y_{i,u} V_{i,t} V_{u,t} \sin(\theta_{i,u} + \delta_{u,t} - \delta_{i,t}) \end{aligned} \tag{3.5}$$

  where

  $P^{\mathrm{D}}_{i,t}$ active power consumed at bus i and time t
  $Q^{\mathrm{D}}_{i,t}$ reactive power consumed at bus i and time t
  $Y_{i,u}$ magnitude of the $(i,u)^{th}$ element of the bus admittance matrix
  $\theta_{i,u}$ angle of the $(i,u)^{th}$ element of the bus admittance matrix
  $\delta_{i,t}$ voltage angle at node i and time t
  $u \in I$

- The relation between consecutive tap ratios,

$$n_{k,j,t} = n_{k,j,t-1} + W_{k,j,t} \Delta V \tag{3.6}$$

  where ΔV is voltage change in per unit value for one tap step.

In the load flow equations the tap ratio of the transformer may change from one time step to another. This tap change affects three elements of the admittance matrix, which increases the number of variables in the model. Clearly, this imposes an extra computational burden on the simulation. Hence the load flow equations in (3.5) are modified so that they do not use the bus admittance matrix directly. The discussion of these modified load flow equations is provided as follows.

3.2.1.3 Modified load flow equations

The link between two buses is usually either a power line or a transformer. The power line can be represented by an equivalent π-model as shown in Fig. 3.2.

A transformer between two buses is represented by the equivalent π-model shown in Fig. 3.3

Hence, for the network which contains both of these elements, i.e. power lines and transformers, the link between any two buses can be represented as in Fig. 3.4.

The active $P^{\mathrm{F}}_{k,j,t}$ and reactive $Q^{\mathrm{F}}_{k,j,t}$ power flow from bus k to any other bus j at time t is given by

$$\begin{aligned} P^{\mathrm{F}}_{k,j,t} &= \left(\frac{V_{k,t}}{n_{k,j,t}}\right)^2 g_{k,j} - \frac{V_{k,t} V_{j,t}}{n_{k,j,t}} y_{k,j} \cos(\delta_{j,t} - \delta_{k,t} + \varphi_{k,j}) \\ Q^{\mathrm{F}}_{k,j,t} &= -V^2_{k,t} \left(\frac{b_{k,j}}{n^2_{k,j,t}} + \frac{b^c_{k,j}}{2}\right) + \frac{V_{k,t} V_{j,t}}{n_{k,j,t}} y_{k,j} \sin(\delta_{j,t} - \delta_{k,t} + \varphi_{k,j}) \end{aligned} \tag{3.7}$$

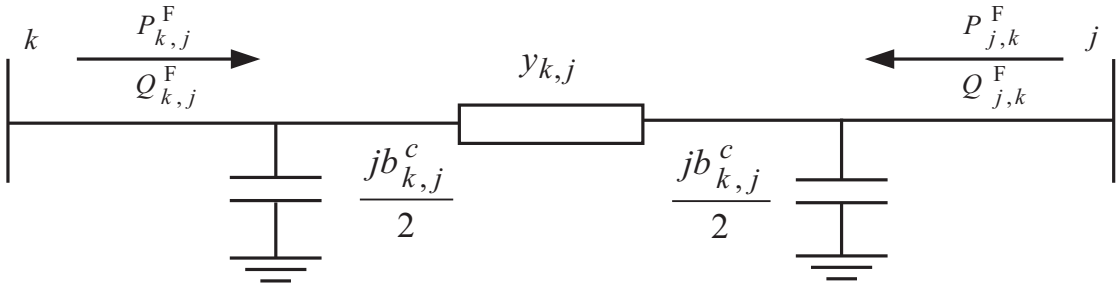

Figure 3.2: π-model of a power line.

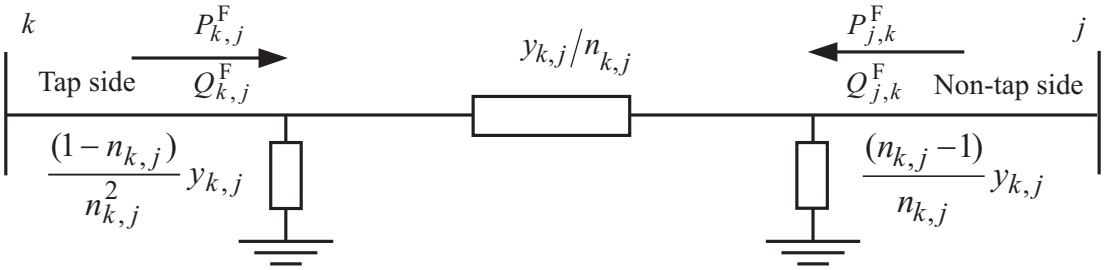

Figure 3.3: Equivalent circuit of a tap changing transformer [68].

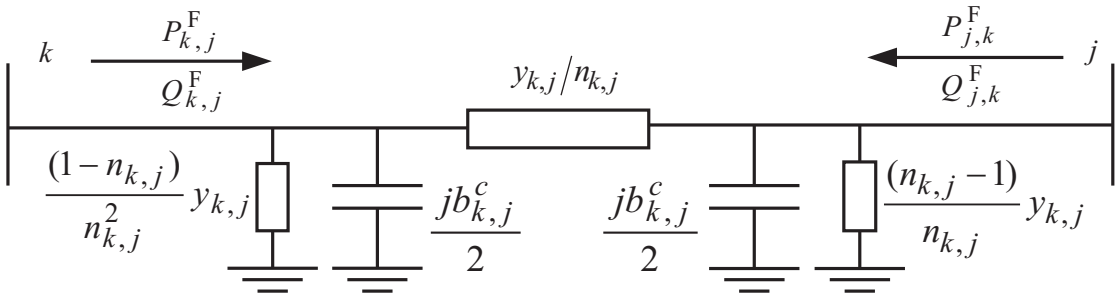

Figure 3.4: An equivalent model for a link between any two nodes.

where

$b_{k,j}$ series susceptance between bus k and bus j
$b^{c}_{k,j}$ shunt susceptance between bus k and bus j
$g_{k,j}$ series conductance between bus k and bus j
$y_{i,u}$ series admittance between bus i and bus u
$\varphi_{k,j}$ angle of the series admittance between bus k and bus j

and the reverse flow from bus j to bus k is given by

$$\begin{aligned} P^{F}_{j,k,t} &= V^{2}_{j,t} g_{j,k} - \frac{V_{j,t} V_{k,t}}{n_{k,j,t}} y_{j,k} \cos(\delta_{k,t} - \delta_{j,t} + \varphi_{k,j}) \\ Q^{F}_{j,k,t} &= -V^{2}_{j,t} \left(b_{j,k} + \frac{b^{c}_{j,k}}{2} \right) + \frac{V_{j,t} V_{k,t}}{n_{k,j,t}} y_{j,k} \sin(\delta_{k,t} - \delta_{j,t} + \varphi_{k,j}) \end{aligned} \tag{3.8}$$

In (3.7) and (3.8), if the link between two buses is a cable or overhead line, the tap ratio is one and the equations will represent the power flow in the circuit shown in Fig. 3.2. On the other hand, if

the link between two buses is a transformer, the shunt capacitance is equal to zero. Then (3.7) and (3.8) represent the power flow in the circuit shown in Fig. 3.3.

Now the load flow equations in (3.5) are replaced by (3.9) and (3.10) below as equality constraints. For bus in $k \in K$:

$$\begin{aligned} P_{k,t} - P^{\mathrm{D}}_{k,t} &= \sum_j P^{\mathrm{F}}_{k,j,t} \\ Q_{k,t} - Q^{\mathrm{D}}_{k,t} &= \sum_j Q^{\mathrm{F}}_{k,j,t} \end{aligned} \tag{3.9}$$

For bus $j \in J$:

$$\begin{aligned} P_{j,t} - P^{\mathrm{D}}_{j,t} &= \sum_k P^{\mathrm{F}}_{j,k,t} \\ Q_{j,t} - Q^{\mathrm{D}}_{j,t} &= \sum_k Q^{\mathrm{F}}_{j,k,t} \end{aligned} \tag{3.10}$$

Equations (3.7) - (3.10) do not contain the variable bus admittance matrix. In other words, there will be only one variable for a single tap change as opposed to four that would be in (3.5). With the reduction in the number of variables, there will be a reduced computational effort.

3.2.2 Modeling the use of reactive power compensation to decrease the frequency of tap changes

In this section we develop the model used for analyzing the use of reactive power from the wind turbines to decrease the FTC.

3.2.2.1 The objective function

When there is a continuously controllable reactive power from wind turbines, it can be used to decrease the FTC. In principle, for a transformer where the tap is located on the primary side, reactive power is consumed to avoid a tap increase during low load condition and produced to avoid a tap decrease during high load condition. However reactive power is not consumed or produced when there is no potential tap change or the available reactive power is not sufficient to prevent a tap change. In the latter case, it is better to use tap regulation directly as unnecessary reactive power flow increases system power losses. In order to model this, the objective function is modified to

$$\min_{W,Q} O_t := \sum_k \sum_j a W^2_{k,j,t} + \sum_i Q^2_{i,t} \tag{3.11}$$

The term on the far right side is added to produce or consume as minimum amount of reactive power as possible from the wind turbines. On the other hand a is a constant of sufficiently large value added to prioritize using RPC, whenever possible, instead of tap changing.

3.2.2.2 The constraints

The equality constraints discussed in (3.6), (3.9), (3.10) and the inequality constraints discussed in (3.2), (3.3) holds true here as well.

The reactive power limits, $Q_{i,t}^{\min}$ and $Q_{i,t}^{\max}$ in (3.4), can be defined in terms of a given minimum operating power factor limit, $\Phi^{\min}$. These limits can also be constrained by the thermal capability of the wind turbine, $S_i^{\max}$. This happens when the wind turbines are operating around the rated power output. Hence for a given wind turbine at bus i, the reactive power limits are given by

$$-Q_{i,t}^{\text{cap}} \leq Q_{i,t} \leq Q_{i,t}^{\text{cap}} \tag{3.12}$$

where

$$Q_{i,t}^{\text{cap}} = \min\left(\sqrt{\left(S_i^{\max}\right)^2 - P_{i,t}^2}, \frac{P_{i,t}\sqrt{(1-(\Phi^{\min})^2)}}{\Phi^{\min}}\right) \tag{3.13}$$

In case $\Phi^{\min}$ is extended to zero, i.e. when the wind turbines are providing reactive power support even when they are not producing active power, (3.12) and (3.13) can be reduced to

$$-\sqrt{\left(S_i^{\max}\right)^2 - P_{i,t}^2} \leq Q_{i,t} \leq \sqrt{\left(S_i^{\max}\right)^2 - P_{i,t}^2} \tag{3.14}$$

3.2.3 The flow chart of the proposed sequential load flow simulation

The model formulated in this paper is to be used in a radial distribution system where there are usually one or two transformers in parallel. Under such condition the binary variable, $W_{k,j,t}$, can be replaced by a continuous variable, $W'_{k,j,t}$, and (3.15) can be used to calculate $W_{k,j,t}$. This results in a model which can be solved more efficiently using solvers developed for standard nonlinear programs, e.g. [69]. However whenever this model is used in networks where there are a couple of tap changing transformers at different locations there could be an optimality problem. Hence under such situation the problem should be solved as mixed integer nonlinear programming model (MINLP).

$$W_{k,j,t} = \begin{cases} \text{round}(W'_{k,j,t}), & \text{if} \quad \left|W'_{k,j,t}\right| \leq \varepsilon \\ \text{ceil}(W'_{k,j,t}), & \text{if} \quad W'_{k,j,t} > \varepsilon \\ \text{floor}(W'_{k,j,t}), & \text{if} \quad W'_{k,j,t} < -\varepsilon \end{cases} \tag{3.15}$$

where ε is a very low value chosen based on the sensitivity of the tap operating system.

The flow chart of the overall simulation is presented in Fig. 3.5.

3.3 Case Study

3.3.1 Network and data description

The case study is based on a rural 11 kV network operated by Falbygdens Energi located in Falköping area in Sweden. The network is fed by a 40 kV grid through a 10 MVA $45\pm8\times1.67\%/11.5$ kV transformer with a percentage impedance of 8%. The tap changer regulates the voltage at the

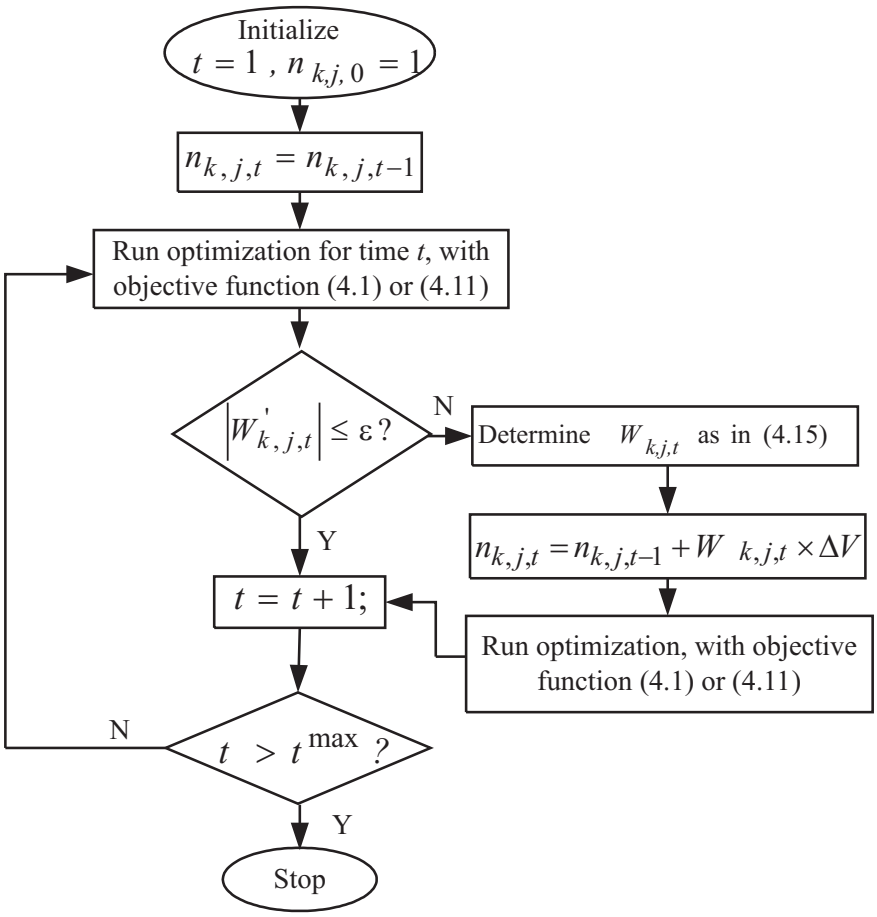

Figure 3.5: The flow chart of the proposed sequential load flow simulation.

secondary side of the transformer with the set point voltage of 10.7 kV and a $\pm$1.2% deadband. In this distribution system, there are 13 wind turbines (composed of Type A, B, and D) installed, with an overall installed capacity of 12.225 MW. From these wind turbines there are hourly measured time series power data available for one year, i.e. 2011. Hourly measured active and reactive power data at the substation are also available for the same year. Active power consumption in the network is then calculated by adding the measured wind power data and active power measurement at the substation. Currently the wind turbines operate at unity power factor (PF) setting, thus the reactive power is assumed to come from consumer loads only.

3.3.2 Effect of wind power on frequency of tap changes

The aim here is to find out if wind power may lead to an increase in the FTC. Thus, no RPC from the wind turbines is considered.

With the data described in the above subsection, the mathematical model developed in Section 3.2 is implemented in GAMS. Two cases are investigated:

- Case 1: only consumer load is assumed to be connected to the network without wind power in the system.

- Case 2: both load and wind power are connected to the system. This is the existing system condition.

Fig. 3.6 shows the number of tap changes at each hour of a day summed over one year. It can

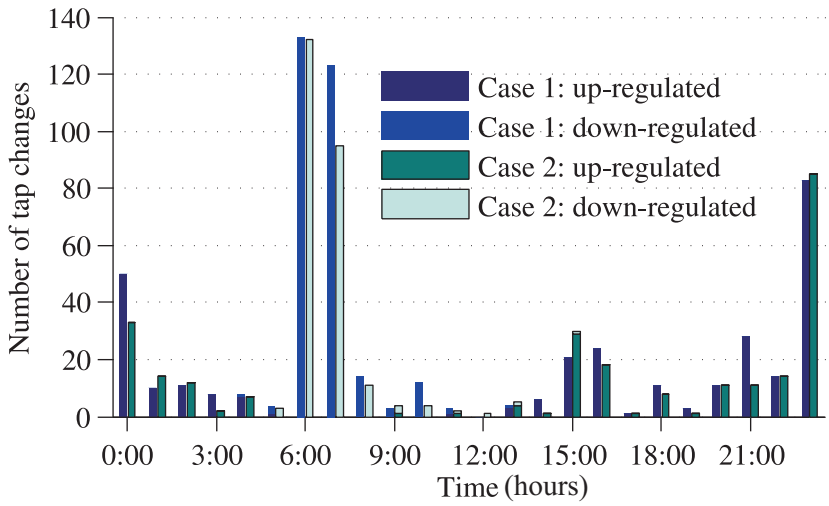

Figure 3.6: Number of tap changes on each hour of a day summed over a year.

be seen that for both cases, the diurnal variation of tap changes follows a similar trend: with a large number of tap changes at 6:00 and 7:00 in the morning and at 23:00 and 0:00 during the night. There are also considerable tap changes at 15:00 and 16:00. Usually the tap changes in the morning (specifically between 5:00 and 10:00) are down regulations to boost the voltage on the secondary side. During this period, the load increases due to the start up of a factory, connected to this distribution system, and residential loads. During the rest of the day, the tap is usually up-regulated due to the dominance of lighter load conditions than in the morning. The total number of tap changes for Case 1 is 585 and for Case 2 is 505 for one year of operation. Thus, in contrary to our expectation, the FTC has decreased when there is wind power in the distribution system. The reason for the decrease in number of tap changes is explained using Fig. 3.7 and Fig. 3.8.

Fig. 3.7 shows the load and wind power profile for a specific day and Fig. 3.8 shows the tap positions of the tap changer in the same day. It can be seen in Fig. 3.8 that between the period 5:00 and 16:00, there are three tap changes in Case 1 compared to a single tap change in Case 2 (see Fig. 3.8). From Fig. 3.7, one can make two observations. On one hand, the variability of load follows the variability of wind power. These results in a less variable net active power. On the other hand, during part of this period (for example between 14:00 and 20:00) when the net active power increases, the reactive power decreases and vice versa. This, according to (3.16) [70], results in a lower voltage change on the secondary side of the transformer compared to Case 1.

$$\Delta V_t \approx RP_{2,t} + XQ_{2,t} \tag{3.16}$$

where

ΔV_t voltage difference between reference node '1' (infinite bus) $V_{1,t}$ and node '2' (secondary side of the transformer) $V_{2,t}$
$P_{2,t}$ active power consumed at node '2'
$Q_{2,t}$ reactive power consumed at node '2'
R resistance between node '1' and '2'
X reactance between node '1' and '2'

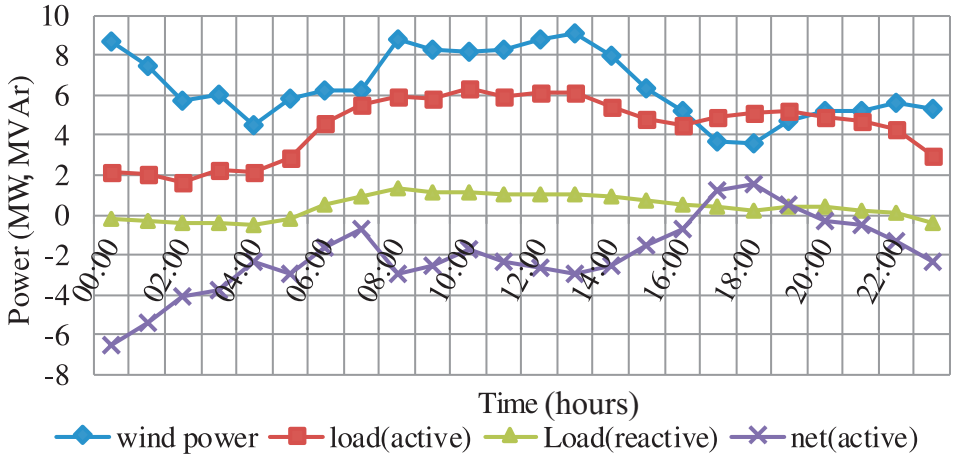

Figure 3.7: Load and wind power profile at specific day of the year.

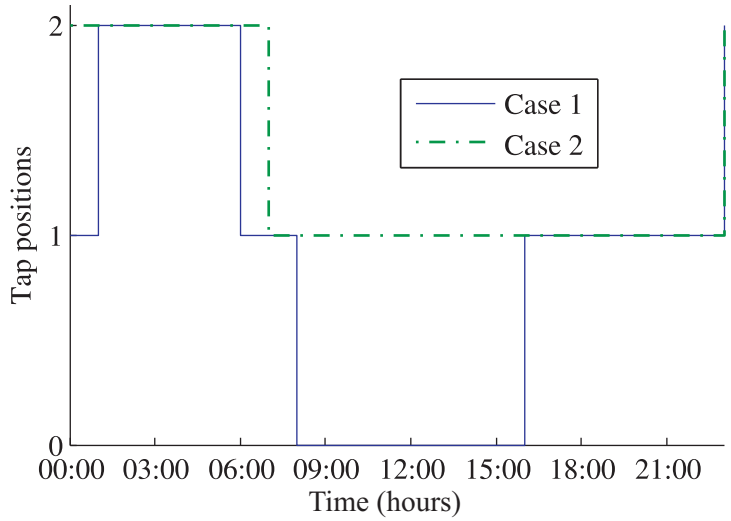

Figure 3.8: Tap position of the tap changer at specific day of the year.

Moreover wind power causes fluctuation mostly in active power. Fluctuations in active power, according to (3.16), will not lead to significant voltage fluctuations when the X/R ratio of the external grid is high.

In Fig. 3.7 and Fig. 3.8, the aim is to show how wind power can contribute to a decrease in the number of tap changes in some days. But wind power do also contribute to an increase in the number of tap changes on some other days. However, in this case, wind power has led to a reduction in the total number of tap changes.

Seasonal variations in the number of tap changes is compared in Fig. 3.9. The figure shows that the effect of wind power on FTC changes from one month to another. Though the FTC has decreased in most of the months, there are also months where the FTC has increased because of the wind power. Thus, an analysis based on only one month data, as it has been done in [67], cannot give the true picture of the effect of wind power on the FTC.

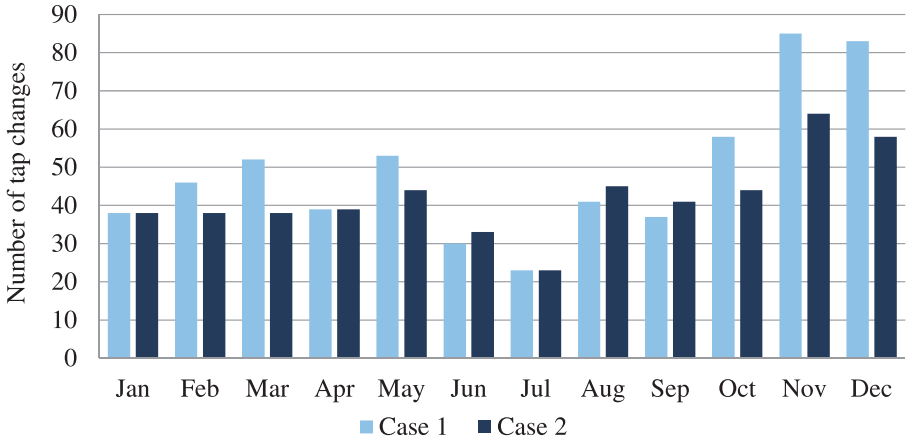

Figure 3.9: Number of tap changes distributed on monthly basis

3.3.3 Analyzing the frequency of tap changes with a different set of wind power data

In the Section 3.3.2, the analysis of the effect of wind power on the FTC is done based on a particular set of data. To test the validity of the observation made in the previous section, an analysis based on different sets of data may be required. To this end, an analysis is done using a number of synthetic data (WPs1-WPs5 in Fig. 3.10) and one more measurement data (WPm), both having a capacity of around 8 MW. The synthetic data is generated using the stochastic model of wind power proposed in [71]. The load data, on the other hand, is kept the same as the one used in Section 3.3.2. This is valid since, though the details of the data could be different from year to year, the general profile of a load data will remain almost the same from one year to another.

As shown in Fig. 3.10, the FTC with the new wind data lays between 549 and 573 which is still below the number tap changes that occur when there is no wind power. But one can observe that compared to the FTC with the original wind power of the same size (WPo) (i.e. 509), there is an increase by around 10%. These increase is not significant, and it can partly be attributed to the reduction in correlation between the load data and the new wind power data compared to the original one.

3.3.4 The frequency of tap changes with different reference voltage at the secondary side of the substation transformer

The discussion up to this point shows wind power contributing to the reduction in FTC. To test if this also holds for some other case, the FTC problem is simulated with different reference voltages

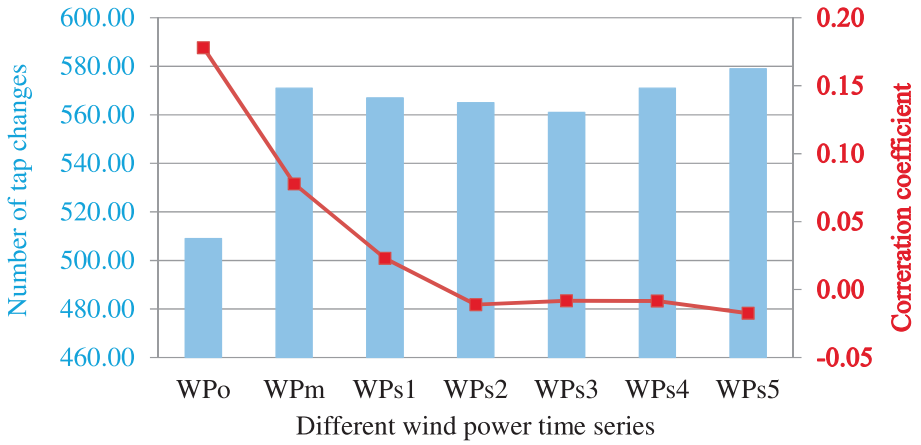

Figure 3.10: Number of tap changes with different wind power time series data

at the secondary side of the transformer for varying levels of wind power. The argument is that if the introduction of wind power should decrease the FTC, it would do so irrespective of the voltage set point. The result of the analysis (presented in Fig. 3.11) shows that wind power does not necessarily lead to a decrease in the FTC. However in general the increase in FTC due to wind power is insignificant for the distribution system studied so far. Thus, wind power in such distribution systems does not pose a reliability concern to the transformer tap changers.

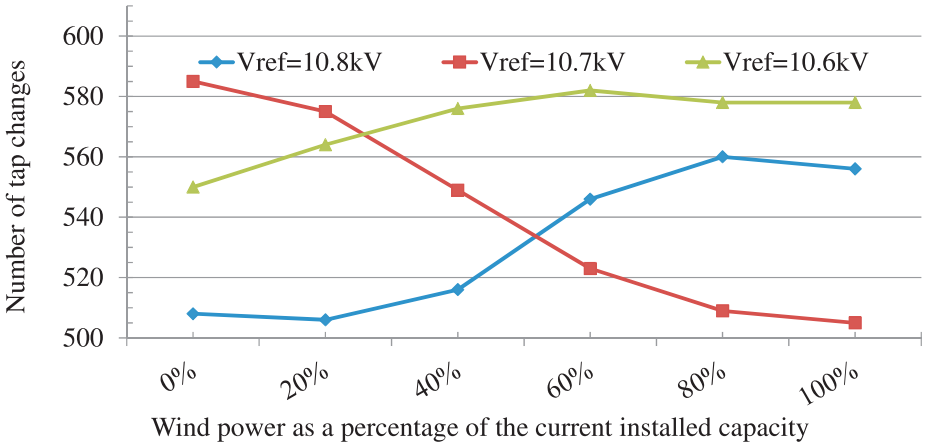

Figure 3.11: The frequency of tap changes for varying level of wind power and different voltage set point.

3.3.5 The frequency of tap changes for varying levels of grid strength

The analysis in the previous sections is done assuming the short circuit capacity (SCC) and the X/R ratio of the external grid to be 171 MVA and 10 respectively. For this distribution system, it is seen that wind power does not pose a significant threat to the FTC. In fact, it may reduce the FTC. In this subsection the same investigation is done for grids with different SCCs and with varying X/R ratios.

Fig. 3.12 shows the trend in FTC as the power penetration level increases for grids with different SCC. The figure shows that, overall, the FTC increases with decrease in SCC. This is understand-

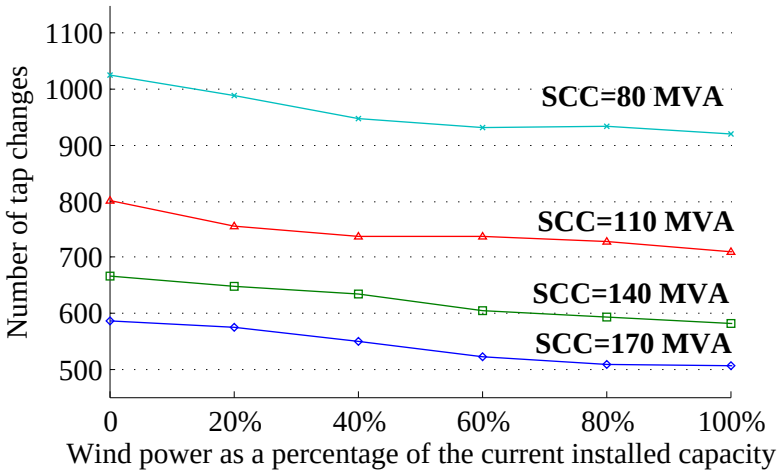

Figure 3.12: Number of tap changes per year for different SCC of external grid with X/R=10.

able as a higher impedance leads to a higher voltage drop for a given loading condition. In other words, for the same variation of transformer loading, the voltage variation will become larger in a weaker grid.

Though the curves in Fig. 3.12 show a general decrease in FTC with an increase in the capacity of wind power, we have noted above using Fig. 3.11 that wind power does not always lead to a decrease in FTC. However, the similarity in the profile of the curves in Fig. 3.12 can be explained as follows.

A tap change occurs when there is a voltage change at the secondary side of a transformer due to a change in power flow. Hence one can roughly approximate the FTC to be proportional to the voltage change that occurs at each time step t due to power flow changes. In the absence of wind power in the system, the change in voltage at the secondary side of the transformer due to load flow changes is given by (3.16). In the presence of wind power in the system, there is additional fluctuations in active power; this fluctuation causes an additional voltage fluctuation at the secondary side of the transformer which can be given by (3.17). The percentage change in voltage change at the secondary side of the transformer can, thus, be given by (3.18). Since the FTC is proportional to the voltage change at the transformer secondary, (3.19) follows from (3.18).

$$\Delta V_{2,t} \approx \Delta P_{2,t} \times R \tag{3.17}$$

where

$\Delta V_{2,t}$ the change in voltage at node '2' relative to the previous value
$\Delta P_{2,t}$ the change in active power consumption at node '2' due to the wind power

$$\frac{\Delta V_{2,t}}{\Delta V_t} = \frac{\Delta P_{2,t}}{P_{2,t} + Q_{2,t} \times \left(X/R\right)} \times 100\% \tag{3.18}$$

and

$$\Delta FTC \propto \frac{\Delta P_{2,t}}{P_{2,t} + Q_{2,t} \times \left(X/R\right)} \times 100\% \tag{3.19}$$

Equation (3.19) implies that the percentage change in FTC, ΔFTC, is proportional to the X/R ratio and is constant for a given X/R ratio irrespective of the SCC of the grid. However the tap change does not only depend on the voltage change at the secondary side of the transformer but also whether the resulting voltage will be outside of the deadband. Hence based on (3.19) one can only roughly expect the implications to hold. Fig. 3.12 proves the same.

The above analysis shows that for an X/R ratio of 10 no significant increase in the FTC is expected due to introduction of wind power operating at unity power factor. Fig. 3.13 provides the results of the analysis with different X/R ratios. The results show that when the X/R ratio gets lower the effect of wind power on the FTC changes becomes considerable. This is clear from (3.19) that for a given active power change, the lower the X/R ratio the bigger is the change in FTC.

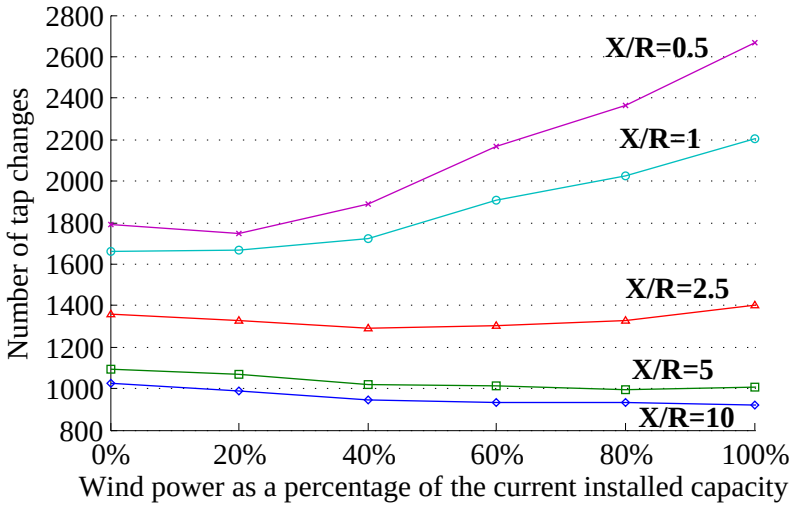

Figure 3.13: Number of tap changes per year in a distribution system connected to 80 MVA external grid having different X/R ratio.

The results presented in Figs. 3.12- 3.13 are based on assuming a wind farm directly connected to the substation, i.e. without any connecting cable in-between. However, almost similar results are observed even when there is a cable or an overhead line connecting the wind power plant to the substation, as shown in Fig. 3.14. The results in the figure compares the FTC with a wind farm located at different distances from substation and connected to the station through different cable types; the external grid here is assumed to have a SCC of 80 MVA with X/R ratio of 5.

Based on the analysis so far, it can be concluded that for distribution networks with an X/R ratio greater than 5, wind power operating at unity power factor does not cause a reliability concern for the tap changers. But for distribution networks with an X/R ratio less than 5, there could be some problems of increase in FTC due to wind power introduction. This is especially true for those grids with an X/R ratio less than 2.5.

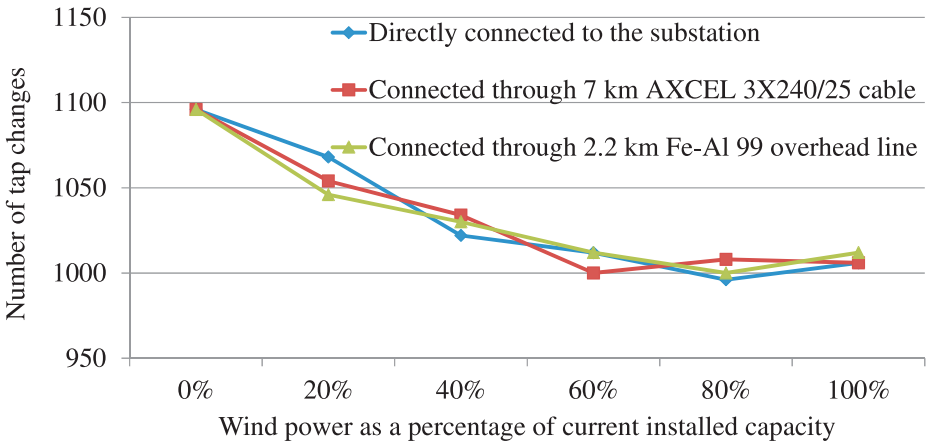

Figure 3.14: Comparing the FTC when the wind power is at varying distance from the substation

3.3.6 The effect on FTC when wind turbines consume reactive power

This section investigates the effect on FTC of wind power operating at a power factor other than unity. This situation may arise when the wind turbines connected to the distribution system are of Type A or B, which cannot provide a controllable reactive power support. As shown in Fig. 3.15, when the wind turbines operate at a PF other than unity there is a considerable increase in the FTC. Of course, the closer the PF to unity is, the lower is the increase in FTC due to wind power. Some DFIG wind turbines work at around 0.99 PF lagging and such operation is not seen to increase the FTC considerably. Hence in distribution system where there is a concern on the number of tap changes, it is necessary to make sure that only wind turbines that are able to operate at or close to unity power factor are being installed.

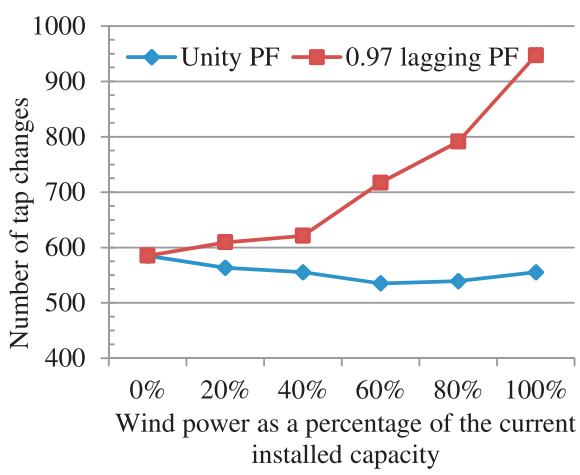

(a) SCC=170 MVA & X/R=10

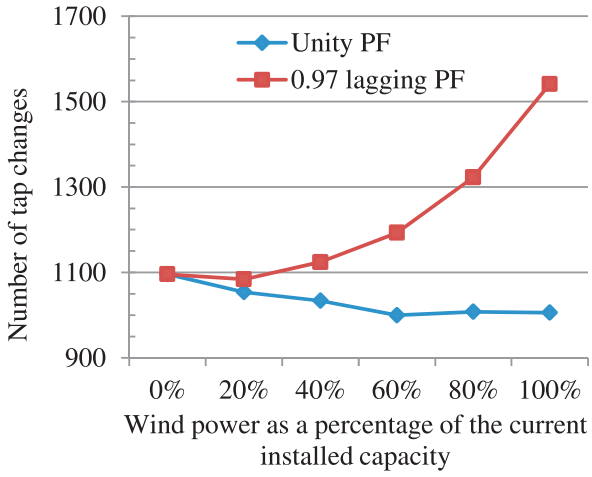

(b) SCC=80 MVA & X/R=5

Figure 3.15: The effect on FTC of wind turbines working at power factor other than unity

3.3.7 Using reactive power compensation to reduce the number of tap changes

This section investigates the use of reactive power from wind turbines to decrease the FTC. The need for reducing the FTC may arise due to the existence of a high level of FTC induced by load changes. It can also be induced by a high level of wind power for the reasons mentioned in Subsections 3.3.5 and 3.3.6. The current practice for decreasing the FTC in such conditions is to increase the deadband of the tap changer, say from 1.2% to 1.6% or more. However this solution may pose voltage quality problems.

Among the available wind turbines in the network (described in Section 3.3.1), a wind farm composed of four 0.8 MW wind turbines is chosen to provide reactive power support to the grid. These wind turbines are of the variable speed design (full converter based) from Enercon and are recently installed at a site close to the substation. Since these wind turbines have started their production as of March 2011, the wind power and load data starting from march 2011 are used for this analysis. The wind power from the rest of the wind turbines is aggregated with the load. The simplified diagram of the resulting system is shown in Fig. 3.16.

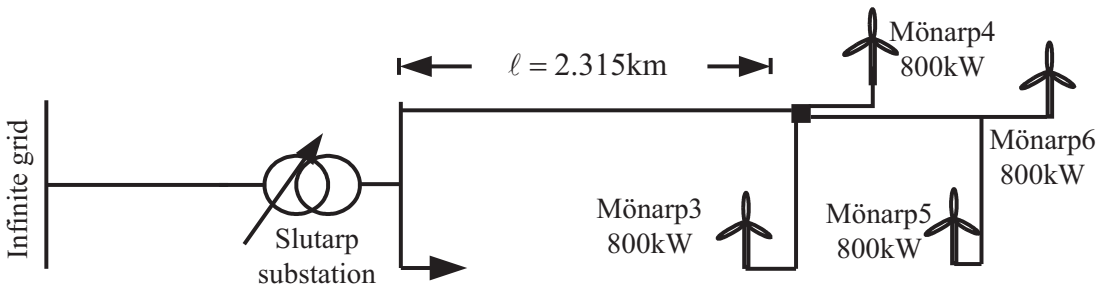

Figure 3.16: Simplified diagram of the 10 kV distribution network.

The majority of grid codes require that wind turbines should have a capability of operating between 0.95 PF lagging and leading at full production [72]. This indicates that, for these wind turbines, the rated power of the converter should be at least five percent higher than the full power output of the wind turbines. Hence $S_i^{\max}$, for each wind turbine, is taken to be five percent higher than the rated power output.

Fig. 3.17 compares the number of tap changes with and without RPC when the wind turbines are controlled to operate between 0.95 lagging and leading power factor so as to avoid a tap change whenever possible. The figure shows a decrease in the FTC by 21%. Reactive power is consumed at light load or at windy conditions when there is a potential tap up-regulation. This brings down the voltage at the substation busbar and avoids an up-regulation of the tap. Reactive power is supplied to boost the voltage during high loading condition to avoid a potential tap down-regulation. In this way, reactive power contributes to the reduction in the number of tap changes. One can also notice that RPC sometimes only delays a tap change to a later time. This is seen in Fig. 3.17 when the number of tap changes decreases at 23:00 while the number of tap changes increases at 00:00. However, this delay of tap changes does not appear to be a significant issue.

Table 3.1 summarizes the main points that can be used in the comparative analysis of using RPC to reduce the FTC. It also includes results from some more scenario analysis. The results in Table 3.1 are for a grid with SCC=171 MVA and X/R=10. Table 3.2 provides the results of the

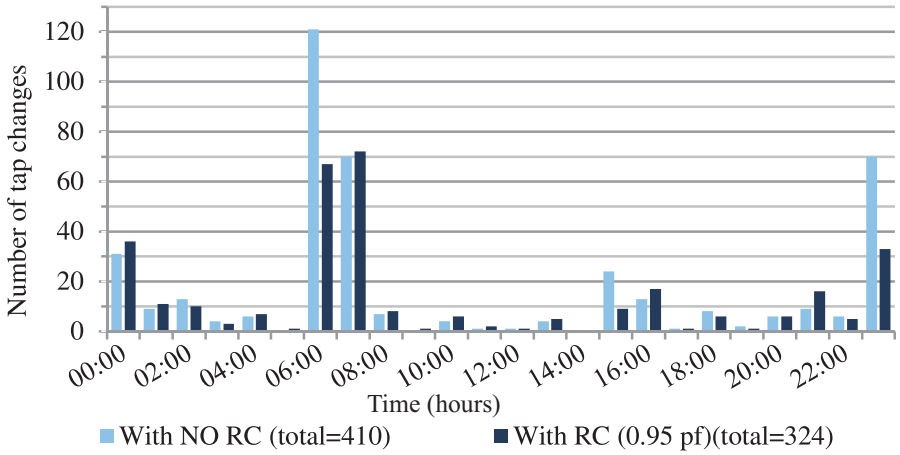

Figure 3.17: Number of tap changes on 24hr basis with and without RPC.

same analysis for a weaker grid having SCC=80 MVA and X/R=1. Moreover in Table 3.1 and 3.2, the wind turbines are located 2.3 km from the substation. On the other hand, Table 3.3 provides the results of the same analysis for wind turbines located 15 km from the substation. The analysis with longer distance is used to see if the magnitude of the impedance between the wind farm and the substation has some effect on the proposed solution. Over all, the results provided in Table 3.1-3.3 shows that RPC can be used for reducing the FTC in most grids.

Table 3.1: Effect of using RPC to reduce the FTC in a distribution system connected to a stronger grid (SCC=171 MVA,X/R=10)

Case	Φ^{min}	**Change in the FTC (ΔFTC)**		**Average power Loss (kW)**	**reactive power from the wind turbines**	
		ΔFTC	%ΔFTC		Average (kVAr)	Maximum (MVAr)
1	1	0	0	16	0	0
2	0.95	-86	-21	16	15	0.7
3	0.90	-124	-30	16	25	0.9
4	0.80	-166	-40	16	36	1.0
5	0.0	-410	-100	14	176	1.0

Table 3.2: Effect of using RPC to reduce the FTC in a distribution system connected to a weaker grid (SCC=80 MVA and X/R=1)

Case	Φ^{min}	**Change in the FTC (ΔFTC)**		**Average power Loss (kW)**	**reactive power from the wind turbines**	
		ΔFTC	%ΔFTC		Average (kVAr)	Maximum (MVAr)
1	1	0	0	86	0	0
2	0.95	-394	-22	85	33	1.0
3	0.90	-502	-28	85	64	1.4
4	0.80	-663	-37	85	121	2.0
5	0.0	-1 738	-97	91	724	3.4

In terms of achieving a specific level of reduction in the FTC, the distance of wind turbines from

Table 3.3: RPC from wind turbines located 15 km away from the substation (SCC=171 MVA,X/R=10)

Case	Φ^{min}	Change in the FTC (ΔFTC)		Average power Loss (kW)	reactive power from the wind turbines	
		ΔFTC	%ΔFTC		Average (kVAr)	Maximum (MVAr)
1	1	0	0	28	0	0
2	0.95	-90	-22	28	16	0.8
3	0.90	-120	-29	28	25	1.0
4	0.80	-166	-40	28	36	1.0
5	0.0	-416	-100	27	176	1.0

the substation has no effect at all. That is, almost the same amount of reactive power is necessary to achieve the same level of reduction in the FTC. Thus, the cable does not make any significant impact on the reactive power requirement from the wind turbines. However, compared to strong grids, in weak grids more reactive power is required from the wind turbines to achieve the same level of reduction in FTC. This is because, in weak grids, higher number of tap changes need to be avoided to achieve the same percentage of reduction in the FTC.

Generally, the change in the network loss relative to the base case (Case 1) is found to be negligible in all cases except in Case 5 of Table 3.2. This is apparent from the fact that, in this case, the network resistance is relatively large and the amount of reactive power consumed or produced by the wind turbines relatively high.

Finally, the analysis presented in this subsection is carried out assuming constant power loads, however similar results are obtained assuming constant impedance load.

3.3.7.1 Reactive power flow in the network

Here we compare the reactive power consumption in the network with and without RPC in the network to see if RPC would result in unfavorable grid operating conditions. The results of the analysis for Case 5 (worst case in terms of reactive power consumption) from Table 3.1 are presented here in Fig. 3.18 and Fig. 3.19. However similar results are observed for the analysis in Tables 3.2 and 3.3.

Fig. 3.18 shows that reactive power is consumed during light load or windy conditions and produced at heavy load conditions. From the point of the external grid, this is beneficial because during low load conditions the voltage in the power system is generally high due to the Ferranti effect, consuming reactive power will mitigate the voltage rise. During high loading condition the grid may approach its voltage stability and low voltage limit and providing local reactive power is vital to improve the voltage stability and level, respectively, of the system. Moreover, as shown in Fig. 3.19, the maximum amount of reactive power supplied from the external grid when RPC is used is not higher than the maximum value when the wind turbines are set to unity PF. However the average reactive power supplied from the external grid is generally higher when RPC is used.

The result presented in fig. 3.19 is for Case 5 where a 100% reduction in the number of tap changes is achieved. In other cases the change in reactive consumption or production from the base case(Case1) is even lower.

In Case 5, the total amount of reactive power used in achieving such a high level of reduction in

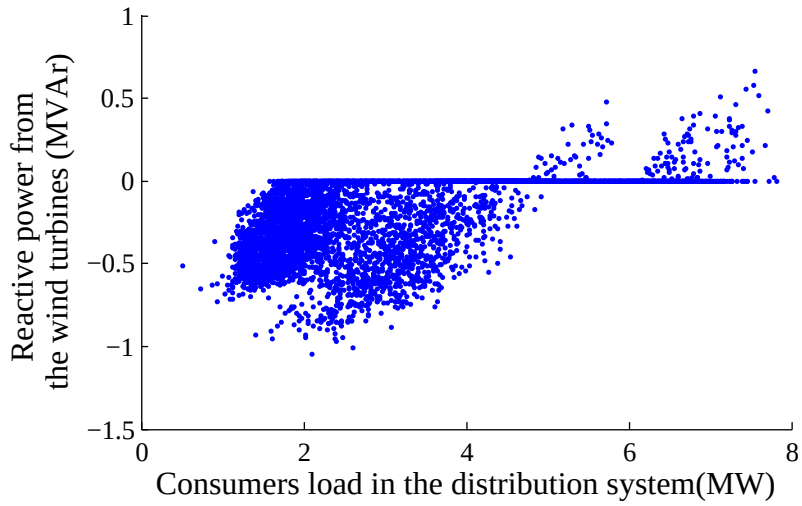

Figure 3.18: Reactive power production from the wind turbines as the function of the load in the system for Case 5

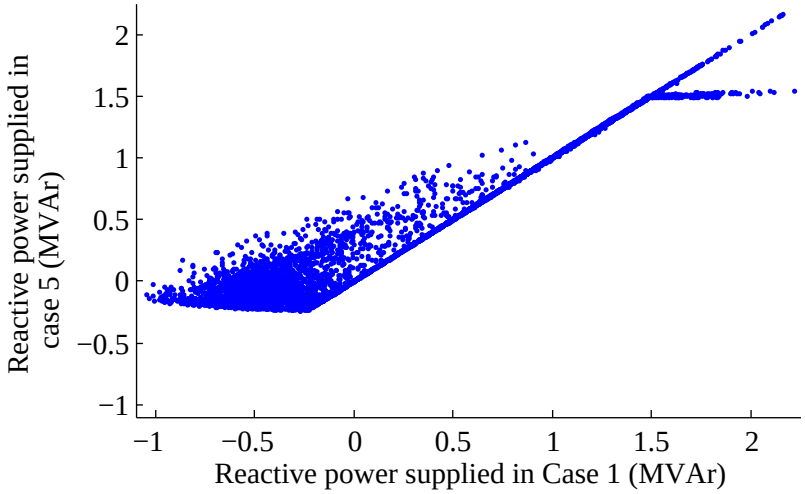

Figure 3.19: Comparison of reactive power supplied from the external grid

FTC depends on the initial tap position of the transformer. The initial tap position should be chosen such that it is in the middle of the tap positions the tap changer has ever operated at. This can be observed from the historical data. In the present case study the transformer is found to operate between the tap positions zero and two. Hence the reference (initial) tap position is chosen to be one. If the reference tap position is chosen to be zero, the average reactive power used from the wind turbines would have been above 700 kVAr. This is even without achieving 100% reduction in the number of tap changes. Moreover the loss could have been higher than the base case.

3.3.7.2 Voltage in the network

Due to a relatively high amount of reactive power consumed by the wind turbines, one may expect the voltage on wind turbine terminals to be below the acceptable level. Fig. 3.20 compares the voltage at the wind turbine terminals between the base case (Case 1) and Case 5 from Table 3.1.

On the contrary, the figure shows that the voltage at the wind turbine terminals remains within ±5% of the nominal (reference) voltage, 10.7kV. Moreover, on average, the voltage at wind turbine terminals are higher in Case 5 than in the base case. When reactive power is consumed to avoid a tap change, the voltage at the secondary side of the transformer is kept at the upper limit of the voltage deadband. This results in a voltage gain at terminals of the wind turbines. Even though there is voltage drop due to reactive power consumption, the overall effect is a general increase in voltage at the wind turbine terminals.

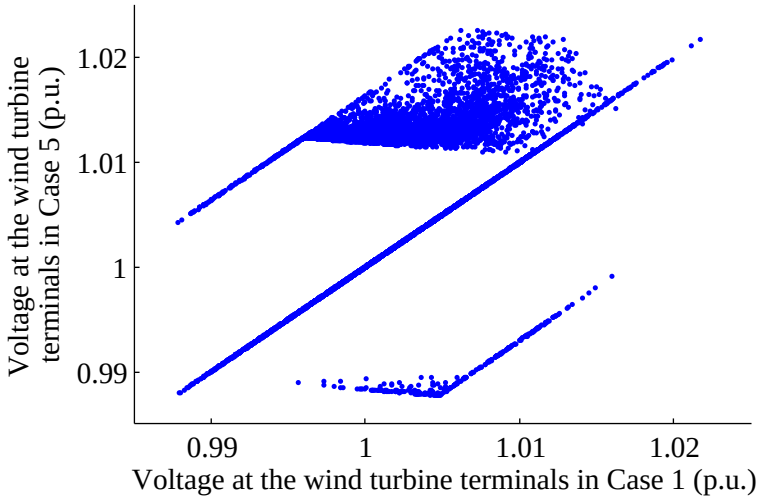

Figure 3.20: Comparison of distribution of voltage on the wind turbine terminals

Moreover, by using this voltage regulation strategy, it is possible to minimize the overvoltage that happens in the system due to the slow reaction time of the tap changers. This is especially of great importance if some other wind turbines in the system are tripped due to fault resulting in a sudden voltage drop in the system.

3.3.7.3 Effect of voltage set point on the effectiveness of reactive power compensation to reduce the number of tap changes

Though the voltage set point at the secondary side of the transformer may be chosen to provide customers with the appropriate voltage level, there is some degree of freedom in the choice. Here we see how the choice of the voltage set point at the secondary side of the transformer can affect the performance of RPC in reducing the FTC.

The voltage set point affects how the tap positions are distributed. For the case presented in Table 3.1, Fig. 3.21 shows the tap position distribution of the substation transformer for two different voltage set points at the secondary side of the transformer.

To totally eliminate the tap changes using RPC, naturally it is more effective to set the tap position at the median of the tap position distribution. The more evenly distributed the tap positions are around the median tap position, generally, the lower is the average reactive power demand from the wind turbines to avoid a tap change. In Fig. 3.21 the tap positions are more evenly distributed around the median when the reference voltage is 10.8 kV. If we compare the average reactive power requirement to avoid tap changes totally, we see that it is 176 kVAr with a 10.7 kV as a reference

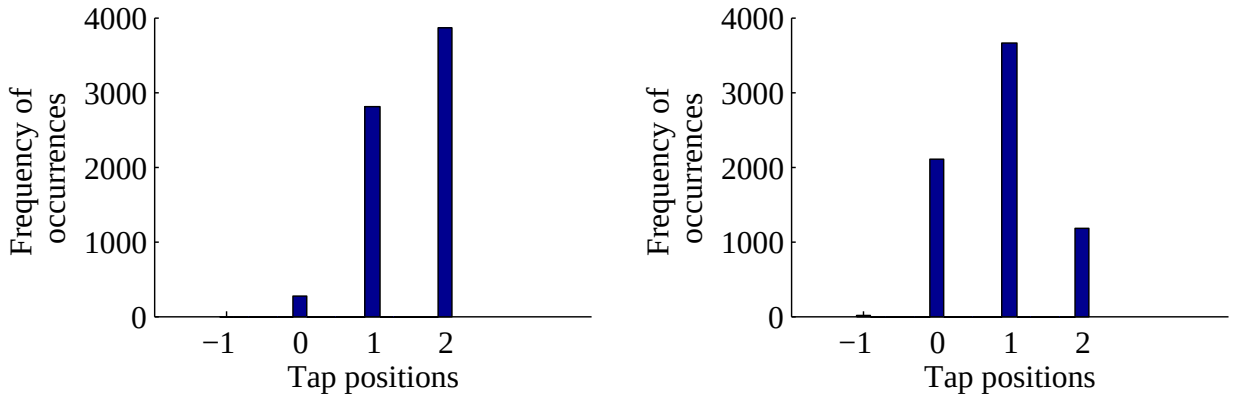

(a) 10.7 kV **(b)** 10.8 kV

Figure 3.21: Tap position distribution of the substation transformer for two different voltage set points:

voltage and 56 kVAr with 10.8 kV. Therefore, the RPC would be more effective if the reference voltage is set to 10.8 kV, showing that the reference voltage chosen can affect the effectiveness of the RPC. This also shows that the demand on reactive power from the wind farms depends on the reference voltage setting.

3.4 Summary

In this chapter an analysis of the effect of wind power on the frequency of tap changes (FTC) is carried out. In general, for distribution networks connected to external grids with $X/R \geq 5$, no significant effect on the FTC is seen due to introduction of wind power. However, in a distribution system connected to grids with a lower X/R ratio wind power can affect the FTC significantly as wind power penetration increases.

An analysis is done to decrease the FTC using reactive power compensation (RPC) from the wind turbines. Two types of distribution systems are considered: one connected to a relatively strong (SCC=171 MVA, X/R= 10) external grid and the other to a weak (SCC=80 MVA, X/R= 1) external grid. The results show that RPC can be used to effectively reduce the FTC in both cases. However, the reactive power required to reduce the FTC by a specific percent depends on the SCC and the X/R ratio. The reactive power requirement decreases with a higher SCC and X/R ratio.

A further investigation on RPC is carried out for wind farms located farther from the substation. However, the change in reactive power requirement and network loss is found to be only minor. Hence the RPC method is found to be effective even when wind farms are far away from the substation.

Finally the practical implementation of RPC to reduce the number of tap changes depends on the maintenance cost of the tap changers involved, the cost of reactive power from the wind turbines, and the change in power loss that occurs within the network due to RPC.

3. EFFECT OF WIND POWER ON FREQUENCY OF TAP CHANGES

4

Siting wind turbines in a distribution system

This chapter investigates the optimal siting of wind turbines or farms in a given distribution system. The chapter starts by presenting background knowledge to the optimal siting problem. Then, the siting problem is discussed with respect to the different integration issues of wind power discussed in Chapter 2. These include overvoltage, overloading, flicker, harmonics, increase in fault level as well as loss considerations.

4.1 Background

The location of a wind turbine or farm is mainly affected by the windiness and the accessibility of a given site. However, it is possible that the distribution system has a couple of sites with nearly the same average wind speed and it may be required to choose one or more sites among them for wind power installation. In this regard, extensive research effort has been devoted to the optimal siting and sizing distributed generations (DGs) [73–99]. The siting problem has been studied to achieve different objectives such as minimize loss reduction [73–80, 83–88, 91, 94, 95, 98, 99], maximize hosting capacity [82, 87, 92, 93], and reliability improvement [81, 83, 87]. Also different methodologies have been proposed to solve the problem. These include but not limited to genetic algorithm [73, 74, 78, 79, 82, 83, 87, 92, 95], particle swarm optimization (PSO) [75, 76, 80, 81, 85, 86, 94], analytical methods [77, 84, 90, 91, 99], fuzzy logic [88], ordinal optimization (OO) [93], and artificial bee colony (ABC) [96].

The main objective of the majority of the papers cited above is loss reduction. However, our main objective in this chapter is to identify the optimal connection point for a wind power plant, so that the hosting capacity of the network is maximized while keeping the power quality and security concern within the acceptable limits.

4.2 Siting wind power

The connection point of a wind turbine determines the power quality and security concerns it poses to a given distribution system. These power quality and security concerns discussed in Chapter 2

include overvoltage, overloading, flicker and harmonic emission, and increase in fault level. In subsequent subsections, the siting problem is investigated according to each power quality and security concern. Each subsection starts by, first, investigating the situation under which each power quality and security concern can become a limiting factor. Then the siting of the wind power under such a situation is discussed.

4.2.1 Overvoltage

The effect of wind power in increasing the voltage level in a distribution system has been shown in Section 2.2.1 using (2.11) (rewritten here as (4.1) with a slight rearrangement).

$$|V_2| \approx |V_1| + PR + QX \tag{4.1}$$

From (4.1) , since the voltage at the substation $|V_1|$ is regulated around a reference voltage, the voltage $|V_2|$ at the PCC will be higher for higher wind power generation P and cable resistance R. Higher cable resistance R arises from longer cable or overhead line. Fig. 4.1 shows the capacity of wind power that can be installed based on the $\pm 5\%$ voltage limit for different cable types with varying lengths. The data for these two cable types are given in Table 2.1. The wind farm is assumed to operate at unity power factor, which is the current operating practice of most wind turbines.

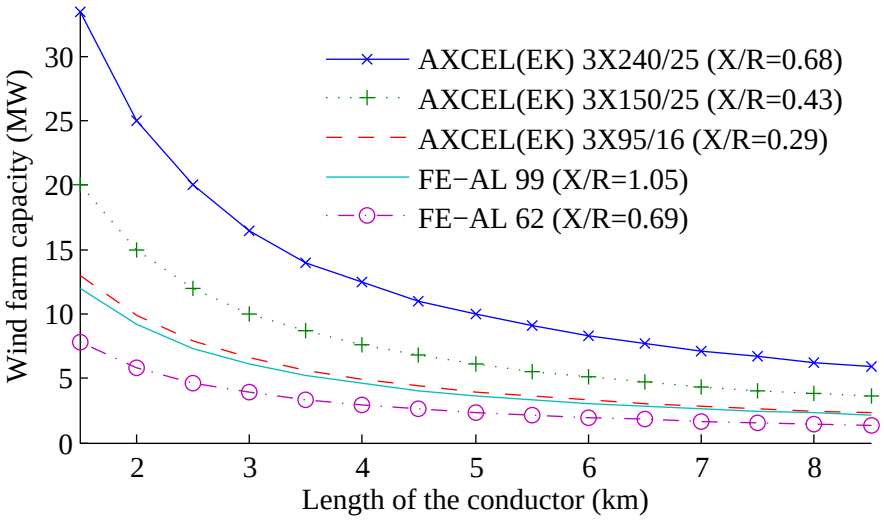

Figure 4.1: The capacity of wind power that can be installed based on $\pm 5\%$ limit

From Fig. 4.1, one can notice that the capacity of wind power that can be installed based on the $\pm 5\%$ voltage limit is severely limited when the wind farm is further away from the substation. Hence when the limiting factor to wind power integration is the voltage rise problem, the wind power hosting capacity of the distribution system can be increased by siting the wind turbines as electrically close to the substation as possible.

The above analysis works when one is investigating the siting of single wind farm along a single feeder. However, in a given distribution system there are usually a number of feeders and laterals and the DSO may need to identify those buses that maximize the hosting capacity of the system.

For example, consider the distribution system shown in Fig. 4.2[1], with the indicated candidate wind farm sites (Buses 2 to 4 and 6 to 9) and the network impedances. It is assumed that the minimum loading condition at the buses is zero MW. The worst case voltage rise occurs in system when the load is at its minimum and the generation is at its maximum. The analysis done assuming these extreme conditions of load and wind power is usually called the worst case analysis. Thus, a simple optimal power flow (OPF) analysis is carried out based on the worst case consideration with the objective of maximizing the hosting capacity while keeping the voltage within ±5%. Table.4.1 shows the hosting capacity that is achieved with different bus combination options.

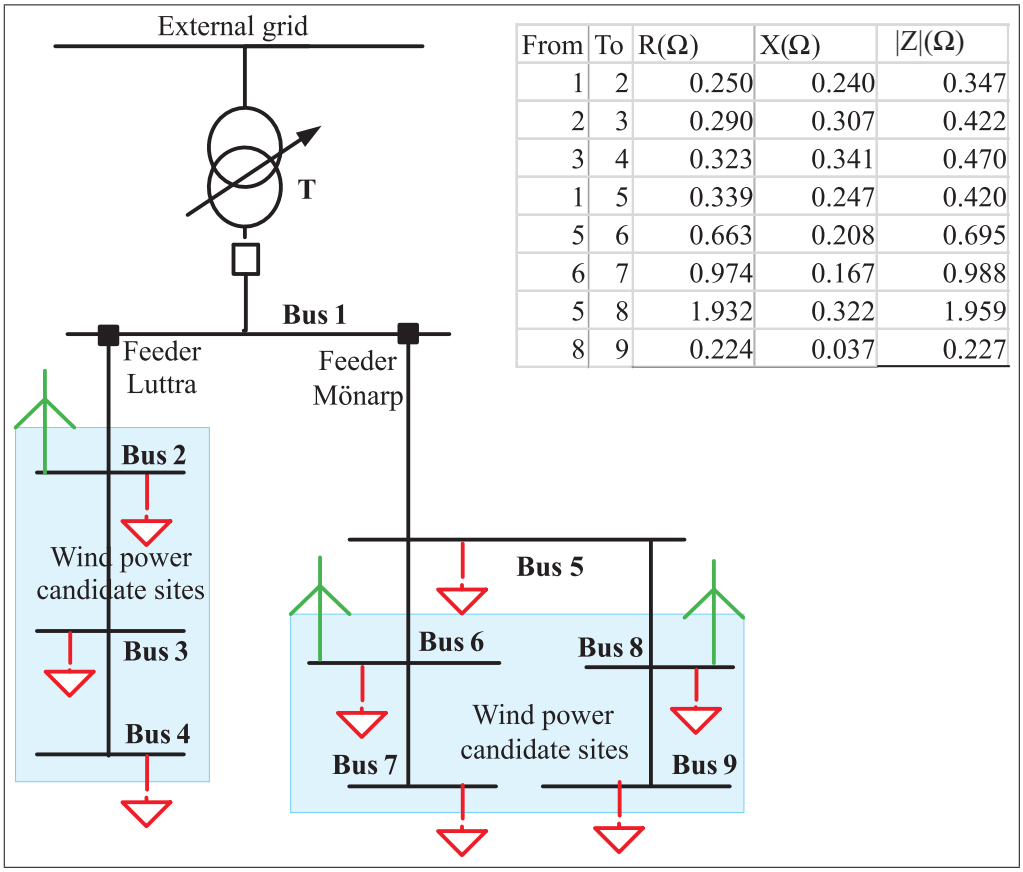

From	To	R(Ω)	X(Ω)	|Z|(Ω)
1	2	0.250	0.240	0.347
2	3	0.290	0.307	0.422
3	4	0.323	0.341	0.470
1	5	0.339	0.247	0.420
5	6	0.663	0.208	0.695
6	7	0.974	0.167	0.988
5	8	1.932	0.322	1.959
8	9	0.224	0.037	0.227

Figure 4.2: siting wind power in distribution system

Table 4.1: Installed wind power capacity with different bus selection alternatives

Option	1			2			3			4			5		
buses	2	6	8	2	3	4	2	8	9	6	7	8	4	7	9
power (MW)	26.0	5.7	2.0	26.0	0.0	0.0	26.0	2.8	0.0	5.7	0.0	2.0	7.6	2.9	2.2
Total (MW)	33.7			26.0			31.0			7.7			12.6		
Loss (MW)	1.6			1.3			1.6			0.4			0.6		
Net (MW)	32.1			24.8			29.5			7.3			12.0		

It is clear from Table.4.1 that wind farm site selection containing Buses 2, 6, 8 has the highest

[1]it is a section of an actual distribution system operated by Falbygdens energi, sectioned out for easier analysis

hosting capacity among the five options considered. That is, distributing the connection points on different feeder maximizes the hosting capacity. Since the voltage at the substation bus is regulated, if the wind turbines are located on different feeders, the maximum capacity of each feeder will be installed without any effect from the wind power on the other feeder. But when they are on the same feeder, the hosting capacity of the feeder will be distributed among the two wind farms. The same is true for the lateral branches of a feeder. That is, if the wind farms, for some reason, should be located at the lateral branches of a feeder, the hosting capacity can be maximized if they are situated in different lateral branches.

Moreover, not connecting the wind turbines as electrically close as possible to the substation, will significantly affect the hosting capacity of the network. For example, from Table 4.1 in case of Option 2, if wind power is installed only on Bus 2, the maximum hosting capacity of Feeder Luttra is 26 MW. Consider now that there is a 2 MW wind turbine installed at Bus 4 on Feeder Luttra. As a result of this pre-installed 2 MW wind power, Bus 2 can now only host 19 MW. Though the hosting capacity is still high, the reduction is significant: -23%. Note that the analysis done here is based on voltage rise consideration only; other consideration, such as overloading, may further limit the hosting capacity of the system as shown in Section 4.2.2.

In conclusion, voltage rise severely limits the capacity of wind power that can be installed in a given distribution system when the connection point is electrically far from the station. Thus, installing wind turbines as close as possible to the substation increases the hosting capacity of a distribution system limited due to voltage rise problem. Moreover when a couple of wind farms are to be connected to a given distribution system, more hosting capacity can be achieved by locating the wind farms at different feeders or lateral branches of a feeder.

4.2.2 Overloading

With overvoltage as the only limiting factor, Fig. 4.1 shows that a considerable amount of wind power can be installed using any of the cables if the wind turbine or farm is located, e.g. at 1.5 km distance from the substation. Table 4.2 shows the current rating of the conductors, the maximum capacity of wind power that the cable can accommodate, and the maximum distance of the wind farm site above which the voltage rise will further limit the capacity of wind power that can be installed. From the table one can see that when the wind turbines are sited electrically close to the substation, the thermal capacity of the cables further limits the wind power hosting capacity of the distribution system. Similar analysis done on the distribution system in Fig. 4.2 shows that the hosting capacity of the system is well below the capacity indicated in Table 4.1 due to the thermal capacity of the cables involved. It can generally be concluded that for wind turbines installed in

Table 4.2: Maximum capacity based on ampacity of different cable types

Cable	Current rating	Pmax (MW)	Maximum cable length (km)
AXCEL(EK) 3X240/25	360	6.7	7.3
AXCEL(EK) 3X150/25	280	5.3	5.7
AXCEL(EK) 3X95/16	215	4.1	4.8
FE-AL 99	435	8.3	2.2
FE-AL 62	305	5.8	2

relatively strong distribution network at sites close to the substation, the capacity of the wind farm is more likely to be limited due to the thermal capacity of the involved components.

Given a situation where the thermal capacity of the network components is the limiting factor, it may be of an interest to decide both the location and the capacity of the wind farm. Consider Feeder Luttra in network of Fig. 4.2, where the thermal rating of the feeder is 280 A with zero MW minimum loading condition. Table 4.3 shows the maximum hosting capacity of the feeder for different choice of a wind turbine connection point.

Table 4.3: Hosting capacity of Feeder Luttra based on thermal limit

Connection point	Capacity (MW)	Voltage at Bus 2 (p.u.)	Voltage at Bus 3 (p.u.)	Voltage at Bus 4 (p.u)	Feeder loss (MW)	Net (MW)
2	5.39	1.011	1.011	1.011	0.06	5.33
3	5.46	1.011	1.024	1.024	0.13	5.33
4	5.53	1.011	1.023	1.037	0.20	5.33

Table 4.3 shows a slightly higher wind power hosting capacity for connection points electrically further from the station. This is due to a higher voltage rise that occurs for connection points further from the station for the same level of current injection. But, the last column of the table shows that the extra hosting capacity gained, becomes a part of the network power losses. The same analysis is also done assuming a higher minimum loading conditions and the results have yielded similar conclusion.

Therefore, in general, one can conclude that installing the wind turbines close to the substation is a preferred option in a distribution system where the hosting capacity is limited due to overloading. On one hand, usually the cables electrically close to the substation have higher ampacity than the cables or overhead lines that are located electrically far from the substation. Hence the hosting capacity can be maximized by installing the wind turbines close to the substation. On the other hand, even if the capacity of the cables along the feeder are similar, it is still better to install wind turbines electrically close the substation. Though this does not increase the hosting capacity of the system, it reduces the power losses as shown in Table 4.3.

4.2.3 Loss consideration

In general power losses do no limit the capacity of installed wind power. However, since increase in power losses leads to loss in revenue, there is a need to minimize the power losses in the system. Thus, in loss minimization, the strategy is usually to supply the power demand in a distribution network as locally as possible. This reduces the current flow through the network cables compared to the case where the loads are supplied from the external grid through the transformers. The reduction in current flow leads to reduced power losses in the system.

Consider the same example on Feeder Luttra discussed in Subsection 4.2.2. Assume now that there are average loads of 0.2 MW, at Buses 2 and 3, and 1 MW, at Bus 4, with a lagging power factor of 0.95. Table 4.4 shows the power generation and loss before and after connecting a DG. The results show that installing an approximately 1.2 MW of wind power at Bus 4 results in the minimum loss in the feeder. Compared with the capacity that is installed based on hosting capacity

maximization, this capacity of wind power is considerably low. When wind turbines are installed based on hosting capacity maximization there is usually a high reverse power flow to the external grid. In such cases installing wind power as electrically close as possible to the substation will result in lower power losses in the system. This is clearly seen on Table 4.3.

Table 4.4: siting wind power based on loss minimization

Buses	Power production (MW)			
	Without DG	With DG at Bus 2	With DG at Bus 3	With DG at Bus 4
External grid	1.412	-0.007	0.105	0.218
2	0	1.414	0	0
3	0	0	1.299	0
4	0	0	0	1.184
Loss (MW)	0.012	0.007	0.004	0.001

4.2.4 Flicker emission

Flicker has been identified as one of the limiting factors in wind power integration before the arrival of variable speed wind turbines [100,101]. Due to better capability of variable speed wind turbines to control their power production with respect to the varying wind speed, flicker emission is not as much a concern as it once was. But it is still interesting to find out the situation at which flicker emission could be a limiting factor in wind power integration.

As noted from the flicker equations (2.12), (2.14), and (2.15), flicker emission from wind turbines can become significant when the grid at the point of common coupling is substantially weak. Hence it is required to investigate if flicker emission could be a limiting factor in weak grids. Consider the network given in Fig. 4.2 where the candidate wind power installation site is taken as Bus 9 (with SCC = 33 MVA). The capacity of wind power that can be installed at the given connection points still satisfying the AMP requirement with respect to flicker emission is given in Table 4.5. Three wind turbine sizes with flicker coefficients varying from 2 to 4.5 are investigated.

Table 4.5: The maximum capacity of wind power that can be installed at each point still fulfilling the AMP limits in terms of flicker emission

flicker coefficient	Wind turbine sizes		
	0.9 MW	1.5 MW	3 MW
2	18.9	12.0	6.0
2.8	9.9	6.0	3.0
3.6	5.4	3.0	3.0
4.4	3.6	3.0	0.0

Based on flicker coefficient data available for various wind turbines, it is not usually difficult to find wind turbine having a flicker coefficient of 2.8. Hence with respect to flicker emission limits the wind farm capacity can easily be as much as 9.9 MW.

Moreover, if the flicker emission limits of the new wind farm is calculated based on the discussion

in Appendix A, it can be as high as $E_{\mathrm{Plt},i} = 0.38$ (assuming that 12 MW wind power is already installed in the system). With this limit in place the capacity of the new wind farm can double the capacity shown in Table 4.5. Hence for flicker to be a limiting factor, the network should already have a substantial amount of flicker emitting installations. Otherwise flicker emission is less likely to be a limiting factor with the advent of current variable speed wind turbines.

However, it is still interesting to investigate the siting of wind turbines in a distribution system to minimize the voltage flicker emission. Consider the case investigated in Table 4.5. At a bus where the SCC is 33 MVA, the capacity of wind power that can be installed based on AMP flicker emission limits is found to be around 9.9 MW with a turbine size of 0.9 MW having a flicker coefficient level of 2.8. Table 4.6 presents the result of the flicker emission when this capacity of wind power is connected at Buses 1, 5, 8, and 9 for different flicker coefficient levels.

Table 4.6: Flicker emission from 9.9 MW wind farm

Bus	S_k(MVA)	$P_{st}(P_{lt})$ with flicker coefficient of			
		2	2.8	3.6	4.4
1	67	0.09	0.12	0.16	0.20
5	57	0.10	0.15	0.19	0.23
8	35	0.17	0.24	0.30	0.37
9	33	0.18	0.25	0.32	0.39

The results show that the flicker emission of wind turbines connected away from the station is higher than those connected close the substation. As it can be observed from (2.12), (2.14), and (2.15), this is because the flicker emission from the wind turbines is inversely proportional to the short circuit capacity of the distribution system at the point of connection. Therefore, it can be concluded that installing wind turbines as close to the substation as possible minimizes the effect of wind power on flicker emission.

4.2.5 Harmonic emission

Appendix B Section B.2 shows that the requirement on low order even harmonics is the most stringent one to fulfill when it comes to harmonic emission limits on wind turbines. As in the flicker case, voltage harmonics emission limits are more difficult to fulfill in case of weak grids. Moreover unlike the flicker case, harmonic emission from LV loads should also be taken into account. Hence, in addition to harmonic contributions from the MV and the upstream network, the harmonic emissions from the LV loads affect the allowed level of harmonic emission from a new wind power installation.

Consider the same example as in Subsection 4.2.4. Consider also, as in the case of example given Section B.2, the MV network already has 12 MW wind power and the peak load in the LV network is 8 MVA. In Table B.2 (column 4) of Appendix B the harmonic voltage contribution limit of the new wind farm is given. For each harmonic order, the maximum amount of wind power that can be installed at Bus 9 while fulfilling the given harmonic limits is calculated. The results of the calculation (for the case of low order even harmonics) is given in Table 4.7.

Based on the data available for this work, the assumed harmonic current emission levels in Table 4.7 are a bit demanding, i.e not every wind turbine in our data set has such a low level of

Table 4.7: Wind farm capacity limits based on harmonic emission

order h	$E_{\mathrm{Uh},i}$ (%)	Harmonic current limits	i_h(%) from wind turbines	Maximum wind farm capacity in MW with	
				4.5 MW wind turbines	0.9 MW wind turbines
2	0.16	2.56	0.29	9.0	9.0
4	0.12	1.02	0.12	9.0	9.0
6	0.13	0.74	0.16	4.5	9.0
8	0.11	0.46	0.10	4.5	9.0
10	0.11	0.37	0.08	4.5	9.0

harmonic emissions. Hence harmonic current emission could be a limiting factor provided that the network already has some distorting installations. Moreover, considering the example network investigated here, harmonic emission is more likely to be a limiting factor than flicker emission.

Therefore, to site a wind farm of a given size for a reduced level of harmonic emission, let us consider (2.21) again which converts the allowed level of voltage harmonics to the allowed level of current harmonics. Here (2.21) is rearranged as (4.2) to facilitate the calculation of voltage harmonics introduced by a wind turbine due to its current harmonics.

$$u_h = \frac{i_h Z_h S_{\max}}{U^2} \tag{4.2}$$

Equation (4.2) shows that a wind turbine which is sited electrically far from the substation, thus experiencing a higher harmonic impedance Z_h, introduces higher voltage harmonics. Hence siting wind turbines as close electrically as possible to the substation can maximize the hosting capacity of a network constrained due to harmonic voltage emission.

4.2.6 Increase in short circuit level

The discussion in Section 2.2.5 indicates that the increase in fault level can become a limiting factor to wind power integration depending on:

- the capacity and technology of the wind turbines in the network,
- the distance of the wind farm from the station,
- the SCC at the station due to the external grid,
- and the rating of the switchgear at the station i.e. the available fault level margin of safety to handle additional fault current from the wind turbines

Therefore, an increase in fault level can only become a limiting factor in a distribution system connected to a quite strong grid where the available margin of safety to handle additional fault level is very low. Moreover the wind turbines connected to the grid need not be of Type D. In general, it is less likely for the grid to be very strong in rural areas, where favorable windy sites are usually located. As the distribution systems in this area are often far from the main grid, they have comparatively low grid strength. Therefore, increased fault level may become a limiting factor only in rare cases.

However, it is still interesting to find out the location of wind turbines in a given distribution system that will minimize the effect of wind power on the switchgear of the system. Consider

the distribution system in Fig. 4.2. Assume that a 4.75 MW wind farm is being investigated for installation on Feeder Luttra. Let this wind farm be composed of five 0.95 MW wind turbines (same wind turbines as those characterized in Table C.4). Fig. 4.2 shows that there are three candidate buses (Bus 2, 3 and 4). Assume that the switchgear at different buses have the same rated capacity. In most cases fault contribution from the external grid is more likely to be higher than the fault contribution from the wind turbines. With higher impedance between the fault source and the fault point, these fault contribution from the external grid substantially decreases when the buses are located electrically further from the station. Therefore, it is less likely for increased short circuit level to be a problem on these buses. Hence in terms of increased short circuit level it is the substation bus that is our main concern.

For the fault at the substation busbar (Bus 1), Table 4.8 shows the fault current contribution from the upstream grid I_k'', the contribution from the wind turbines I_{kW}'', and the total three phase fault current at the substation I_{kT}'' for different connection points (PCC) of the wind turbines. Here the fault current calculation is done using the IEC approach [42] where no load is assumed in the system. Moreover no other wind turbine is also assumed to operate in the system.

From the table, one can notice that the fault current contribution at the substation decreases as the wind turbines are sited further from the substation. Hence the total fault level at the substation decreases. Though the magnitude differences may not seem to be significant here, it may become significant depending on the capacity of the wind farm and the difference in electrical distance between the different candidate sites. Thus, in distribution systems where the available fault level margin of safety is relatively low, when the wind turbines are not of Type D, installing wind farms away from the station could be an option to increase the hosting capacity of the network.

Table 4.8: Fault current at the substation for the different locations of the wind turbines

PCC	I_k'' (kA)	I_{kW}'' (kA)	I_{kT}'' (kA)
Bus 2	3.711	1.437	5.147
Bus 3	3.711	1.339	5.045
Bus 4	3.711	1.242	4.944

4.3 Summary

This chapter has analyzed the different integration issues of wind power as a possible limiting factor based on which siting of wind turbines or farms are proposed. Depending on the location of the wind turbines with respect to the substation transformer, the electrical characteristic of the network at the point of connection, and the wind turbine technology, mostly one integration issue will be dominant. For voltage flicker and harmonics to become a limiting factor in wind power integration, the network should already have a substantial amount of fluctuating or distorting installations. Even in this case the distribution network should have a comparatively very low value of SCC at the substation. Otherwise if the SCC at the substation is relatively high and if it is the SCC at the connection point which is considerably low, then, in this case, voltage rise may most likely become a limiting factor. Moreover, the increase in fault level with respect to the fault handling capability

of the switchgear is a concern only in cases where the external grid is very strong and the available margin of safety to handle additional fault contribution is very low. Voltage rise and thermal overloading can become limiting factors irrespective of the grid condition. Voltage rise usually depends on the electrical distance of the new installation with respect to the substation while overloading depends on the thermal rating of the involved network components such as transformer and cables. Thus, in majority of the cases, voltage rise becomes a problem for installations further from the substation and overloading is a limiting factor when the installations are electrically close to the substation.

In a distribution system where the hosting capacity is limited due to overvoltage, overloading, voltage flicker, and harmonics, it is found that installing wind turbines as electrically close to the substation as possible, maximizes the hosting capacity of a distribution system. Moreover, when more than one PCC is sought, the PCCs should be distributed on different feeders as well as laterals. Even with regard to loss consideration, when large scale integration of wind power is sought, installing wind turbines or farms electrically close to the substation minimizes the loss in the system. It is also mentioned in Chapter 3 that the effect of wind power on the FTC is almost independent of the location of wind farms in a given distribution system. Therefore, based on the integration issues of wind power discussed in this thesis, the increase in fault level is the only reason that one may need to install wind turbines away from the substation when trying to maximize the wind power hosting capacity of distribution systems.

5

Wind power hosting capacity of a distribution system

This chapter deals with the determination of the optimal hosting capacity of a distribution system. The chapter starts with a discussion of the traditional worst-case approach of assessing the hosting capacity of a distribution system. Then the role of active management strategies in increasing the hosting capacity of a given distribution system is discussed. Incorporating these active management strategies, an optimization model is developed to assess the optimal hosting capacity of a given distribution system. A discussion on stochastic wind power and load data modeling is also included in this chapter. This will provide a useful tool for load and wind power data generation whenever the available load and wind power data are not of the required size or type. The chapter concludes by presenting and discussing results from two case studies.

5.1 Assessing the hosting capacity of a distribution system

5.1.1 Worst case analysis

Current distribution systems are operated passively. This means these systems are not actively controlled to insure that system components operate only within the allowed range of voltage and thermal loading. Therefore, while permitting a given wind power installation, distribution system operators (DSOs) consider the worst condition under which the system can operate. Under this operating condition, the philosophy is the the system should function with every power quality and reliability indices of the system being within the acceptable limit.

In Chapter 4, voltage rise and overloading of system components have been identified as the most common problematic effects of wind power. Voltage rise occurs due to reverse power flow. If the power generation from a wind turbine/farm is locally consumed the reverse power flow decreases. Thus, the worst case reverse power flow, corresponding to the maximum voltage rise, happens when the load is at its minimum and the power generation is at its maximum. The same holds true for the overloading which happens due to wind power production. That is, the higher the reverse power flow, the more likely it is for the network elements to be overloaded. Hence the

maximum generation and the minimum loading condition in the system ends up being the worst condition. The maximum loading together with the minimum generation can cause overloading and undervoltage. However, the same condition can arises in the system even without wind power installation. Thus, the analysis of such condition is not necessary to assess the wind power hosting capacity of the system. The analysis based on such assumption of minimum load and maximum wind power generation is called worst case analysis. In the worst case analysis, the objective is for the voltage to remain within, e.g., $\pm$ 5% of the nominal voltage and the power flow to remain within the thermal ratings of the system elements. Based on the worst case, a number of optimization approaches have been proposed to assess the hosting capacity of a distribution system [78, 79, 87, 92, 102]. Optimal power flow (OPF) based approach is proposed in [102] to determine the available headroom for DG. Genetic algorithm (GA) [78, 87], and combined OPF and GA [79, 92] are used to determine the optimal position and size of DGs.

5.1.2 Active management strategies

The approach based on maximum generation and minimum load ensure the network from potential power quality and security concerns. However, due to high variability of both load and wind power generation with a low level of correlation, maximum generation and minimum load condition in the system rarely, if ever, coincides in practice. Hence this approach unnecessarily hinders the penetration of wind power into the electricity grid. It also deprives DSOs from potential benefit they could gain. Hence the use of active management strategies have been proposed to deal with this rare event and increase the penetration of wind power into the electricity grid [3–9]. The discussion of these active management strategies is presented in the following subsections.

5.1.2.1 Reactive power compensation

The main objective of using reactive power compensation (RPC) is to alleviate the voltage rise problem, although it can be used for loss minimization and mitigating other integration issues of wind power, such as voltage flickers [103, 104]. In case of voltage rise mitigation using RPC, reactive power is consumed by the wind turbines or by some other components such as static VAR compensator (SVC) or static synchronous compensator (STATCOM) so as to bring down the voltage at the terminal of the wind farm within the $\pm$5% limit.

5.1.2.2 Coordinated on-load tap changer voltage control

The traditional or the existing practice of controlling tap changers is based on two main principles, as discussed in Section 2.2.1.1. The first one is based on keeping the voltage within a given dead-band around some reference voltage. In the second approach the controllers are augmented with line-drop compensation to boost voltages more during heavy loading condition [27]. Due to introduction of wind power, however, the voltages at different feeders may differ widely. This makes it difficult to properly regulate the voltages at different feeders with just one substation OLTC. Even if separate regulators are assigned for each feeder, the power factor of the feeder where wind power is installed can vary considerably depending on the wind condition. This makes voltage regulation very difficult especially for second approach [27]. Even for the first approach, a better voltage regulation, hence, higher hosting capacity can be achieved with the use of coordinated OLTC voltage

control in a distribution system limited due to voltage rise problem. In coordinated OLTC voltage control, the OLTC is controlled to keep the voltage on various critical points in the system within the acceptable voltage limits. These critical points are usually the end and beginning of feeders or laterals and can be identified more specifically using load flow studies.

5.1.2.3 Wind energy curtailment

The principle behind wind energy curtailment is to curtail part of wind power production in case of overvoltage or overloading. This is the only solution in case of overloading unless some expensive solutions, such as energy storage and capacity enhancement, are made. In case of overvoltage, coordinated OLTC control is the preferred solution as there is no need for extra reactive power or consumption from external grid nor does it involve wind power curtailment.

5.1.3 Costs and benefits of wind power

The active management strategies (AMSs) subject the DSO and the wind farm owner (WFO) to costs of their own. For example, wind energy curtailment causes loss in revenue for the WFO and cannot be used unlimitedly. Similarly, RPC, if used excessively, may lead to unacceptable power losses in the network. Therefore, one needs to identify the capacity of wind power that can be installed using AMSs while maximizing the profit gained by the DSO and the WFO. To this end, different costs and benefits of DSO and WFO need to be analyzed. The next subsections discuss the main costs encountered and benefits gained by WFO and DSO due to integration of wind power. The focus is only on the monetary costs and benefits. Hence, for example, the extra benefit gained by a society due to environmental benefits of wind power is not taken into account. Moreover, the discussion of some financial tools from economics, which are used in our cost-benefit analysis, is included.

5.1.3.1 Costs & benefits of a distribution system operator

Costs of a distribution system operator: The DSO may encounter a significant cost during the connection stage of the wind turbine. The DSO faces these costs only if there is a need to reinforce the network [105]. Otherwise the connection costs up to the point of common coupling are endured by WFO. Since this study focuses on increasing the hosting capacity using the existing system, no connection cost is assumed on the DSO. Other sources of cost for the DSO due to the connection of wind power may include:

- Increase in network losses due to reverse power flow
- Curtailed wind energy, depending on the agreement between the DSO and WFO
- Infrastructure for implementing AMSs

Benefits of a distribution system operator: Network investment deferral can be seen as the major benefit of distributed generations in general. However, due to uncontrollability of the energy source (i.e wind speed) at the wind turbines and low correlation between load and wind power data, wind farms can only make minor contribution to network investment deferral. In other words, wind power cannot be relied on to meet the peak power demand in a distribution system as the power output from wind turbines depends on the wind condition in the area.

On the other hand, in countries like Sweden and UK, the WFO pays the DSO network fee for using the network [106]. This network fee usually breaks down into a combination of any of the following ones as determined by different regulatory frameworks [107–109]:

- Fixed charge per month or per year
- A fee based on kW installed or maximum power injected per month or per year
- A fee based on kWh energy transmitted by the network
- A fee based on kVarh reactive power consumed and transmitted

5.1.3.2 Costs & benefits of a wind farm owner

Costs of a wind farm owner: The overall expenses of the WFO are affected by numerous parameters such as the capital and variable costs of the wind turbine, the discount rates, and the economic life time of the wind turbine [110].

Capital costs: The capital cost includes the costs of the wind turbines, foundation, road construction, grid connection and other project development and planning costs. Usually, these costs contribute to 80% of the total cost of the project over its entire life [110]. The actual value of the capital cost differs significantly between countries as well as between projects. According to the report by European Wind Energy Association (EWEA) [2], the capital cost in Europe differs between 1 million €/MW and 1.35 million €/MW and the average turbine installed in Europe costs 1.23 million €/MW. Future forecasts by both European commission and European wind energy association show that the capital cost will be lower than what it is today [2]. Moreover, the lifetime of the wind turbine is around 20 years for onshore wind turbines and 25 years for offshore ones [2].

Variable costs: Variable costs include expenses pertaining to [110]

- operation and maintenance (O&M) cost, which includes regular maintenances, repairs and spare parts
- Land rental
- Insurances and taxes
- Administration, including audits, management activities, forecasting services and remote control measures.

The current estimate of these variable costs obtained from EWEA is between 12 to 15 €/MWh [2].

Benefits of a wind farm owner: In most countries, renewable energy, including wind power, is supported through regulating either the price or quantity of electricity from these sources [2]. In price based schemes, the supplier of electricity from renewable sources receive subsidy per kW of capacity installed, or payment per kWh produced and sold. This can be in terms of soft loans during the investment stage or the supplier is able to sell the electricity at a fixed feed-in tariff or at a fixed premium (in addition to the electricity market price).

Tendering and Tradable green certificate (also known as renewable portfolio standard models in US and Japan states) systems are the two commonly used quantity based schemes. In the former case, a tender is launched by a government body to supply a given amount of electricity with a guaranteed tariff for a specified period of time. In the latter case, the supplier of electricity from renewable sources sell two products: electricity, which is sold in electricity markets, and green

certificate, which is sold in a market for fulfilling the political obligation to supply renewable energy [2].

In Sweden, green certificate is used to support energy from renewable sources. The average green certificate price in Sweden for 2011 was 27.92 €/MWh [111] and the average electricity price at spot market was 47.85 €/MWh [112]. Hence the average revenue gained in 2011 by producing a MWh of electricity from wind power was 75.77 €.

5.1.3.3 Tools for cost benefit analysis

When dealing with costs and benefits occurring at different time, there are a number of tools that can be used to facilitate decision making about an investment. Here two of them are presented.

Present worth analysis is a method by which costs and savings at different time are compared for decision making.

Given f_n^{pw} as a present worth factor, then the amount of net cash flow B_n at a future year n is equal to A amount at present, where B_n and A are related as follows

$$A = B_n f_n^{\mathrm{pw}} \tag{5.1}$$

Using the discount rate, r, the present worth factor, f_n^{pw}, of money at year n is given by [113]

$$f_n^{\mathrm{pw}} = \frac{1}{(1+r)^n} \tag{5.2}$$

The net present value, v^{np}, of cash flows occurring at a different time is the sum of the present worth of individual cash flows i.e.

$$v^{\mathrm{np}} = \sum_{n=1}^{N} B_n f_n^{\mathrm{pw}} \tag{5.3}$$

Where N is the total period of the investment in years. If identical net cash flows occur in every year t starting from year one i.e. $B_n = B, \forall\, n$, then we have

$$v^{\mathrm{np}} = B \times f^{\mathrm{npw}} \tag{5.4}$$

where

$$f^{\mathrm{npw}} = \frac{(1+r)^N - 1}{r(1+r)^N} \tag{5.5}$$

Levelized values, v^{l}, is the constant annual cost of the project having the same present worth as the actual cost of the project.

$$v^{\mathrm{l}} = v^{\mathrm{np}} \frac{r(1+r)^N}{(1+r)^N - 1} \tag{5.6}$$

Levelized costs can give a better platform for comparing different projects with different life times [113].

5.2 Modeling the hosting capacity problem

Based on the discussions in Section 5.1, this section develops an optimization model that that can be used to determine the optimal hosting capacity of a distribution system and the optimal usage level of active management strategies.

5.2.1 The Objective function

Since the optimal capacity could be different based on who covers the different costs incurred due to the active management strategies involved, separate objective functions are developed for each actor, i.e. DSO and WFO. The aim of the objective functions, in each case, is to maximize the net benefit of the corresponding actor taking into account the different costs and benefits discussed in Section 5.1. Moreover, some costs of wind power integration, such as curtailed energy, may be covered by either the DSO or the WFO.

Both objective functions are subject to the same equality and inequality constraints provided in the subsequent sections.

5.2.1.1 The Objective function of the DSO

The objective function of the DSO is developed assuming that the DSO agrees to pay the WFO for the curtailed energy. Hence, the DSO's objective is to maximize the net benefit it gets while covering the cost of curtailed energy and increase network losses over the economic life time of the wind turbine and is formulated as

$$\max_{n_i, P^{\text{cur}}_{i,t}} O = \sum_i a_i n_i - \sum_i \sum_t b_i P^{\text{cur}}_{i,t} - c\Delta P^{\text{loss}} + d \tag{5.7}$$

where

a_i, b_i, c, and d	are coefficients to be calculated based on cost benefit data of the DSO
n_i	is number of wind turbines with 1 MW capacity
$P^{\text{cur}}_{i,t}$	is curtailed power in MW at each bus i and time t
ΔP^{loss}	is the change in power losses P^{loss} due to wind power introduction, where

$$P^{\text{loss}} = \frac{1}{T} \sum_t^T \sum_k \sum_{j<k} g_{k,j} \left(\left(\frac{V_{k,t}}{n_{k,j,t}} \right)^2 + V_{j,t}^2 - \frac{2 \cdot V_{k,t} \cdot V_{j,t}}{n_{k,j,t}} \cos(\delta_{j,t} - \delta_{k,t}) \right) \tag{5.8}$$

In (5.7), the first term accounts for revenue from network fee while the second and the third term represents the cost of curtailed and increase in network losses respectively. The last term represents any constant revenue or expense, e.g. subscription fee, investment cost of the infrastructure for implementing AMSs. Moreover, the coefficients of each term should be calculated as the present worth of the associated costs or benefits during the life time of the wind turbine. Moreover, one can calculate b_i (excluding the cost of curtailed energy) to investigate the case where the DSO covers only the cost of increase in network losses.

5.2.1.2 The objective function of the WFO

Similarly, the objective function of the WFO is developed assuming the WFO bears the cost of curtailed energy. Hence the objective function which maximizes the net benefit of the WFO is formulated as

$$\max_{n_i, P^{\text{cur}}_{i,t}} O = \sum_i \alpha_i n_i - \sum_i \sum_t \beta_i P^{\text{cur}}_{i,t} - \kappa \tag{5.9}$$

In (5.9) the first term accounts for revenues (including electricity and green certificate sell) and costs (investment cost, O&M costs) per kW of installed capacity while losses in revenue due to curtailed energy is accounted for by the second term. The last term represents any constant revenues or expenses. Similar to the case of DSO, the coefficients in (5.9) should also be calculated as the present worth of the associated costs or benefits during the life time of the wind turbine.

5.2.2 The constraints

The objective functions proposed in the previous subsection are subject to different equality and inequality constraints. These constraints are described below.

5.2.2.1 Equality constraints

The equality constraints are the load flow equations [68]

$$\begin{aligned} P_{i,t} - P^D_{i,t} &= \sum_j Y_{i,u} V_{i,t} V_{u,t} \cos(\theta_{i,u} + \delta_{u,t} - \delta_{i,t}) \\ Q_{i,t} - Q^D_{i,t} &= -\sum_j Y_{i,u} V_{i,t} V_{u,t} \sin(\theta_{i,u} + \delta_{u,t} - \delta_{i,t}) \end{aligned} \tag{5.10}$$

where for buses to which wind power is connected, $P_{i,t}$ can be replaced by

$$P_{i,t} = n_i P^{\text{W}}_{i,t} - P^{\text{cur}}_{i,t} \tag{5.11}$$

and $P^{\text{W}}_{i,t}$ is the available wind power at time t and at bus i [p.u.]

However, whenever the hosting capacity is limited due to the voltage rise problem, the limits on the tap ratio may be violated. Under such a condition, there is a need to constrain the tap ratio within its limit. One way of doing this can be to model the elements of the admittance matrix that are affected by the tap ratio as decision variables. Another way could be to use the modified load flow equations proposed in Section 3.2.1.3. The first approach, besides the variables of the original load flow equations (5.10), will have some elements of the admittance matrix and the tap ratio as additional variables while the second approach will have only the tap ratio as an additional variable. Hence the second approach takes less simulation time. Thus, the modified load flow equations derived in Section 3.2.1.3 ((3.9 revisited) and (3.10 revisited)) replace (5.10).

For bus in $k \in K$:

$$\begin{aligned} P_{k,t} - P^{\text{D}}_{k,t} &= \sum_j P^{\text{F}}_{k,j,t} \\ Q_{k,t} - Q^{\text{D}}_{k,t} &= \sum_j Q^{\text{F}}_{k,j,t} \end{aligned} \tag{3.9 revisited}$$

where

$$P^{\mathrm{F}}_{k,j,t} = \left(\frac{V_{k,t}}{n_{k,j,t}}\right)^2 g_{k,j} - \frac{V_{k,t}V_{j,t}}{n_{k,j,t}} y_{k,j}\cos(\delta_{j,t} - \delta_{k,t} + \varphi_{k,j})$$
$$Q^{\mathrm{F}}_{k,j,t} = -V^2_{k,t}\left(\frac{b_{k,j}}{n^2_{k,j,t}} + \frac{b^c_{k,j}}{2}\right) + \frac{V_{k,t}V_{j,t}}{n_{k,j,t}} y_{k,j}\sin(\delta_{j,t} - \delta_{k,t} + \varphi_{k,j}) \quad \text{(3.7 revisited)}$$

For bus $j \in J$:

$$P_{j,t} - P^{\mathrm{D}}_{j,t} = \sum_k P^{\mathrm{F}}_{j,k,t}$$
$$Q_{j,t} - Q^{\mathrm{D}}_{j,t} = \sum_k Q^{\mathrm{F}}_{j,k,t} \quad \text{(3.10 revisited)}$$

where

$$P^{\mathrm{F}}_{j,k,t} = V^2_{j,t} g_{j,k} - \frac{V_{j,t}V_{k,t}}{n_{k,j,t}} y_{j,k}\cos(\delta_{k,t} - \delta_{j,t} + \varphi_{k,j})$$
$$Q^{\mathrm{F}}_{j,k,t} = -V^2_{j,t}\left(b_{j,k} + \frac{b^c_{j,k}}{2}\right) + \frac{V_{j,t}V_{k,t}}{n_{k,j,t}} y_{j,k}\sin(\delta_{k,t} - \delta_{j,t} + \varphi_{k,j}) \quad \text{(3.8 revisited)}$$

5.2.2.2 Inequality constraints

The inequality constraints include:

- the limit on the thermal capacity (current limit) of network components; this includes the limit on the ampacity of network cables $I^{\mathrm{rat}}_{k,j}$, as given by (5.12)[1], and the power rating of the substation transformer $S^{\mathrm{rat}}_{k,j}$, as given by (5.13),

$$y^2_{k,j}(V^2_{k,t} + V^2_{j,t} - 2V_{k,t}V_{j,t}\cos(\delta_{j,t} - \delta_{k,t})) \leq \left(I^{\mathrm{rat}}_{k,j}\right)^2 \quad \forall k > j \tag{5.12}$$

$$y^2_{k,j}V^2_{k,t}\left(\left(\frac{V_{k,t}}{n_{k,j,t}}\right)^2 + V^2_{j,t} - \frac{2\cdot V_{k,t}\cdot V_{j,t}}{n_{k,j,t}} \times \cos(\delta_{j,t} - \delta_{k,t})\right) \leq \left(S^{\mathrm{rat}}_{k,j}\right)^2 \quad \forall k > j \tag{5.13}$$

- the limit on the available range of tap ratio,

$$n^{\min}_{k,j} \leq n_{k,j,t} \leq n^{\max}_{k,j} \tag{5.14}$$

- the voltage limits on each bus,

$$V^{\min}_i \leq V_{i,t} \leq V^{\max}_i \tag{5.15}$$

[1] In π- model of a line (Fig. 3.2), the current that passes through the resistive element and causes thermal overheating can be calculated using $I_{k,j} = y_{k,j}e^{i\varphi_{k,j}}(V_{k,t}e^{i\delta_k} - V_{j,t}e^{i\delta_j})$ and this gives (5.12). Similar analysis on the π-model of a transformer (Fig.3.3) gives (5.13).

- the limit on cost of curtailed energy, mainly compared to the cost of alternative investment such as reinforcement,

$$\gamma \sum_i \sum_t P_{i,t}^{\text{cur}} + C^{\text{am}} \leq \chi \tag{5.16}$$

where

γ the net present worth of a MWh of electricity from wind power[€/MWh]
C^{am} the net present value of the cost of active management strategy
χ the net present value of the cost of the alternative investment

If the projects (the AMS system and reinforcement) are known to have different life time, it would be more reasonable to compare based on levelized costs rather than the net present value.

- whenever necessary, a limit on the curtailed energy as a percentage of the total available wind energy at each bus i can be set as,

$$\sum_t P_{i,t}^{\text{cur}} \leq \sigma_i \sum_t n_i P_{i,t}^{\text{W}} \tag{5.17}$$

where σ_i is the maximum allowed percentage of curtailed energy with respect to the total available wind energy

- and the limit on available active and reactive power at each bus.

$$\begin{aligned} P_{i,t}^{\min} \leq P_{i,t} \leq P_{i,t}^{\max} \\ Q_{i,t}^{\min} \leq Q_{i,t} \leq Q_{i,t}^{\max} \end{aligned} \tag{5.18}$$

$P_{i,t}$ and $Q_{i,t}$ do not need to be bounded at the slack bus. Hence $P_{i,t}^{\min}$ and $Q_{i,t}^{\min}$ can be assigned $-\infty$ and $P_{i,t}^{\max}$ and $Q_{i,t}^{\max}$ can be set to $+\infty$. For buses with wind power, where $P_{i,t}$ is replaced as in (5.11), the constraint on $P_{i,t}^{\text{cur}}$ can be given by (5.19),

$$0 \leq P_{i,t}^{\text{cur}} \leq n_i P_{i,t}^{\text{W}} \tag{5.19}$$

and $Q_{i,t}^{\min}$, $Q_{i,t}^{\max}$ are given by (5.20).

$$\begin{aligned} Q_{i,t}^{\min} &= -n_{i,t} P_{i,t}^{\text{W}} \frac{\sqrt{1-\eta^2}}{\eta} \\ Q_{i,t}^{\max} &= n_{i,t} P_{i,t}^{\text{W}} \frac{\sqrt{1-\eta^2}}{\eta} \end{aligned} \tag{5.20}$$

where η is the minimum operating power factor level of the wind turbine. For the rest of the buses all limits–$P_{i,t}^{\min}$, $P_{i,t}^{\max}$, $Q_{i,t}^{\min}$, and $Q_{i,t}^{\max}$–should be zero.

5.3 Stochastic wind power and load data modeling

Determining the optimal wind power capacity of a given network depends on the load and wind power condition in the system. Consumer loads and wind power are stochastic by nature. Whenever available, time series load and wind power data can be used to represent this stochastic nature.

However, time series data are rarely available at every bus in a given distribution system. This demands for another way of generating load and wind power data. Moreover, when time series data are available, the length of the series can be large. Depending on the network size and the number of equality and inequality constraints involved, this may result in longer convergence time of the optimization model. Hence this section provides a discussion of a mathematical (statistical) model that captures the stochastic nature of load and wind power data as well as the correlation that exists between them. Using this model, data of required size can be generated based on existing measurement data or some established models such as load duration curves (for load data) and Weibull distribution (for wind power data).

A statistical modeling usually means coming up with a simple (or mathematically tractable) model without the knowledge of the physical aspects of the situation. However the model should try to capture the important characteristics of the physical situation such as the appropriate density shape of the univariate margins and the appropriate dependence structure [114]. Though a number of alternatives have been proposed to model multivariate random processes [115], the copula method is found to be more flexible and more suited for modeling the stochastic nature of load and wind power data [9, 116, 117]. Hence, in this thesis, the copula approach is chosen for modeling the stochastic nature of load and wind power data, which is briefly discussed below.

5.3.1 Using copula to model the stochastic nature of load and wind power

Copulas provide an easy way to model and generate random vectors when one believes that the dependence structure between the random variables can be expressed independent of the marginal distributions of the random variables [115]. The univariate marginal distribution functions can be modeled by using parametric or non-parametric models while the dependence structure is captured by using a copula. In this thesis, the Weibull distribution is used for modeling the wind data. However, since the parametric models are not flexible enough, a non-parametric model [118] is used to model the load data. The dependence structure among the data is captured using the Gaussian copula.

The following subsection introduce the concept of copula and the copula types investigated for use in stochastic modeling of load and wind power data.

5.3.1.1 Copula: definition

Given p uniform random variable u_1, u_2, ..., u_p in the unit interval, where these random variables are not necessarily assumed to be independent, the dependence between them is expressed as follows using copula [119].

$$\mathrm{C}(u_1, u_2, ..., u_p) = prob(U_1 \leq u_1, U_2 \leq u_2, ..., U_3 \leq u_3) \tag{5.21}$$

where C is the copula and U is a uniform random variable and u is the corresponding realization. Thus given p random variables x_1, x_2, ..., x_p with the corresponding marginal distribution $F_1(x_1)$, $F_2(x_2)$,..., $F_p(x_p)$, their multivariate distribution function can be given by

$$F(x_1, x_2, ..., x_p) = \mathrm{C}[F_1(x_1), F_2(x_2), ..., F_p(x_p)] \tag{5.22}$$

The marginal functions $F_1(x_1)$, $F_2(x_2)$, ..., $F_p(x_p)$ can assume any distribution independent of each other and the copula structure. There are both parametric and non-parametric copulas. Copulas are usually grouped into copula families.

5.3.1.2 Families of copula

There are a number of families of copulas which have different capabilities in dependence modeling and have their own pros and cons. The two main families of copula are: the elliptical copula and the Archimedean copula. Elliptical copulas have elliptical contoured distributions. Their key advantage is that one can specify different levels of correlation between the marginals. Their key disadvantages are that elliptical copulas do not have closed form expressions and are restricted to have radial symmetry which means they cannot model asymmetric dependence [120]. Unlike elliptical copulas, Archimedean copulas have a simple closed form and they can model asymmetry available in empirical data. The Archimedean copulas reduce the study of multivariate copula to a single univariate function. However, these copulas use only one parameter which limits their flexibility in modeling the dependence of multivariate vectors. Though there are variants of Archimedean copulas that provide better flexibilities for modeling multivariate random variables [121], they are computationally intensive [122]. Therefore, due to their low computation complexity and high versatility in dependence modeling, elliptical copulas are preferred in this thesis for modeling the dependence among load and wind power data.

5.3.1.3 Elliptical copulas

Elliptical copulas are of two types: Gaussian copula and t-copula. Both copulas have a dispersion matrix, ρ, and t-copula has one more parameter, the degree of freedom, v. As reported in [122], the Gaussian copula does not model upper tail dependence unless $\rho = 1$, whereas the t-copula could do that for different values of ρ. However the degree at which it models upper tail dependence gets weaker as the degree of freedom increases. While both copulas can cover the modeling of dependence from perfect negative dependence (countermonotonicity, $\rho = -1$) to perfect positive dependence (comonotonicity, $\rho = 1$), the t-copula does not model independence unless v tends to infinite [123].

However, on one hand, no tail dependence is seen between load and wind power data, hence there is no need for the ability to model tail dependence. On the other hand, the Gaussian copula has a much lower computational complexity than the t-copula. Hence, the Gaussian copula is used in this thesis for modeling the dependence among load and wind power data. Mathematically the Gaussian copula is represented by [122]:

$$\mathrm{C}(u_1, u_2, .., u_p; \rho) = \Phi_\rho[\Phi^{-1}(u_1), \Phi^{-1}(u_2), ..., \Phi^{-1}(u_p)] \tag{5.23}$$

where Φ_ρ the standardized multivariate normal distribution with correlation matrix ρ and Φ^{-1} the inverse of the normal distribution.

5.3.2 Estimating parameters of the Gaussian copula from empirical data

In general the maximum likelihood method [124] can be used for estimating the parameters of a copula based on observed data set. In this method, the parameters of both the marginal functions

and the dependence structure are jointly estimated which makes the method computationally intensive. An alternative approach is to estimate the parameters of each margin independently before the parameters of the dependence structure. This approach is called the inference functions for margins (IFM) method. Yet another approach is to transform the observed data set $(x_1^t, ..., x_N^t)$ into the uniform variate $(u_1^t, ..., u_N^t)$ using an empirical distribution and then to determine the parameter of the copula using the uniform variate. This method is called the canonical maximum likelihood method or CML. The IFM (or CML) estimator for the Gaussian copula is given as [124][1]:

$$\rho_{CML} = \frac{1}{T}\sum_{t=1}^{T} \varsigma_t^{\top} \varsigma_t \tag{5.25}$$

where $\varsigma_t = (\Phi^{-1}(u_1^t), ..., \Phi^{-}1(u_N^t))$.

5.3.3 Sample generation using the Gaussian copula

The reason behind searching for a statistical model to represent the stochastic nature of load and wind power data is to finally generate synthetic data of a required length. This generated data can further be used to make load flow calculations.

For Gaussian copula, random numbers having the required dependence structure is generated from the Gaussian distribution. Then, the Gaussian (normal) cumulative distribution function is applied to get a random uniform variables, $(U_1, ..., U_N)$. Finally, $X_i = F_{X_i}^{-1}(U_i)$ gives the synthetic data that possess the dependence structure as well as the margins of the original random variables (in our case load and wind power data).

5.4 Case study

This section provides the results of two independent case studies. The first one is based on a widely studied 69 bus system found in literature [125]. The second one is based on a real case study: a rural 11kV distribution system operated by Falbygdens Energi located in Falköping area in Sweden. Further description of the distribution systems will be given in the respective sections below.

5.4.1 Cost-benefit data

Here the main focus is to discuss the monetary value of the assumed costs and benefits of both the DSO and the WFO. It is based on these costs and benefits that the coefficient of the objective functions of the DSO and the WFO are calculated for each scenario. Moreover, these same cost benefit data are used for both case studies.

[1] this is asymptotically equivalent to calculating the Spearman's correlation and to deduce the correlation parameter using the relation [122]:

$$\rho = 2\sin\frac{\pi}{6}\rho \tag{5.24}$$

5.4.1.1 Cost-benefit data of the distribution system operator

The monetary values of the benefits of the DSO are taken to be the network fees charged by Falbygdens Energi. These fees are shown in Table 5.1[1] [107].

Table 5.1: Network fees for rated power above 1.5 MW connected to 11 kV network

Subscription fee (ρ^{sf}) [€/yr]	Peak power fee (ρ^{pf}) [€/MW/mon]	Distribution fee (ρ^{df}) [€/MWh]	Transmission benefit (ρ^{tb}) [€/MWh]
3975	812	1.30	-2.27

The different fees in Table 5.1 are explained as follows:

- Subscription fee (ρ^{sf}): a yearly fee paid for subscription of service.
- Peak power fee (ρ^{pf}): the monthly fee paid by WFO based on the maximum one hour average wind power injected.
- Distribution fee (ρ^{df}): the amount paid by WFO per MWh of electrical energy injected.
- Transmission benefit (ρ^{tb}): the payment made by the DSO to the WFO to account for the benefits of distributed power production. On the other hand, Falbygdens energi gets the same level of reduction in payments made to the transmission system operator.

The costs of the DSO are the expense due to increase in network losses and the refund made to the WFO for curtailed energy. The monetary value of the cost of increase in power losses is taken to be the average spot market price for Sweden in 2011: 47.85 €/MWh. For the curtailed energy the DSO is assumed to pay the WFO the opportunity cost of the curtailed energy. This equals to the average spot market price plus the average cost of a green certificate: 75.77 €/MWh. Besides the DSO will lose some portion of the revenue from network fee due to wind energy curtailment. On the other hand, the DSO needs to invest on communication and control infrastructure that implements the AMSs. The review of investment costs of AMS from different projects shows that the cost varies between 100 k€ - 850 k€ [126–131]. The costs vary depending on the number of points being monitored and controlled and the type of active management strategies being implemented. However, as pointed out in [132], the DSO may refund this cost by increasing the network fees. Of course, this will put additional cost on the WFO. Since some of these projects include the cost of research and development (R & D), the cost of AMS is expected to decrease in the future. Hence the capital cost of AMS in forth coming analysis is assumed to be 100 k€ per substation with 12 k€ for each additional wind power connection point, as in [126]. That is, its taken to be roughly 200 k€ for Case study I with eight PCCs and 100 k€ in Case study II with one PCC.

Based on these cost-benefit data, the formulas for calculating the coefficients of the objective function of the DSO in (5.7) are given as:

[1]The data are original given in SEK. It is converted into € using the all time average exchange rate, 9.2319 SEK = 1 €, obtained from European central bank

$$
\begin{aligned}
a_i &= f^{\mathrm{mp}} n^{\mathrm{mon}} \rho^{\mathrm{pf}} + f_i^{\mathrm{cf}} \rho^{\mathrm{df}} \\
b_i &= \frac{f^{\mathrm{mp}} n^{\mathrm{mon}} \rho^{\mathrm{pf}}}{\sum_t^T P_{i,t}^{\mathrm{W}}} + \frac{h^{\mathrm{yr}}}{T} (\rho^{\mathrm{df}} + C^{\mathrm{e}} + C^{\mathrm{gc}}) \\
c &= C^{\mathrm{e}} h^{\mathrm{yr}} \\
d &= \rho^{\mathrm{sf}}
\end{aligned}
\tag{5.26}
$$

where

f^{mp}	the average monthly peak power from the wind turbines [p.u.]
n^{mon}	number of months per year
f_i^{cf}	capacity factor in numbers of hours of full power production in a year
h^{yr}	number of hours per year
T	sample length
C^{e}	cost of electricity based on spot market [€/MWh]
C^{gc}	cost of green certificate [€/MWh]

Here, it is assumed that the cash flows of the DSO due to the wind power do not change from year to year. Thus, the expression for coefficients are formulated to maximize the annual net benefit of the DSO. This provides the possibility to assess the net benefit of the DSO with different discount rates.

5.4.1.2 Cost-benefit data of the wind farm owner

As for the WFO, most of the monetary values of costs and benefits are given in Section 5.1.3, which are summarized in Table 5.2, including the network fees presented in Table 5.1.

Table 5.2: An estimate of costs and benefits of a WFO

Benefit	Revenue from electricity sale (C^{e}) [€/MWh]		47.85
	Revenue from green certificate sale (C^{gc}) [€/MWh]		27.92
	Revenue from transmission benefit (ρ^{tb}) [€/MWh]		2.27
Costs	Investment cost (C^{c}) [€/MW]		1 225 000
	O&M costs (C^{v}) [€/MWh]		14.5
	AMS implementation cost (C^{am}) [€]		100-200 k
	Network fee	Distribution fee (ρ^{df}) [€/MWh]	1.3
		Peak power fee (ρ^{pf}) [€/MW/month]	812
		Subscription fee (ρ^{sf}) [€/yr]	3975

Based on the cost and benefits of the WFO presented in Table 5.2, the formulas for calculating the coefficients of the objective function of the WFO in (5.9) are given in (5.27). One should note that these coefficients correspond to the case where the WFO concedes the cost of curtailed energy but not that of increase in power losses. In the case where the WFO concedes both costs, another coefficient is added to account for the loss increase.

$$
\begin{aligned}
\beta_i &= \left((C^{\mathrm{e}} + C^{\mathrm{gc}} + \rho^{\mathrm{tb}} - C^{\mathrm{v}} - \rho^{\mathrm{df}}) f_i^{\mathrm{cf}} - f^{\mathrm{mp}} n^{\mathrm{mon}} \rho^{\mathrm{pf}} \right) \times f^{\mathrm{npw}} \\
\alpha_i &= \beta_i - C^{\mathrm{c}} \\
\kappa &= \rho^{\mathrm{sf}} \times f^{\mathrm{npw}} + C^{\mathrm{am}}
\end{aligned}
\tag{5.27}
$$

where

f^{npw} the net present worth factor given in (5.5) and n which is the life time of the wind turbine is taken to be 20 years
C^{v} variable costs of wind power [€/MWh]
C^{c} capital cost of wind power [€/MW]

5.4.1.3 Comparing energy curtailment with grid reinforcement

Using constraint (5.16) a comparison is made between wind energy curtailment and investment on capacity enhancement of the substation transformer to determine if and when investing on substation capacity enhancement could be a better option. Substation capacity enhancement is chosen because it is the constraint that needs major investment to increase the hosting capacity of the system. The cost of curtailed energy is taken as $\gamma = 75.77$ €/MWh. This includes the loss in revenue from both green certificate and energy sell. The cost of new substation construction is roughly estimated to be 93 000€/MVA[1] [133]. Thus (5.16) can be rewritten as:

$$75.77 \sum_i \sum_t P_{i,t}^{\text{cur}} + C^{\text{am}} \leq 93000 \sum_i n_i \tag{5.28}$$

Besides substation capacity enhancement it is possible to investigate enhancement in the form of reconductoring, new cable installation, etc.

5.4.2 Case study I: 69 bus system

5.4.2.1 Network and data description

Network description: This is an 11-kV radial distribution system having two substations, four feeders, 69 nodes, and 68 branches as shown in Fig. 5.1. It is also assumed that

- each substation has a 10 MVA transformer with $X(\%) = 8$ and $X/R = 16$
- the external grid has a SCC of 250 MVA with $X/R = 10$
- only those buses within the shaded area are available for connection

Data description: To use the optimization model developed in Section 5.2, load and wind power data are needed as an input. In [125] average load data on each bus are provided. Assuming the load duration curve of Fig 5.2, synthetic data of 1000 samples are generated for the load at each buss. Full correlation is assumed among load data on different buses. The synthetic data generation is done in such a way that the mean value of the synthetic load data is equal to the values given in [125] for the corresponding bus.

For wind power data, the Weibull distribution has been used to generate the wind speed data, which are converted into wind power data using the power curve of a typical wind turbine. Moreover, since usually wind power and load data have only a low level of correlation [117], independence is assumed between wind and load data. However, wind power data at different sites are assumed to

[1] Its average value is given in the reference as 112 000$/MVA, but it is converted into € here using the all time average exchange rate between € and $ i.e. 1.2103

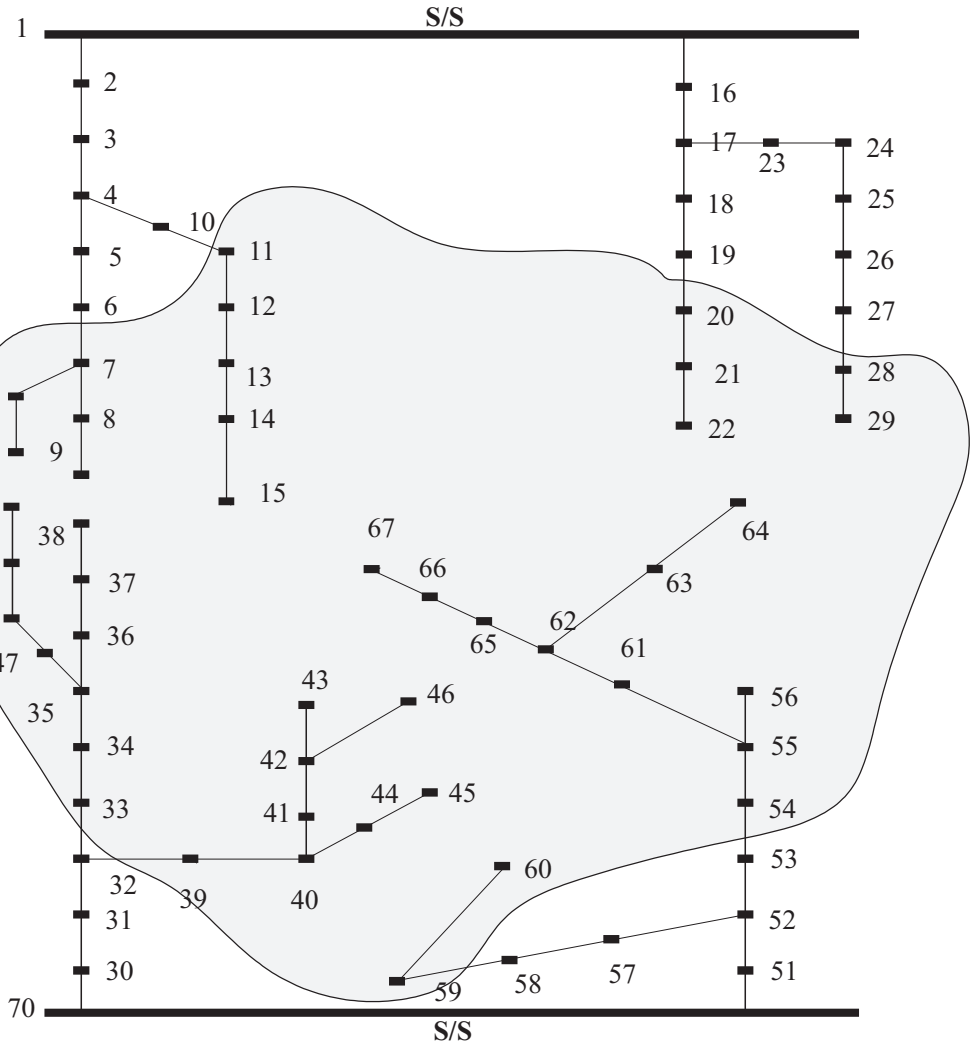

Figure 5.1: The 69 bus system [125]

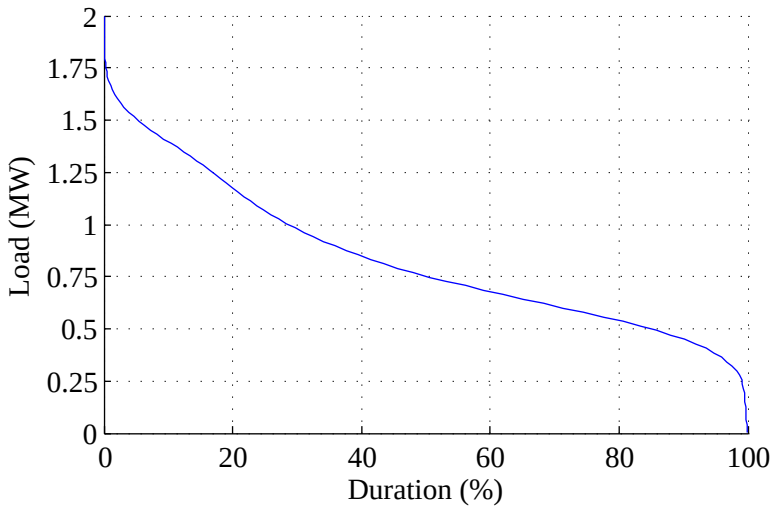

Figure 5.2: Load duration curve

be fully correlated. This is valid since in a distribution system of this size the correlation between the wind speeds at different area are high. For example, in the network analyzed as Case study II, there are wind turbines from around eleven locations in the network. The correlation between them varies between 0.83 and 0.96.

5.4.2.2 Siting the wind farms for maximizing the hosting capacity of the network

Before any optimization is done on the hosting capacity of the network, the optimal siting of the wind farms should be chosen based on the objective in consideration: maximizing the wind power hosting capacity of the network, in this case. Based on the discussion in Chapter 4, buses 7, 11, 20, 28, 33, 39, 54, 59 can be determined as those combination of buses which result in maximum hosting capacity.

5.4.2.3 Hosting capacity and the active management strategies

In this section the role of each active management strategy in increasing the hosting capacity of the system is presented. Two cases of average wind speeds are considered:

- Case 1: with average speed of 7.5 m/s with a shape factor of 2 resulting in a capacity factor of 33.4%
- Case 2: with average speed of 6.5 m/s with a shape factor of 2 resulting in a capacity factor of 25.6%

Fig. 5.3 shows the capacity of wind power that can be installed using different AMSs. The hosting capacity is found to be the same for both Case 1 and 2. This is partly because the same load data are taken for both cases. This means that the amount of wind power that can be installed in both cases is the same for the first three scenarios–no active management strategy (No AMS), coordinated OLTC voltage control (C-OLTC), and reactive power compensation (RPC)–as the hosting capacity depends on the minimum loading condition rather than the wind power condition on the system. In the fourth scenario, which is the case of wind energy curtailment (WEC), wind energy is curtailed so as to achieve the same level of hosting capacity as in the case of RPC. Consequently, 0.8% and 0.5% of the wind energy is respectively curtailed for Case 1 and Case 2. With this amount of curtailed energy, together with RPC and C-OLTC, the final capacity with all AMSs involved is calculated, which is shown as the last bar of Fig. 5.3.

Fig. 5.3 shows that the hosting capacity can be increased significantly by using AMSs. The actual increase in hosting capacity in case of RPC depends on the level of reactive power available from the wind turbines–here operation up to a minimum power factor of 0.95 is assumed. However, even if there is sufficient amount of reactive power, after some level, the thermal capacity of the involved components, such as cables and transformers, limits the amount of wind power that can be installed using RPC. In the case of energy curtailment, the hosting capacity can be increased infinitely in theory. However, the economics of the wind power installation determine the amount of wind energy one is willing to curtail.

Table 5.3 shows the amount of energy lost annually due to introduction of wind power using the various AMSs. It can be seen that for both cases (Case 1 and Case 2) that energy is saved due to loss reduction when wind power is installed using No AMS and C-OLTC. This is mainly due to low level wind power in the system. In case of RPC, due to extra consumption of reactive power

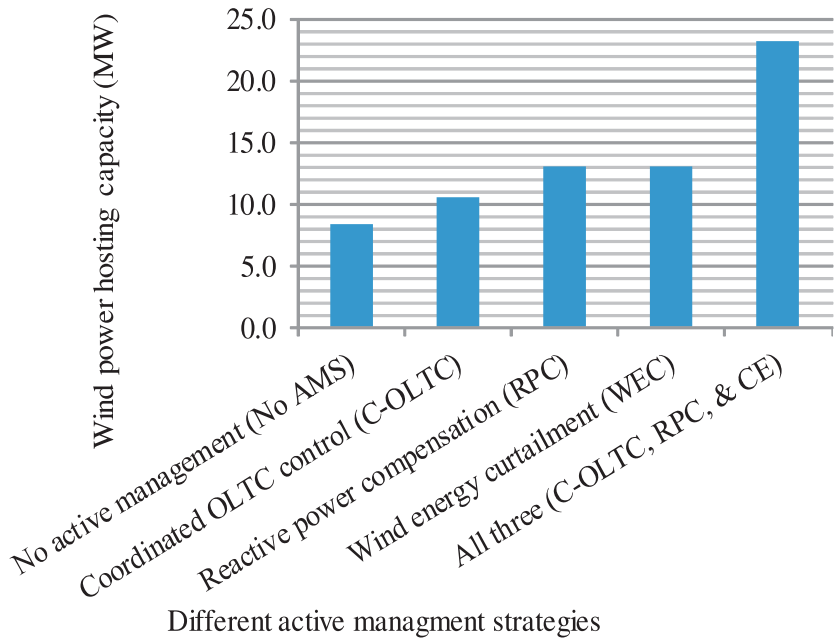

Figure 5.3: The role of AMS in increasing the hosting capacity (for both Case 1 & 2)

there is an increase in power losses. In case of WEC there is a loss in energy due to curtailment and gain in energy due to saving in power losses.

Table 5.3: Lost energy due to active management strategies (AMSs)

AMS type	Increase in Losses (MWh)		Curtailed energy (MWh)		**Total energy lost (MWh)**	
	Case 1	Case 2	Case 1	Case 2	**Case 1**	**Case 2**
No AMS	-524	-495	0	0	**-524**	**-495**
C-OLTC	-341	-410	0	0	**-341**	**-410**
RPC	-21	-267	0	0	**-21**	**-267**
WEC	-68	-289	305	144	**236**	**-145**
RC & WEC & C-OLTC	3267	1639	572	266	**3838**	**1905**

Moreover, given the same capacity of wind power, wind farms with higher capacity factors result in higher losses in the system, as shown in Table 5.3. This is because on one hand the current flow through the network will be higher which results in higher losses. On the other hand, with a higher capacity factor, the curtailed energy increases due to the increase in coincidence of high wind power and low load condition in the system.

5.4.2.4 Optimal hosting capacity of the distribution system

The analysis in this section is done by limiting RPC in such away that the minimum operating power factor is equal to or greater than 0.95 while the optimal level of curtailed energy is determined. Moreover any present worth calculation in this section is done with a discount rate of 5%.

Case DSO$^{\text{CE\&Loss}}$: In this case the DSO is assumed to pay the cost of curtailed energy and power loses in the network.

Table 5.4 also shows the optimal capacity, the optimal curtailed energy, increase in network power losses, and the net benefit (NB) generated by each actor during the life time of the wind farm. The cases refer to the two cases of wind speed considered in Section 5.4.2.3. When calculating the net benefit of the WFO using (5.7) the formula for coefficient β_i in (5.27) is modified as the WFO does not pay for curtailed energy. Similar modification is done to the coefficient b_i in Case WFO$^{\text{CE\&Loss}}$ below.

For Case 2, compared to the No AMS case considered in Section 5.4.2.3, the hosting capacity of the network is increased by as much as 136 $\%\left(=\frac{19.8-8.4}{8.4}\times 100\right)$, with a corresponding increase in NB generated by the DSO and WFO. Such an increase is achieved mainly by using RPC with very little support from wind energy curtailment.

Table 5.4: The optimal hosting capacity of the system for Case DSO$^{\text{CE\&Loss}}$

Cases	Case 1	Case 2
Hosting capacity (MW)	16.7	19.8
Curtailed energy (%)	0.01	0.02
Increase in average power losses (kW)	33	41
NB of the DSO(€)	2 550 000	2 810 000
NB of the WFO(€)	15 200 000	7 700 000

Inline with the observation made in Section 5.4.2.3, RPC is favored instead of wind energy curtailment as it results in lower energy loss. Moreover, the cost of wind energy curtailment includes not only the cost of electricity curtailed but also the cost of green certificate not sold. However, RPC causes power losses for which the DSO covers the cost of electricity only.

With respect to the DSO, lower capacity factor wind farms are preferred in this system as can be seen in Table 5.4. This is because, for a given wind farm size, wind farms with higher capacity factor introduce higher power flows and cause more loss than lower capacity factors. However, the network fee arrangement does not favor that much wind farms with higher capacity factor. To explain the situation, in this analysis, there are two main components of the network fee: the peak power fee and the distribution fee. The peak power fee is assumed to be invariant with respect to the capacity factor of the wind farm. This is based on the observation of one year measurement data available from wind turbines of various capacity factor i.e. the average monthly peak power is not seen to increase with capacity factor. Hence, in this analysis, the average monthly peak power is taken to be 0.94 pu for both cases, i.e. Case 1 and Case 2. The other is the distribution fee which depends on the capacity factor of the wind farm. But compared to the cost of power loss due to a MWh of electricity from the wind farm, the income generated from distribution fee is not significant.

Clearly, for the WFO, the net benefit increases with the capacity of the wind farm. As can be seen in Table 5.4, though the capacity of the wind farm is greater in Case 2, due to higher capacity factor the WFO have generated more NB in Case 1.

Over all, as can be seen in Fig. 5.4, the main source of income for the DSO is the network fee while the main cost of the DSO is the increase in power loses in the system. Though the cost of the

increase in power losses are considerably low compared to the revenue gained from network fee, it is the main limiting factor that hinders further increase in hosting capacity. Moreover, the figure also shows that the cost of curtailed energy is negligible.

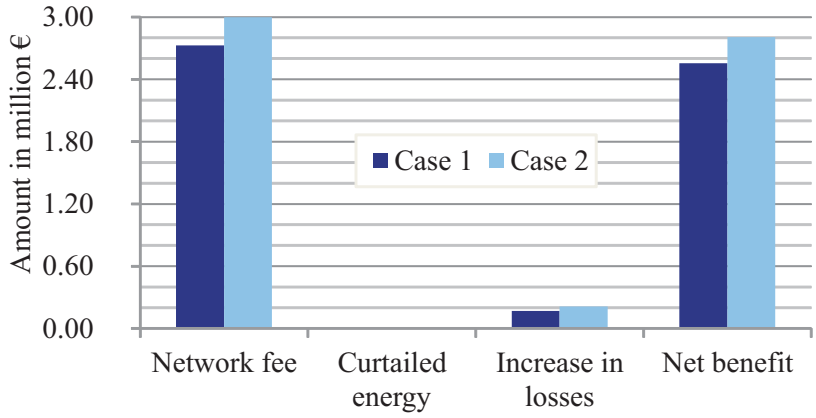

Figure 5.4: The cash flows of the DSO

Case WFO$^{\text{CE\&Loss}}$: In this case the WFO is assumed to pay the cost of curtailed energy and power loses in the network.

Table 5.5 shows that the optimal capacity of the network is increased compared to the DSO$^{\text{CE\&Loss}}$ case by 33 % $\left(= \frac{26.3-19.8}{19.8} \times 100\right)$. This is a staggering increase of 213 %$\left(= \frac{26.3-8.4}{8.4} \times 100\right)$ compared to the No AMS case. The optimal level of energy curtailment has also increased to 3% compared to the DSO$^{\text{CE\&Loss}}$ case . This is because RPC alone cannot assist a further increase in hosting capacity when the thermal rating is also a limiting factor. The power losses in the system have also increased considerably. Now, since no cost is assumed on the DSO, the NB of the DSO has increased significantly. The NB of the WFO has also increased.

Table 5.5: The optimal hosting capacity of the system for Case WFO$^{\text{CE\&Loss}}$

Cases	Case 1	Case 2
Hosting capacity (MW)	26.3	26.2
Curtailed energy (%)	3.0	1.6
Increase in average power losses (kW)	472	236
NB of the DSO(€)	4 200 000	3 940 000
NB of the WFO(€)	20 100 000	8 300 000

When it comes to the determination of the limiting factor to the increase in hosting capacity, the two cases of wind farm capacity factor can be seen separately. In Case 1, the hosting capacity is limited as a further increase in hosting capacity using energy curtailment is found to be less profitable than investing on a new substation. In other words, a further increase in hosting capacity is limited by the constraint in (5.28). In Case 2 the hosting capacity is limited as further curtailment is less profitable due to costs of power losses and curtailed energy.

Moreover, different cash flows of the WFO are shown in Fig. 5.5. Though there is a substantial income from electricity and green certificate sell, this income covers a number of costs. However,

the AMS costs (which includes the cost curtailed energy and the implementation cost of AMSs) is very low compared to costs like investment cost and operation and maintenance costs (O&M costs).

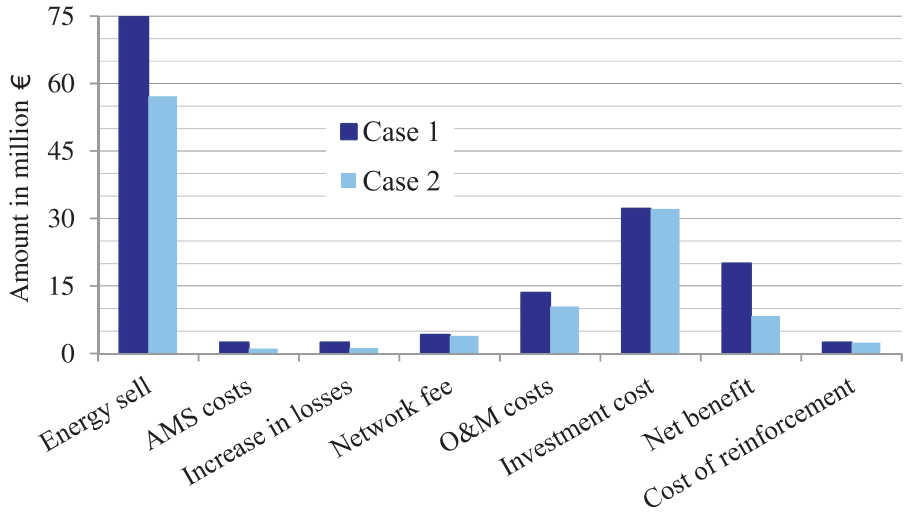

Figure 5.5: The different cash flows of the WFO

One can also further investigate the case where the DSO covers for the cost of power losses in the network and the WFO bears the cost of curtailed energy. However, as seen in Fig.5.4, since there is only a negligible cost associated with curtailed energy in the $DSO^{CE\&Loss}$ case, waiving the cost of curtailed energy from the DSO will not increase the hosting capacity of the network with respect to the DSO. Hence unless the WFO covers part of or all of the increase in loss due to the wind farm, the hosting capacity of the network will be limited to 16.7 MW in Case 1 and 19.8 MW in Case 2.

5.4.3 Case study II: Falbygdens Energi's network

5.4.3.1 Network and data description

Network description: Case study II is based on a rural 11 kV distribution system operated by Falbygdens Energi located in Falköping area in Sweden. The network is fed by a 40 kV grid through a $45 \pm 8 \times 1.67\%/11.5$ kV, 10 MVA transformer. The tap changer of the transformer regulates the low voltage side of the transformer at 0.97 ± 0.012 pu[1]. The voltage in the distribution system should be within $\pm 5\%$ of the nominal value, i.e. 0.97 pu. There are 13 wind turbines, with an overall installed capacity of 12.225 MW, already connected to the distribution system. A new wind farm is to be connected directly to the substation with an independent cable (see Fig 5.6). The distance of the wind farm from the substation is 5 km.

Data description: The existing 13 wind turbines in the distribution system have a varying capacity factor (CF) between 20% and 28% based on the available one year measurement data. From each

[1] 11 kV is taken as the base voltage

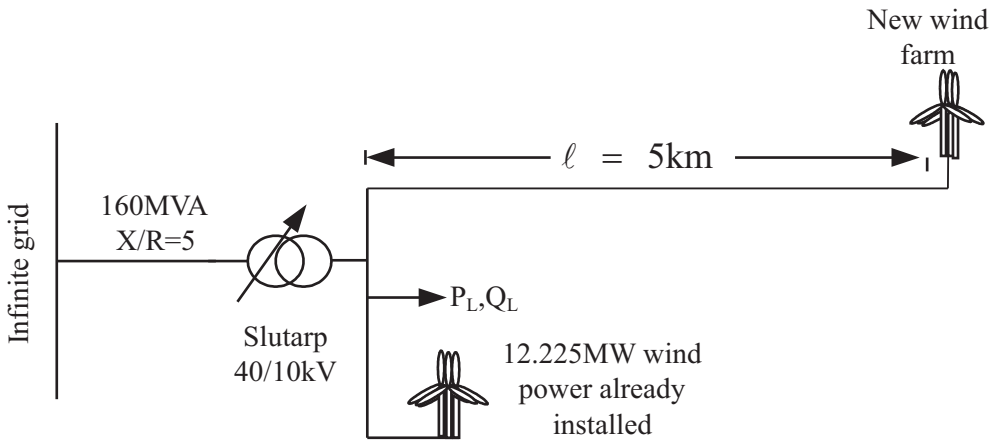

Figure 5.6: Simplified network of Fabygdens Energi

of these wind turbines there is one year hourly measured active power data. Hourly measured active and reactive power data at the substation are also available for the same period. Adding the wind power data and the active power data from the substation, the load along with active power losses in the network is extracted. This calculation shows the minimum loading condition in the system to be 0.5 MW. The reactive power is assumed to come from the load. These time series load and wind power data are directly used in the optimization model.

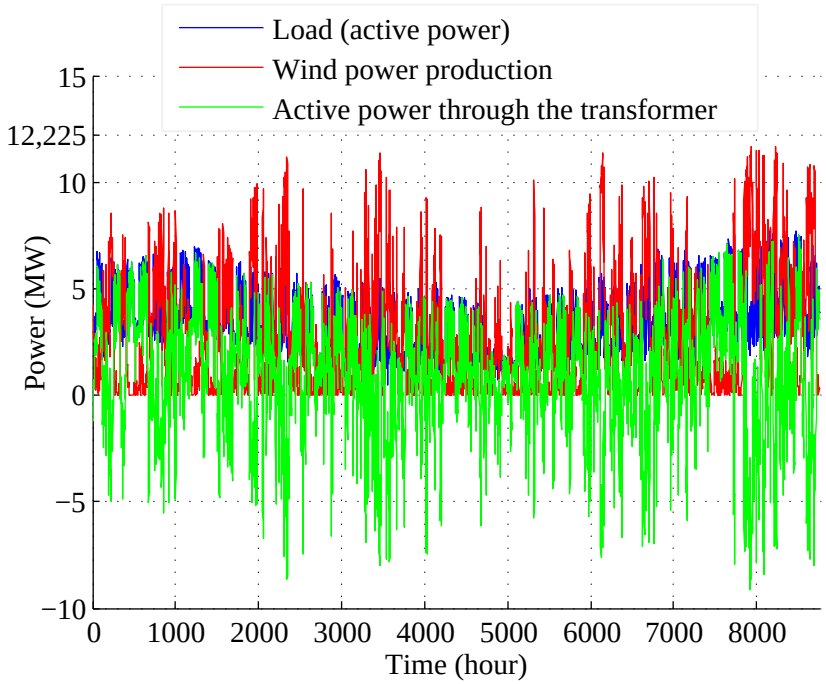

Figure 5.7: The load, wind and reverse power flow condition in the existing system

Fig 5.7 shows the existing condition of load and wind power and the power flow through the substation transformer. Though the substation transformer is 10 MVA with minimum loading condition of 0.5 MW and installed wind power capacity of 12.225 MW, the maximum reverse power flow through transformer based on the one year measurement data shown in Fig 5.7 is 9.14 MW.

5.4.3.2 Optimal hosting capacity of the distribution system

It should be noted that, with the given transformer size and the observed minimum loading condition, even without additional wind power, there is a probability of overloading the substation transformer. Hence the optimal hosting capacity of the system is calculated using energy curtailment and coordinated OLTC voltage control as an AMS. RPC is not used here since coordinated OLTC voltage control is enough to deal with the voltage rise during high wind power output. Thus, the wind turbines are assumed to operate at unity power factor.

Case $\text{DSO}^{\text{CE\&Loss}}$: Similar to the same case considered in Section 5.4.2.4, here the DSO is assumed to cover the cost of curtailed energy and power losses in the system. Then, the optimal hosting capacity is determined for three cases of wind power capacity factor: 28%, 24%, and 20%. The results of the analysis, presented in Table 5.6, show that with a small percentage of curtailed energy a significant increase in hosting capacity can be achieved. With the existing transformer size and the minimum loading condition, it is only possible to install 10.5 MW of wind power without overloading the transformer. But by allowing 1% WEC, the hosting capacity can be increased up to 16.825 MW (= 12.225 MW + 4.6 MW). This amounts to an increase of 60% in hosting capacity of the distribution system.

Table 5.6: Optimal level of additional wind power in the system with respect to the DSO

Capacity factor	28%	24%	20%
Additional capacity (MW)	4.6	4.0	4.4
Curtailed Energy (%)	0.9	1.3	1.6
Increase in average power losses (kW)	27	18	19
Cost of curtailed energy (€)	100 000	110 000	120 000
Cost of increased network losses (€)	140 000	90 000	90 000
Revenue due to network fee (€)	760 000	630 000	660 000
DSO's net benefit (€)	520 000	430 000	450 000
WFO's net benefit (€)	2 634 000	1 086 000	31 000
Cost of grid reinforcement (€)	430 000	370 000	410 000

The increase in hosting capacity gained here is not as much as the $\text{DSO}^{\text{CE\&Loss}}$ case in Section 5.4.2.4. This is due to the fact that here it is mainly energy curtailment and coordinated voltage control that are used to increase the hosting capacity unlike in the aforementioned case, where RPC is used. And, as mentioned previously, the loss increase due to RPC costs less than the energy loss due to curtailment.

Table 5.6 shows also different cash flows of the DSO during the life time of the project due to this additional wind power. These cash flows are calculated assuming a discount rate of 5%. Compared to the cost of grid reinforcement needed, the cost of curtailed energy is less than one third. This clearly shows the advantage of using AMSs, such as WEC, to increase the hosting capacity of a distribution system.

Moreover, the limiting factors with respect to the DSO in this case study are costs of both curtailed energy and increase in network power losses; in the same scenario considered in Case study I, the limiting factor was the loss increase. It is interesting to see that, even though the cables between

the wind farm and the substation are not as lossy as in the network in Case study I , the increase in network losses still plays a significant role in determining the hosting capacity of the network.

Unlike the case studied in Section 5.4.2.4, Table 5.6 does not show the hosting capacity to follow a specific trend with the CF of the wind turbine. This is because the effect of increase in loss with capacity factor is not as severe as in the Case study I.

In summary, the analysis shows that, in networks of different types, DSO can use AMSs to increase the hosting capacity of the network thereby increasing the benefit obtained from wind power as well as promoting the cost effective way of integrating wind power to the power system.

Case WFO^{CE} : In Case study I, though it seems unlikely, we have considered the case where the WFO covers the cost of curtailed energy and increase in network loss. Otherwise, the hosting capacity will be limited to a lower value as determined in the Case $\text{DSO}^{\text{CE\&Loss}}$. In contrast, here we consider the case where the WFO covers only the cost of curtailed energy. The increase in loss will be covered by the DSO.

Table 5.7 presents the optimal hosting capacity, WEC level, and the net benefit of the WFO for three cases, which differ based on the CF of the wind power and the discount rate (DR) of the investment. The cases are:

- Case 1: CF = 28% and DR = 5%.
- Case 2: CF = 28% and DR = 7.5%.
- Case 3: CF = 24% and DR = 5%.

Table 5.7: Optimal wind power capacity with respect to WFO for different capacity factors and discount rates

Case	1	2	3
Additional capacity(MW)	7.0	7.5	6.0
Curtailed Energy (%)	3.3	4.1	3.8
Increase in average power losses (kW)	53	59	34
WFO's net benefit (€/life time)	3 420 000	1 250 000	1 190 000
DSO's net benefit(€/lifetime)	810 000	847 000	731 000

The different cash flows of the WFO are provided in Fig 5.8. These include revenues from energy sell (which includes the revenue from both electricity and green certificate sell), the cost due to network fee, O&M costs, the expected investment cost, the cost of AMSs (which includes the cost of curtailed energy and the implementation cost of AMSs), and the net benefit.

Compared to the the same case in Table 5.6 where the wind turbine has a capacity factor of 28%, the additional curtailment in wind power, e.g. $\frac{3.3\%-0.9\%}{0.9\%} = 2.7$, does not result in a comparable boost in hosting capacity of the network, e.g. $\frac{7.0-4.6}{4.6} = 0.5$. But still a significant increase in hosting capacity, 83% $\left(= \frac{12.225+7.0-10.5}{10.5}\right)$, is achieved with a relatively small curtailed energy, 3.3%. Moreover the AMS costs, as shown in Fig 5.8, is very low compared to other costs of the WFO.

Table 5.7 shows also that the hosting capacity decrease with the decrease in CF of the wind turbine in case of the WFO. This is reasonable as less CF implies less revenue for the WFO. Hence the

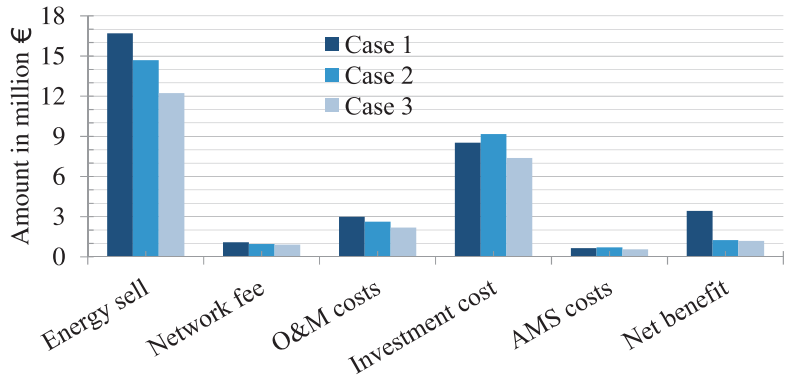

Figure 5.8: Expected cash flows of the WFO for each scenario shown in Table 5.7

WFO has less motivation to install more wind power when parts of the energy production is to be curtailed. However, in contrast to our expectation, the table shows that when the DR is increased i.e. from Case 1 to Case 2, more wind power is installed. This is because the hosting capacity in the analysis is limited due to the constraint in (5.28) i.e. a further increase in hosting capacity using WEC is found to be less profitable than investing on new substation. Since grid reinforcement is assumed to be composed of upfront costs only, it does not depend on DR. However, higher DR decreases the net present value of the cost of curtailed energy. This means with higher DR, larger wind power capacity can be installed by curtailing more wind energy.

Fig. 5.9 presents more clearly the idea discussed in the above paragraph. The analysis is done for wind power having a CF of 28%. The figure shows that the hosting capacity of the distribution

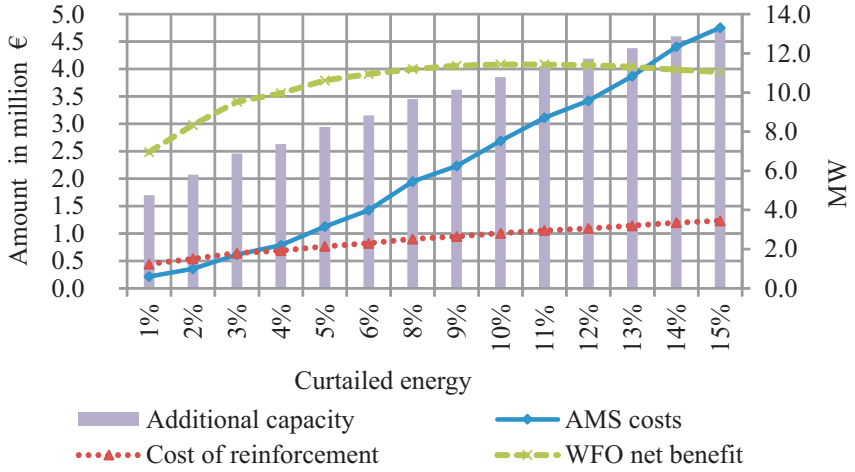

Figure 5.9: Comparing the investment options of the WFO

system can be increased indefinitely using curtailment. But the net benefit of the WFO increases only until the curtailed energy reaches 10%. Even curtailing this level of energy is unreasonable as grid reinforcement can generate more profit. In fact, as can be seen from Fig. 5.9, WEC is attractive only up to 3.3%.

On the other hand, Fig. 5.10 shows the costs and benefits of the DSO when the WFO bears the

cost of curtailed energy. Despite significant loss in revenue due to increased power losses, the DSO continues to generate more revenue as the capacity of wind power in the system is increased. However, this observation holds true only for this case study. In Case study I, we have noticed that the increase in loss alone determines the optimal hosting capacity of the network with respect to the DSO. For example, in case of a wind farm with capacity factor 33.4%, almost immediately after 16.7 MW capacity of wind power the net benefit of the DSO would have declined if a similar analysis is done.

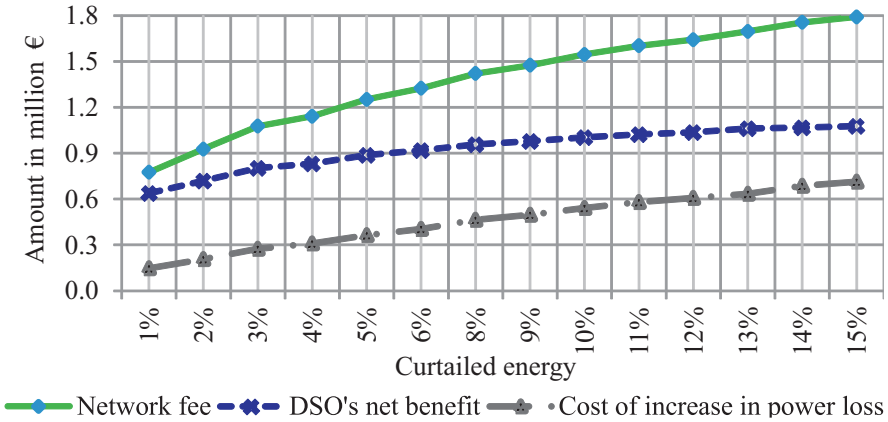

Figure 5.10: Costs and benefits of the DSO

5.5 Summary

The analyses in this chapter have identified voltage rise and thermal overloading as the two most likely limiting factors of wind power integration to a distribution system. Consequently, three active management strategies (AMSs) have been investigated to increase the hosting capacity of a distribution network constrained due to these limiting factors. The AMSs include coordinated on-oad tap changer voltage control (C-OLTC), reactive power compensation (RPC), and wind energy curtailment (WEC). C-OLTC is a preferred option to deal with voltage rise problems followed by RPC. If both solutions fail to achieve their objective, they can be assisted by WEC. To deal with the overloading of system components due to wind power the only solution considered in this thesis is WEC.

To further facilitate the investigation, a mathematical model based on cost-benefit analysis is developed. The model also assesses the profitability of using AMSs with respect to grid reinforcement. The result of the investigation shows that the wind power hosting capacity of a distribution system can be increased up to twice the capacity that could be installed based on worst case analysis.

The optimal level of hosting capacity and curtailed energy depends on the capacity factor of the wind power plant and the discount rate. With respect to the WFO, higher capacity factor implies higher hosting capacity. But it is also affected by the discount rate, the cost of curtailed energy, and the cost of grid reinforcement. On the other hand, the optimal level of curtailed energy in our analysis is found to be of low magnitude. After some level, e.g. a maximum of 3.8% in Case study II, it is not attractive to curtail more wind energy in order to increase the hosting capacity of the network.

6

Conclusions and future work

This thesis provides an analysis of wind power in distribution systems aimed at maximizing the wind power hosting capacity of such systems. Various power quality and reliability effects of wind power is analyzed. In particular, the effect of wind power on the frequency of tap changes is investigated using a model developed in this thesis. A mitigation solution based on reactive power compensation from the wind turbines is proposed to decrease the frequency of tap changes. The thesis also identifies the limiting factors of wind power integration based on which the siting of wind turbines in a given distribution system is proposed. Finally an optimization model is developed that can be used to assess the optimal hosting capacity of distribution systems. Different investigations in the thesis are supported by case studies based on a real-life network, and measured load and wind power data obtained from Falbygdens Energi.

6.1 Main conclusions

The main conclusions of the thesis are:

- In addition to the common integration issues of wind power (such as overvoltage, overloading, etc) some DSOs are concerned about the effect wind power on increasing the frequency of tap changes (FTC).
  - ◇ Based on our analysis, for distribution systems connected to strong external grids (with $X/R \geq 5$), no significant effect on the FTC is seen due to the introduction of wind power. However, in a distribution system connected to an external grid with lower X/R ratio, the FTC can be affected significantly due to the introduction of wind power.
  - ◇ A further investigation is carried out to decrease the FTC using the reactive power available from variable speed wind turbines. The result shows that the methodology is very effective. However, the reactive power required to reduce the FTC by a specific percent depends on the SCC and the X/R ratio. The reactive power requirement decreases with higher SCC and X/R ratio.
- Our analysis identifies the following conditions at which each of the different integration issues could become a limiting factor.

- ◇ Overvoltage has been identified as one of the main limiting factors in radial distribution networks. It usually occurs when wind turbines are connected to a PCC away from the station where the grid is weak.
- ◇ Overloading of network components such as cables and transformers becomes a limiting factor when the wind turbines are installed close to the substation so that overvoltage is not a problem.
- ◇ Harmonics and flicker can become a limiting factor in a distribution system connected to a relatively weak external grid and the wind farm is close to the substation, so that overvoltage is not a problem. However, with the advent of variable speed wind turbines, flicker is less likely to be a limiting factor. Rather it is harmonic emission limits that may become limiting factors, especially the limits on low order even harmonics are more stringent to fulfill for wind turbines.
- ◇ Increased fault level can become a limiting factor in rare cases where the distribution system is connected to a relatively strong grid, and the wind turbines, which are of Type A, B, or C, connected close to the station. Moreover the substation has higher overload capacity, so overloading is not a problem. However, it depends on the rating of the switchgear which will determine the short-circuit capacity margin left to handle additional fault current from the wind turbines.
- ◇ Protection malfunctioning, more or less, does not become a limiting factor but it needs investigation to ensure such a condition does not arise.
- ◇ In general, however, the usual and main limiting factors of wind power integration are voltage rise and overloading.

- Moreover, with the different limiting factors in place corresponding to the different characteristic of the distribution system and the wind turbines, the optimal siting problem has been investigated in this thesis. The main conclusions are:
  - ◇ In a distribution system where there are a couple of equally favorable sites/buses to wind power connection, then the ones electrically close to the substation–distributed on different feeders or laterals–would maximize the hosting capacity of the distribution system.
  - ◇ Installing the wind turbines away from the substation would effectively limit the hosting capacity of the feeder, especially if the limiting factor is the voltage rise problem.
  - ◇ The only case when one may want to connect the wind turbines away from the substation is if the wind power hosting capacity the distribution system is limited due to increased fault level.
- For a distribution system whose hosting capacity is limited due to voltage or overloading, different active management strategies are proposed in literature to increase the hosting capacity of the network. To assess the optimal use of these active management strategies thereby determine the optimal hosting capacity of the network, an optimization model based on cost benefit analysis is developed in this thesis. This model is applied to two separate case studies and the following conclusions are made:
  - ◇ Coordinated OLTC voltage control and reactive power compensation can be effectively used to increase the wind power hosting capacity of a distribution system limited due voltage rise problem. A case study based on such systems has shown an increase in hosting capacity up to double the capacity that would be installed based on worst case analysis. Such an increase is achieved with very little help from energy curtailment.

◇ Energy curtailment is the only option investigated in this theses to increase the hosting capacity of a network constrained due to thermal overloading of network components. A case study carried out shows that the optimal hosting capacity of such a network depends on who covers the cost of curtailed energy: the DSO or the WFO. In either case the hosting capacity is increased considerably. In the case of the DSO, the hosting capacity of the network is increased by as much as 60% by allowing a mere 1% WEC. For the WFO the increase in hosting capacity depends on the CF of the wind turbines and the DR. In our analysis, the hosting capacity is increased by as much as 83% with the curtailed energy being only 3.3%. Unlike the case of DSO, here the hosting capacity is limited as the alternative option, i.e. grid reinforcement, becomes more attractive than curtailment if the WFO wants to install more. Hence when determining the optimal level of wind power curtailment, one should not only focus on the profitability of the WEC but also a comparison should be made with an alternative option, such as grid reinforcement.

6.2 Future work

This thesis tries to cover a number of issues of wind power integration in a distribution systems. The following issues need more investigation:

- Though voltage flickers are less likely to be limiting factor in a typical distribution system, its assessment would be more complete if it is supported by measuring the actual flicker level in the system.
- Given low order harmonics are more stringent to fulfill by wind turbines and could become a limiting factor to further integration of wind power to the system, it would be valuable if such investigation is supported by the measurement of the harmonic emissions in the system. If there is such a problem, mitigating solutions need to be investigated.
- Moreover, we have continuously used the IEC approach when assessing the flicker and the harmonic emissions from different wind turbines. It would be valuable if the result arrived at based on this analysis is compared against simulation results.
- Though a rough fault current contribution from wind turbines is analyzed, mostly based on IEC standard, such analysis can more accurately be made using simulations.

Moreover, in Chapters 3 and 5 active management strategies are analyzed to deal with the problem of increased FTC, voltage rise, and thermal overloading. However, these analyses are done based on only a static consideration and the actual control and operation of a system with these active management strategies is not investigated. Therefore, the structure and control of a system with active management strategies requires further investigation. This investigation includes:

- The identification of buses or components where overvoltage and thermal overloading may occur
- The identification of the wind turbines that need to curtail their wind power output or provide reactive power compensation
- The control of wind energy curtailment to relieve thermal overloading
- The control of OLTC and reactive power from the wind turbines to avoid a voltage rise

- When it comes to the use of reactive compensation for reducing the FTC, the investigation of the control strategy to achieve the same
- Moreover, one can also investigate the control of the wind turbines in the system for loss minimization

Moreover in addition to the active management strategies investigated in this thesis, others such as demand side management and energy storage, which may include electric vehicles, can be analyzed to increase the wind power hosting capacity of distribution systems.

References

[1] J. L. Sawin, E. Martinot, and Others, "Renewables 2013 global status report," tech. rep., REN21, Paris, France, June 2012.

[2] S. Krohn, P.-E. Morthorst, and S. Awerbuch, "The economics of wind energy," tech. rep., European Wind Energy Association (EWEA), Brussels, Mar. 2009.

[3] S. Liew and G. Strbac, "Maximising penetration of wind generation in existing distribution networks," *Generation, Transmission and Distribution, IEE Proceedings-*, vol. 149, pp. 256 –262, May 2002.

[4] P. Siano, P. Chen, Z. Chen, and A. Piccolo, "Evaluating maximum wind energy exploitation in active distribution networks," *Generation, Transmission Distribution, IET*, vol. 4, pp. 598 –608, May 2010.

[5] J. Mutale, "Benefits of active management of distribution networks with distributed generation," in *Power Systems Conference and Exposition, 2006. PSCE '06. 2006 IEEE PES*, pp. 601 –606, Nov. 2006.

[6] A. Shafiu, T. Bopp, I. Chilvers, and G. Strbac, "Active management and protection of distribution networks with distributed generation," in *IEEE Power Engineering Society General Meeting, 2004*, pp. 1098 –1103 Vol.1, June 2004.

[7] J. Zhang, H. Fan, W. Tang, M. Wang, H. Cheng, and L. Yao, "Planning for distributed wind generation under active management mode," *International Journal of Electrical Power & Energy Systems*, vol. 47, pp. 140–146, May 2013.

[8] L. Ochoa, C. Dent, and G. Harrison, "Distribution network capacity assessment: variable DG and active networks," *IEEE Transactions on Power Systems*, vol. 25, no. 1, pp. 87–95, 2010.

[9] S. N. Salih, P. Chen, and O. Carlson, "Maximizing wind power integration in distribution system," in *10th International Workshop on Large-Scale Integration of Wind Power into Power Systems as well as on Transmission Networks for Offshore Wind Power Plants*, Oct. 2011.

[10] L. Ochoa, C. Dent, and G. Harrison, "Maximisation of intermittent distributed generation in active networks," in *SmartGrids for Distribution, 2008. IET-CIRED. CIRED Seminar*, pp. 1 –4, June 2008.

[11] T. Ackermann, *Wind Power in Power Systems*. John Wiley & Sons, Apr. 2005.

[12] A. Dai and C. Deser, "Diurnal and semidiurnal variations in global surface wind and divergence fields," *Journal of Geophysical Research: Atmospheres (1984–2012)*, vol. 104, no. D24, p. 31109–31125, 1999.

[13] D. Heide, L. von Bremen, M. Greiner, C. Hoffmann, M. Speckmann, and S. Bofinger, "Seasonal optimal mix of wind and solar power in a future, highly renewable europe," *Renewable Energy*, vol. 35, pp. 2483–2489, Nov. 2010.

[14] R. Gasch and J. Twele, *Wind Power Plants: Fundamentals, Design, Construction and Operation*. Springer, Dec. 2011.

[15] C. Achberger, D. Chen, and H. Alexandersson, "The surface winds of sweden during 1999–2000," *International Journal of Climatology*, vol. 26, no. 2, p. 159–178, 2006.

[16] B. Fox, *Wind power integration: connection and system operational aspects*, vol. 50. of *IET power and energy series*. Institution of Engineering and Technology, Jan. 2007.

[17] A. D. Hansen, F. Iov, F. Blaabjerg, and L. H. Hansen, "Review of contemporary wind turbine concepts and their market penetration," *Wind Engineering*, vol. 28, no. 3, p. 247–263, 2004.

[18] N. Jenkins, R. Allan, P. Crossley, D. Kirschen, and G. Strbac, *Embedded Generation (IEE Power)PBPO0310*. Power \& Energy Ser. 31, Institution of Engineering and Technology, July 2000.

[19] L. Holdsworth, X. Wu, J. Ekanayake, and N. Jenkins, "Comparison of fixed speed and doubly-fed induction wind turbines during power system disturbances," *Generation, Transmission and Distribution, IEE Proceedings-*, vol. 150, no. 3, pp. 343–352, 2003.

[20] M. Bongiorno and T. Thiringer, "A generic DFIG model for voltage dip ride-through analysis," *IEEE Transactions on Energy Conversion*, vol. 28, no. 1, pp. 76–85, 2013.

[21] M. Stiebler, *Wind Energy Systems for Electric Power Generation*. Springer, Oct. 2008.

[22] T. Thiringer, J. Paixao, and M. Bongiorno, "Monitoring of ride-through ability of a 2MW wind turbine in tvååker, halland," Elforsk rapport 09:26, Feb. 2009.

[23] T. Lund, P. Sørensen, and J. Eek, "Reactive power capability of a wind turbine with doubly fed induction generator," *Wind Energy*, vol. 10, no. 4, p. 379–394, 2007.

[24] S. Engelhardt, I. Erlich, C. Feltes, J. Kretschmann, and F. Shewarega, "Reactive power capability of wind turbines based on doubly fed induction generators," *IEEE Transactions on Energy Conversion*, vol. 26, no. 1, pp. 364–372, 2011.

[25] O. Anaya-Lara, *Wind energy generation: modelling and control*. John Wiley & Sons, Jan. 2009.

[26] N. Ullah, K. Bhattacharya, and T. Thiringer, "Wind farms as reactive power ancillary service providers #x2014;technical and economic issues," *IEEE Transactions on Energy Conversion*, vol. 24, no. 3, pp. 661–672, 2009.

[27] T. A. Short, "Voltage regulation," in *Electric Power Distribution Handbook*, CRC Press, Sept. 2003.

[28] "AMP - anslutning av mindre produktion till elnätet,"

[29] EN CENELEC, "EN 50160: 1999–Voltage characteristics of electricity supplied by public distribution systems," *European standard (supersedes 1994 edition)*, 1999.

[30] IEC Standard 61000-4-15, "Electromagnetic compatibility (EMC) - part 4-15: Testing and measurement techniques - flickermeter - functional and design specifications," Aug. 2010.

[31] Z. Chen, "Issues of connecting wind farms into power systems," in *Transmission and Distribution Conference and Exhibition: Asia and Pacific, 2005 IEEE/PES*, pp. 1 –6, 2005.

[32] J. Mur-Amada and . A. Bayod-Rújula, "Flicker emission of wind farms during continuous operation," *Parameters*, vol. 1, p. 50.

[33] A. Larsson, "Flicker emission of wind turbines during continuous operation," *IEEE Transactions on Energy Conversion*, vol. 17, pp. 114 –118, Mar. 2002.

[34] IEC standard 61400-21, "Wind turbines-part 21: Measurement and assessment of power quality characteristics of grid connected wind turbines," Aug. 2008.

[35] IEC 61000-2-12, "Electromagnetic compatibility (EMC) – part 2-12: Compatibility levels for low-frequency conducted disturbances and signaling in public medium-voltage power supply systems," 2003.

[36] IEC 61000-3-6, "Electromagnetic compatibility (EMC) - part 3-6: Limits - assessment of emission limits for the connection of distorting installations to MV, HV and EHV power systems," 2008.

[37] A. Robert, T. Deflandre, E. Gunther, R. Bergeron, A. Emanuel, A. Ferrante, G. Finlay, R. Gretsch, A. Guarini, J. Gutierrez Iglesias, D. Hartmann, M. Lahtinen, R. Marshall, K. Oonishi, C. Pincella, S. Poulsen, P. Ribeiro, M. Samotyj, K. Sand, J. Smid, P. Wright, and Y. Zhelesko, "Guide for assessing the network harmonic impedance," in *Electricity Distribution. Part 1: Contributions. CIRED. 14th International Conference and Exhibition on (IEE Conf. Publ. No. 438)*, vol. 1, pp. 3/1–310 vol.2, June 1997.

[38] W. Xu, E. Ahmed, X. Zhang, and X. Liu, "Measurement of network harmonic impedances: practical implementation issues and their solutions," *IEEE Transactions on Power Delivery*, vol. 17, pp. 210–216, Jan. 2002.

[39] R. Langella and A. Testa, "A new method for statistical assessment of the system harmonic impedance and of the background voltage distortion," in *International Conference on Probabilistic Methods Applied to Power Systems, 2006. PMAPS 2006*, pp. 1–7, June 2006.

[40] K. Duda, D. Borkowski, and A. Bien', "Computation of the network harmonic impedance with chirp-z transform," *Metrology and Measurement Systems*, vol. 16, no. 2, p. 299–312, 2009.

[41] I. 62271-100:, "High-voltage switchgear and controlgear - part 100: Alternating current circuit-breakers," Apr. 2008.

[42] IEC 60909-0, "Short-circuit currents in three-phase a.c. systems-part 0: Calculation of currents," 2001.

[43] T. Sulawa, Z. Zabar, D. Czarkowski, Y. TenAmi, L. Birenbaum, and S. Lee, "Evaluation of a $3-\phi$ bolted short-circuit on distribution networks having induction generators at customer sites," *IEEE Transactions on Power Delivery*, vol. 22, pp. 1965 –1971, July 2007.

[44] P. Bousseau, E. Gautier, I. Garzulino, P. Juston, and R. Belhomme, "Grid impact of different technologies of wind turbine generator systems (WTGS)," (Madrid), June 2003.

[45] T. N. Boutsika and S. A. Papathanassiou, "Short-circuit calculations in networks with distributed generation," *Electric Power Systems Research*, vol. 78, pp. 1181–1191, July 2008.

[46] E. Muljadi, N. Samaan, V. Gevorgian, J. Li, and S. Pasupulati, "Short circuit current contribution for different wind turbine generator types," in *2010 IEEE Power and Energy Society General Meeting*, pp. 1 –8, July 2010.

[47] J. Morren and S. W. H. De Haan, "Short-circuit current of wind turbines with doubly fed induction generator," *IEEE Transactions on Energy Conversion*, vol. 22, no. 1, pp. 174–180, 2007.

[48] P. Karaliolios, A. Ishchenko, E. Coster, J. Myrzik, and W. Kling, "Overview of short-circuit contribution of various distributed generators on the distribution network," in *Universities Power Engineering Conference, 2008. UPEC 2008. 43rd International*, p. 1–6, 2008.

[49] F. Sulla, J. Svensson, and O. Samuelsson, "Symmetrical and unsymmetrical short-circuit current of squirrel-cage and doubly-fed induction generators," *Electric Power Systems Research*, vol. 81, pp. 1610–1618, July 2011.

[50] G. Pannell, D. Atkinson, and B. Zahawi, "Analytical study of grid-fault response of wind turbine doubly fed induction generator," *IEEE Transactions on Energy Conversion*, vol. 25, no. 4, pp. 1081–1091, 2010.

[51] Z. Zheng, G. Yang, and H. Geng, "Short circuit current analysis of DFIG-type WG with crowbar protection under grid faults," in *2012 IEEE International Symposium on Industrial Electronics (ISIE)*, pp. 1072–1079, 2012.

[52] M. Wang, A. Vandermaar, and K. Srivastava, "Review of condition assessment of power transformers in service," *IEEE Electrical Insulation Magazine*, vol. 18, pp. 12 – 25, Dec. 2002.

[53] J. Jagers, J. Khosa, P. D. Klerk, and C. Gaunt, "Transformer reliability and condition assessment in a south african utility," 2007.

[54] S. Tenbohlen, T. Stirl, G. Bastos, J. Baldauf, P. Mayer, M. Stach, B. Breitenbauch, and R. Huber, "Experienced-based evaluation of economic benefits of on-line monitoring systems for power transformers," *CIGRE Session 2002*, 2002.

[55] M. Minhas, J. Reynders, and P. de Klerk, "Failures in power system transformers and appropriate monitoring techniques," in *High Voltage Engineering, 1999. Eleventh International Symposium on (Conf. Publ. No. 467)*, vol. 1, pp. 94 –97 vol.1, 1999.

[56] C. W. G. 05, "An international survey on failures in large power transformers in service," *Electra*, no. 88, pp. 21 –47, 1983.

[57] R. Jongen, P. Morshuis, J. Smit, A. Janssen, and E. Gulski, "A statistical approach to processing power transformer failure data," in *Cired 19th International Conference on Electricity Distribution*, 2007.

[58] H.-U. Schellhase, R. Pollock, A. Rao, E. Korolenko, and B. Ward, "Load tap changers: investigations of contacts, contact wear and contact coking," in *Proceedings of the Forty-Eighth IEEE Holm Conference on Electrical Contacts, 2002*, pp. 259 – 272, 2002.

[59] P. Kang and D. Birtwhistle, "On-line condition monitoring of tap changers-field experience," in *Electricity Distribution, 2001. Part 1: Contributions. CIRED. 16th International Conference and Exhibition on (IEE Conf. Publ No. 482)*, vol. 1, p. 5 pp. vol.1, 2001.

[60] M. Foata, C. Rajotte, and A. Jolicoeur, "On-load tap changer reliability and maintenance strategy," (Paris), 2006.

[61] M. Redfern and W. Handley, "Duty based maintenance for on-load transformer tap changers," in *Power Engineering Society Summer Meeting, 2001*, vol. 3, pp. 1824 –1829 vol.3, 2001.

[62] P. Kang and D. Birtwhistle, "Condition assessment of power transformer onload tap changers using wavelet analysis and self-organizing map: field evaluation," *IEEE Transactions on Power Delivery*, vol. 18, pp. 78 – 84, Jan. 2003.

[63] B. Handley, M. Redfern, and S. White, "On load tap-changer conditioned based maintenance," *Generation, Transmission and Distribution, IEE Proceedings-*, vol. 148, pp. 296 –300, July 2001.

[64] E. G. Romero, *Voltage control in a medium voltage system with distributed wind power generation*. Master thesis, Lund University, Lund, 2007.

[65] P. Carvalho, P. Correia, and L. Ferreira, "Distributed reactive power generation control for voltage rise mitigation in distribution networks," *IEEE Transactions on Power Systems*, vol. 23, pp. 766 –772, May 2008.

[66] D. S. Romero, *Voltage regulation in distribution systems - Tap changer and Wind Power*. Master thesis, Lund University, Lund, 2010.

[67] S. S. Baghsorkhi and I. A. Hiskens, "Impact of wind power variability on sub-transmission networks," in *Proceedings of the IEEE Power and Energy Society General Meeting*, July 2012.

[68] H. Saadat, *power system analysis*. PSA publishings, 2010.

[69] A. Wächter and L. T. Biegler, "On the implementation of an interior-point filter line-search algorithm for large-scale nonlinear programming," *Mathematical Programming*, vol. 106, pp. 25–57, 2006.

[70] P. Chen, *Stochastic modeling and analysis of power system with renewable generation*. PhD thesis, Aalborg university, Aalborg, Jan. 2010.

[71] P. Chen, T. Pedersen, B. Bak-Jensen, and Z. Chen, "ARIMA-Based time series model of stochastic wind power generation," *Power Systems, IEEE Transactions on*, vol. 25, pp. 667 –676, May 2010.

[72] B. Singh and S. N. Singh, "Wind power interconnection into the power system: A review of grid code requirements," *The Electricity Journal*, vol. 22, no. 5, pp. 54 – 63, 2009.

[73] S. Chandrashekhar Reddy and P. Prasad, "Power quality improvement of distribution system by optimal placement of distributed generators using GA and NN," in *Proceedings of the International Conference on Soft Computing for Problem Solving (SocProS 2011) December 20-22, 2011* (K. Deep, A. Nagar, M. Pant, and J. C. Bansal, eds.), vol. 130 of *Advances in Intelligent and Soft Computing*, pp. 257–267, Springer Berlin / Heidelberg, 2012.

[74] M. H. Aliabadi, M. Mardaneh, and B. Behbahan, "Siting and sizing of distributed generation units using GA and OPF," in *Proceedings of the 2nd WSEAS International Conference on Circuits, Systems, Signal and Telecommunications*, p. 202–206, 2008.

[75] Y. Alinejad-Beromi, M. Sedighizadeh, and M. Sadighi, "A particle swarm optimization for sitting and sizing of distributed generation in distribution network to improve voltage profile and reduce THD and losses," in *Universities Power Engineering Conference, 2008. UPEC 2008. 43rd International*, pp. 1 –5, Sept. 2008.

[76] N. Jain, S. N. Singh, and S. C. Srivastava, "Particle swarm optimization based method for optimal siting and sizing of multiple distributed generators," in *Proceedings of 16th National Power Systems Conference*, p. 669–674, 2010.

[77] A. Kazemi and M. Sadeghi, "Sitting and sizing of distributed generation for loss reduction," in *Power and Energy Engineering Conference, 2009. APPEEC 2009. Asia-Pacific*, pp. 1 –4, Mar. 2009.

[78] B. Kuri, M. Redfem, and F. Li, "Optimisation of rating and positioning of dispersed generation with minimum network disruption," in *IEEE Power Engineering Society General Meeting, 2004*, pp. 2074 –2078 Vol.2, June 2004.

[79] M. Mardaneh and G. Gharehpetian, "Siting and sizing of DG units using GA and OPF based technique," in *TENCON 2004. 2004 IEEE Region 10 Conference*, vol. C, pp. 331 – 334 Vol. 3, Nov. 2004.

[80] R. H. Mohammed Mansoor O., "Optimal siting and sizing of distributed generation by adaptive particle swarm optimization for power distribution system," in *ICTT Electrical Engineering Papers*, 2010.

[81] S. Reddy, P. Prasad, and A. Laxmi, "Reliability improvement of distribution system by optimal placement of DGs using PSO and neural network," in *2012 International Conference on Computing, Electronics and Electrical Technologies (ICCEET)*, pp. 156 –162, Mar. 2012.

[82] P. Siano, G. P. Harrison, A. Piccolo, and A. R. Wallace, "Strategic placement of distributed generation capacity," in *International Conference on Electricity Distribution*, p. 1–4, 2007.

[83] C. Tautiva, A. Cadena, and F. Rodriguez, "Optimal placement of distributed generation on distribution networks," in *Universities Power Engineering Conference (UPEC), 2009 Proceedings of the 44th International*, pp. 1 –5, Sept. 2009.

[84] N. Acharya, P. Mahat, and N. Mithulananthan, "An analytical approach for DG allocation in primary distribution network," *International Journal of Electrical Power & Energy Systems*, vol. 28, pp. 669–678, Dec. 2006.

[85] A. Afraz, F. Malekinezhad, S. J. s. Shenava, and A. Jlili, "Optimal sizing and sitting in radial standard system using PSO," *American journal of scientific research*, no. 67, pp. 50–58, 2012.

[86] A. J. Ardakani, A. K. Kavyani, S. A. Pourmousavi, S. H. Hosseinian, and M. Abedi, "Siting and sizing of distributed generation for loss reduction," *International Carnivourous Plant Society*, 2007.

[87] G. Celli, E. Ghiani, S. Mocci, and F. Pilo, "A multiobjective evolutionary algorithm for the sizing and siting of distributed generation," *Power Systems, IEEE Transactions on*, vol. 20, no. 2, p. 750–757, 2005.

[88] A. L. Devi and B. Subramanyam, "Optimal DG unit placement for loss reduction in radial distribution system-a case study," *ARPN Journal of Engineering and Applied Sciences*, vol. 2, Dec. 2007.

[89] L. Devi and B. Subramanyam, "Sizing of DG unit operated at optimal power factor to reduce losses in radial distribution; a case study," *Journal of Theoretical and Applied Information Technology*, p. 973–980, 2008.

[90] S. Ghosh, S. Ghoshal, and S. Ghosh, "Optimal sizing and placement of distributed generation in a network system," *International Journal of Electrical Power & Energy Systems*, vol. 32, pp. 849–856, Oct. 2010.

[91] T. Gözel and M. H. Hocaoglu, "An analytical method for the sizing and siting of distributed generators in radial systems," *Electric Power Systems Research*, vol. 79, pp. 912–918, June 2009.

[92] G. Harrison, A. Piccolo, P. Siano, and A. Wallace, "Distributed generation capacity evaluation using combined genetic algorithm and OPF," *International Journal of Emerging Electric Power Systems*, vol. 8, no. 2, pp. 750 – 757, 2007.

[93] R. A. Jabr and B. C. Pal, "Ordinal optimisation approach for locating and sizing of distributed generation," *Generation, Transmission & Distribution, IET*, vol. 3, no. 8, p. 713–723, 2009.

[94] S. Kansal, B. B. R. Sai, B. Tyagi, and V. Kumar, "Optimal placement of distributed generation in distribution networks," *International Journal of Engineering, Science and Technology*, vol. 3, no. 3, 2011.

[95] D. M. P. Lalitha, D. V. C. V. Reddy, N. S. Reddy, and V. U. Redddy, "A two stage methodology for siting and sizing of dg for minimum loss in radial distribution system using rcga," *International Journal of Computer Applications*, vol. 25, pp. 10–16, July 2011. Published by Foundation of Computer Science, New York, USA.

[96] M. P. Lalitha, N. S. Reddy, and V. C. V. Reddy, "Optimal DG placement for maximum loss reduction in radial distribution system using ABC algorithm," *International Journal of Reviews in Computing*, 2009.

[97] M. H. Moradi and M. Abedini, "A combination of genetic algorithm and particle swarm optimization for optimal DG location and sizing in distribution systems," *International Journal of Electrical Power & Energy Systems*, 2011.

[98] V. Rashtchi and M. Darabian, "A new BFA-Based approach for optimal sitting and sizing of distributed generation in distribution system," *International Journal of Automation and Control Engineering(IJACE), International Journal of Automation and Control Engineering(IJACE)*, vol. 1, Nov. 2012.

[99] C. Wang and M. Nehrir, "Analytical approaches for optimal placement of distributed generation sources in power systems," *IEEE Transactions on Power Systems*, vol. 19, pp. 2068 – 2076, Nov. 2004.

[100] S. Lundberg, T. Petru, and T. Thiringer, "Electrical limiting factors for wind energy installations in weak grids," *International Journal of Renewable Energy Engineering*, vol. 3, no. 2, pp. 305–310, 2001.

[101] S. Lundberg, *Electrical limiting factors for wind energy installations*. Master thesis, Chalmers University of Technology, Göteborg, Sweden, 2000.

[102] G. Harrison and A. Wallace, "Optimal power flow evaluation of distribution network capacity for the connection of distributed generation," *Generation, Transmission and Distribution, IEE Proceedings-*, vol. 152, pp. 115 –122, Jan. 2005.

[103] T. Sun, Z. Chen, and F. Blaabjerg, "Flicker mitigation of grid connected wind turbines using STATCOM," in *Power Electronics, Machines and Drives, 2004. (PEMD 2004). Second International Conference on (Conf. Publ. No. 498)*, vol. 1, pp. 175 – 180 Vol.1, Apr. 2004.

[104] T. Sun, Z. Chen, and F. Blaabjerg, "Flicker study on variable speed wind turbines with doubly fed induction generators," *Energy Conversion, IEEE Transactions on*, vol. 20, no. 4, p. 896–905, 2005.

[105] R. Barth and C. Weber, "Distribution of the integration costs of wind power," Deliverable D7.1, IER-Stuttgart University, 2005.

[106] G. Harrison, A. Piccolo, P. Siano, and A. Wallace, "Exploring the tradeoffs between incentives for distributed generation developers and DNOs," *IEEE Transactions on Power Systems*, vol. 22, pp. 821 –828, May 2007.

[107] "Inmatningstariffer 2011." http://feab.nu/Inmatningstariffer-2011-2012.htm.

[108] "Nätpriser - inmatning till lokalnät."

[109] "Statement of use of system charging."

[110] M. I. Blanco, "The economics of wind energy," *Renewable and Sustainable Energy Reviews*, vol. 13, pp. 1372–1382, Aug. 2009.

[111] S. Kraftnät. https://certifikat.svk.se.

[112] N. P. Spot. http://www.nordpoolspot.com.

[113] H. L. Willis and W. G. Scott, *Distributed Power Generation: Planning and Evaluation*. Marcel Dekker, 2000.

[114] J. Harry, *Multivariate models and dependence concepts*. Chapman & Hall, 1997.

[115] B. Biller and S. Ghosh, "Chapter 5 multivariate input processes," in *Simulation* (S. G. Henderson and B. L. Nelson, eds.), vol. 13 of *Handbooks in Operations Research and Management Science*, pp. 123 – 153, Elsevier, 2006.

[116] H. V. Haghi, M. T. Bina, M. Golkar, and S. Moghaddas-Tafreshi, "Using copulas for analysis of large datasets in renewable distributed generation: Pv and wind power integration in iran," *Renewable Energy*, vol. 35, no. 9, pp. 1991 – 2000, 2010.

[117] G. Papaefthymiou and D. Kurowicka, "Using copulas for modeling stochastic dependence in power system uncertainty analysis," *Power Systems, IEEE Transactions on*, vol. 24, pp. 40 –49, Feb. 2009.

[118] B. Adrian W and A. Azzalini, *Applied Smoothing Techniques for Data Analysis*. New York: Oxford University Press, 1997.

[119] E. W.Frees and E. A. Valdez, "Understanding relationships using copulas," *North American Actuarial Journal*, vol. 2, p. 1–25, 1998.

[120] V. S. BVBA, *Help File for ModelRisk*. 2007. Version 4.

[121] K. Aas and D. Berg, "Models for construction of multivariate dependence - a comparison study," *The European Journal of Finance*, vol. 15, no. 7-8, pp. 639–659, 2009.

[122] B. Eric, V. Durrleman, A. Nikeghbali, G. Riboulet, and T. Roncalli, "Copulas for finance a reading guide and some applications," *Recherche*, 2000.

[123] P. Fischbach, *Copula-Models in the Electric Power Industry*. Master thesis, University of St.Gallen, St. Gallen, Switzerland, Aug. 2010.

[124] V. Durrleman, A. Nikeghbali, and T. Roncalli, "Which copula is the right one," *Exchange Organizational Behavior Teaching Journal*, p. 19, 2000.

[125] D. Das, "A fuzzy multiobjective approach for network reconfiguration of distribution systems," *IEEE Transactions on Power Delivery*, vol. 21, pp. 202–209, Jan.

[126] D. Pudjianto, D. M. Cao, S. Grenard, and G. Strbac, "Method for monetarisation of cost and benefits of DG options," *Bericht im Rahmen des Europäischen Projektes DG Grid, Manchester/London (download http://www. dggrid. org/results/result_reportpudjianto. pdf)*, 2006.

[127] E. E. N. Ltd, "IFI/RPZ report for EPN/LPN/SPN," tech. rep., 2010.

[128] S. E. Networks, "Innovation funding incentive annual report," tech. rep., 2012.

[129] S. GRENARD, A. QUERIC, and O. CARRE, "Technical and economic assessment of centralised voltage control functions in presence of DG in the french MV network," in *Proceedings of the 21st International Conference on Electricity Distribution*, 2011.

[130] KEMA, "Smart grid strategic review: The orkney islands active network management scheme," tech. rep., Mar. 2012.

[131] Z. Hu and F. Li, "Cost-benefit analyses of active distribution network management, part II: investment reduction analysis," *IEEE Transactions on Smart Grid*, vol. 3, no. 3, pp. 1075–1081, 2012.

[132] J. Gordijn and H. Akkermans, "Business models for distributed generation in a liberalized market environment," *Electric Power Systems Research*, vol. 77, pp. 1178–1188, July 2007.

[133] P. Balducci, L. Schienbein, T. Nguyen, D. Brown, and E. Fatherlrahman, "An examination of the costs and critical characteristics of electric utility distribution system capacity enhancement projects," in *Transmission and Distribution Conference and Exhibition, 2005/2006 IEEE PES*, pp. 78 –86, May 2006.

[134] G. Beaulieu and G. Borloo, "Power quality indices and objectives," in *Electricity Distribution, 2005. CIRED 2005. 18th International Conference and Exhibition on*, p. 1–5, 2005.

[135] IEC 61000-2-2, "Electromagnetic compatibility (EMC) - part 2-2: Environment - compatibility levels for low-frequency conducted disturbances and signalling in public low-voltage power supply systems," Mar. 2002.

[136] IEC/TR 61000-3-7, "Electromagnetic compatibility (EMC) - part 3-7: Limits - assessment of emission limits for the connection of fluctuating installations to MV, HV and EHV power systems," Feb. 2008.

[137] V. J. Gosbell, D. A. Robinson, S. Perera, and A. Baitch, "The application of IEC 61000-3-6 to MV systems in australia," in *Quality and Security of Electrical Supply Conference Proceedings*, Research Online, 2001.

[138] S. Chen, T. Lund, M. Zamastil, V. Akhmatov, H. Abildgaard, and B. Gellert, “Short-circuit calculations considering converter-controlled generation components,” in *2012 IEEE Energytech*, pp. 1–6, 2012.

REFERENCES

Appendices

Appendix A

More on flickers

A.1 Flicker emission limit calculation from planning level

The flicker emission limits at any voltage level is based on their cumulative effect as felt by customers located on the low voltage side. A flicker severity index exceeding unity will be felt disturbing to the majority of individuals; a flicker severity index between 0,7 and 1,0 is noticeable, but not disturbing [134]. Hence compatibility level of these flicker emissions at LV are given near unity (P_{st}= 1 and P_{lt}= 0.8) [135]. That is, the flicker emission levels that occur in low voltage systems should be below this value with 95% probability based on a statistical distribution representing both time and spatial variations. From the compatibility levels the system operator can assign different flicker emission planning levels for different voltage levels in the system. Some indicative values of planning level for MV and HV are shown in Table A.1 where the flicker transfer coefficients between the different voltage levels–HV to MV, MV to LV–are assumed be unity.

Table A.1: Indicative values of planning levels for flicker in MV, HV, and EHV power systems [136]

	Planning level	
	MV	HV-EHV
P_{st}	0.9	0.8
P_{lt}	0.7	0.6

The composite effect of flicker emission from different installation in the particular voltage level should not exceed the planning level with 95% probability, as mentioned above. From this planning level, emission limits are imposed on each installation. The flicker emission transferred from upstream voltage systems should be taken into account when determining the maximum global flicker contribution, G_{PstMV}, from all installations in a given voltage level. This can be done as in [136]

$$G_{\mathrm{PstMV}} = \sqrt[\alpha]{L^{\alpha}_{\mathrm{PstMV}} - T^{\alpha}_{\mathrm{PstUM}} \cdot L^{\alpha}_{\mathrm{PstUS}}} \tag{A.1}$$

Where

L_{PstMV} the planning level for flicker, in P_{st} or P_{lt} in the MV system
L_{PstUS} the planning level for flicker in the upstream voltage level
T_{PstUM} the transfer coefficient of flicker (P_{st} or P_{lt}) from the upstream system to MV system
α the summation law exponent, commonly equal to 3

Examples of transfer coefficient, T_{PstUM}, obtained from simultaneous flicker measurements at 220 kV, 70 kV, 15 kV, and 230 V voltage levels are shown in Table A.2 [136].

Table A.2: Examples of flicker transfer coefficients

Voltage level	T_{PstAB}
220 kV to 70 kV	0.82
70 kV to 15 kV	0.91
150 kV to 230 V	0.98-1.0

Once the maximum global flicker contribution is determined, the flicker emission limits, i.e $E_{\text{Pst},i}$ and $E_{\text{Plt},i}$, for each installation at MV level can be apportioned taking into account their capacity S_i with respect to the total system capacity S_{tot} as shown [136]

$$\begin{aligned} E_{\text{Pst},i} &= G_{\text{PstMV}} \cdot \sqrt[\alpha]{\frac{S_i}{S_{\text{tot}} - S_{\text{LV}}}} \\ E_{\text{Plt},i} &= G_{\text{PltMV}} \cdot \sqrt[\alpha]{\frac{S_i}{S_{\text{tot}} - S_{\text{LV}}}} \end{aligned} \tag{A.2}$$

where S_{LV} is the total capacity of the installations that are or can be directly connected at the LV network.

The IEC/TR 61000-3-7 technical report recommends the values, $E_{\text{Pst},i} = 0.35$ and $E_{\text{Plt},i} = 0.25$, to be used in case the capacity of the installation is too low that the above approach imposes impractically low flicker limit. The same limits are specified by Swedish AMP manual for each wind power installation in a given MV distribution networks, i.e. typically 10-20kV networks [28].

A.2 Calculation examples

A 9 MW wind farm consisting of variable wind speed wind turbines is to be connected to a distribution network, which has a short circuit capacity of 67 MVA at the point of connection. Assume that this network has 12 MW of wind power already installed somewhere else and the capacity of the total installation at LV level S_{LV} is 8 MVA. It is required to investigate the voltage quality problems that could arise with this wind farm.

A collection of variable speed wind turbine technical data shows that the voltage change factor is usually located between 0.1 and 0.9[1], the flicker coefficient lies between 2 and 4, and the flicker step factor lies between 0.01 and 0.2. Flicker calculation of this wind farm is done assuming different wind turbine sizes in the farm and flicker coefficient of the wind turbine. The summation formula in (2.13) is used for the calculation. The result is presented in Table A.3 and Table A.4.

The results show that a wind farm composed of smaller wind turbines introduces less voltage flicker to the network. Moreover, should the limits specified by the Swedish AMP manual be

[1] due to switching operation at rated power

Table A.3: Flicker emission, $P_{st}(P_{lt})$, of a wind farm during continuous operation

Flicker coefficient, $c(\psi_k)$	Size of each wind turbine			
	0.9 MW	1.5 MW	3 MW	4.5 MW
1.5	0.06	0.08	0.12	0.14
2.5	0.11	0.14	0.19	0.24
3.5	0.15	0.19	0.27	0.33
4.5	0.19	0.25	0.35	0.43

Table A.4: Flicker emission, $P_{st}(P_{lt})$, of a wind farm during switching operation

Flicker step factor, $k_f(\psi_k)$	Size of each wind turbine			
	0.9 MW	1.5 MW	3 MW	4.5 MW
0.01	0.00	0.01	0.01	0.01
0.08	0.04	0.05	0.09	0.12
0.15	0.07	0.10	0.16	0.22
0.22	0.10	0.15	0.24	0.32

followed strictly at each connection point, flicker emission may become a limiting factor to install 9 MW with some wind turbine types(see the last two rows of column 4 and 5 of Table A.3).

On the other hand, taking the planning level data from Table A.1, the maximum global flicker contribution at the MV level can be calculated as $G_{\mathrm{PstMV}} = 0.6$ and $G_{\mathrm{PstMV}} = 0.5$ using (A.1) with $\alpha = 3$. Then using (A.2), the flicker emission limits of the given installation can be calculated as $E_{\mathrm{Pst},i} = 0.45$ and $E_{\mathrm{Plt},i} = 0.38$. Therefore, the given capacity of wind power can be accommodated by the system at the given connection point for most of the cases.

As for the voltage change that may occur due to switching operation within the wind farm, since the different switching operations are less likely to occur at the same time, no summation effect needs to be taken into account [34]. Hence the voltage change increases directly with the size of the individual wind turbine as shown in Table A.5. The results in Table A.5 show also that for the

Table A.5: Voltage change in the network due to switching operation of the wind farm

Voltage change factor, $k_u(\psi_k)$	Size of each wind turbine			
	0.9 MW	1.5 MW	3 MW	4.5 MW
0.10	0.13	0.22	0.45	0.67
0.35	0.47	0.78	1.57	2.35
0.60	0.81	1.34	2.69	4.03
0.85	1.14	1.90	3.81	5.71

voltage change during switching operation to be a concern the size of the wind turbines need to be 4.5MW and a voltage change factor to be above 0.6.

In summary, based on the data available for three coefficients of various wind turbines– flicker coefficients, flicker step factor, and voltage change factor– and the result in Tables A.3, A.4 and A.5, the flicker emission during continuous operation can be seen as the main voltage quality concern.

A. MORE ON FLICKERS

Appendix B

More on Harmonics

B.1 Harmonic current allocation for each installation from planning level

Utilities as well as national and international standards specify harmonic emission limits in a given distribution system. Similar to the flicker case, the IEC standard specifies the harmonic objectives based on compatibility and planning levels of voltage harmonics. Compatibility levels are only specified for LV and MV systems while indicative planning levels are given for both MV and HV-EHV systems [134]. Table B.1 shows the compatibility levels and indicative planning levels as specified by IEC standard [35, 36]. The specification of harmonic voltage limits by Swedish AMP manual is also included for comparison.

Moreover, similar to the case of flicker, harmonic emission limits for each installation can be calculated from the planning level. Once again the contribution from the HV-EHV system should be taken into account as in (B.1).

$$G_{\mathrm{hMV+LV}} = \sqrt[\beta]{L_{\mathrm{hMV}}^{\beta} - T_{\mathrm{hUM}}^{\beta} \cdot L_{\mathrm{hUS}}^{\beta}} \tag{B.1}$$

Where

$G_{\mathrm{hMV+LV}}$	global harmonic emission at MV including LV loads
L_{hMV}	the planning level of harmonic emission at MV
L_{hUS}	the planning level of harmonic emission in the upstream voltage level
T_{PhUM}	the transfer coefficient of harmonic emission from the upstream system to MV system

The transfer coefficient can be determined by simulation or measurement. For simplified evaluation it can be taken as 1 but it, in practice, can be less or greater than 1 [36]. However from the planning levels indicated in Table B.1, in case the transfer coefficient is taken to be 1, the global harmonic emission for some harmonic orders from the MV networks becomes zero. In this case appropriate sharing of the harmonic emissions between the different voltage levels should be performed.

Table B.1: Harmonic voltage specification according to IEC and the AMP manual

Harmonic order, h	Harmonic voltage magnitude (% fundamentable voltage)			
	MV (1 to 35 kV)			HV-EHV (> 35 kV)
	IEC compatibility level	IEC indicative planning level	AMP limits	IEC indicative planning level
2	2	1.6	2	1.5
3	5	4	5	2
4	1	1	1	1
5	6	5	6	2
6	0.5	0.5	0.5	0.5
7	5	4	5	2
8	0.5	0.4	0.5	0.4
9	1.5	1.2	1.5	1
10	0.5	0.4	0.5	0.4
11	3.5	3	3.5	1.5
12	0.46	0.2	0.5	0.2
13	3	2.5	3	1.5
14	0.43	0.2	0.5	0.2
15	0.4	0.3	0.5	0.3
16	0.41	0.2	0.5	0.2
17	2	1.6	2	1
18	0.39	0.2	0.5	0.2
19	1.76	1.2	1.5	1
20	0.38	0.2	0.5	0.2
21	0.3	0.2	0.5	0.2
22	0.36	0.2	0.5	0.2
23	1.41	1.2	1.5	0.7
24	0.35	0.2	0.5	0.2
25	1.27	1.2	1.5	0.7
THD	8	6.5		3

From the global harmonic emission level, each installation will have emission levels $E_{\mathrm{Uh},i}$ apportioned to it based on its capacity S_i compared to the total system capacity S_{tot}, including provisions for future load growth. The apportioning can be done using (B.2). It can be observed that, unlike the case of flicker emission, the harmonic emission from the LV loads is not ignored.

$$E_{\mathrm{Uh},i} = G_{\mathrm{hMV+LV}} \cdot \sqrt[\beta]{\frac{S_i}{S_{\mathrm{tot}}}} \tag{B.2}$$

In case the calculation above results in some harmonic voltage emission limits less 0.1%, it shall be set to 0.1% unless there are some strict limits why it should not be [36]. The apportioning of

voltage harmonics for different installation using (B.2) does not result in proportional sharing of harmonic current emission limits between the installations when the installations are located at varying distance from the substation [137]. This would not be fair considering that most distorting installation act as a harmonic current source. Hence an apportioning approach which takes this problem into account while utilizing efficiently the absorption capacity of the system is proposed in [137].

B.2 Calculation examples

Consider that same case as in Section A.2. Moreover assume the peak value of the load connected to the LV system is 8 MVA. In Table B.2, the harmonic emission level of the wind farm is analyzed for voltage harmonic limits in the network. From the AMP voltage harmonic limits $L_{\mathrm{hMV}(\%)}$ and the indicative planning levels of HV-EHV networks (shown in Column 5 of Table B.1) given by the IEC standard [36], the global harmonic contribution of the MV and LV network $G_{\mathrm{hMV+LV}}$ is calculated using (B.1). Equation (B.2) is then used to calculate the allowed voltage harmonics $E_{\mathrm{Uh},i}$ from the wind farm. This is changed into the allowed level of current harmonics from the wind farm using (2.21) (presented in Column 5). With a typical current harmonics of a variable wind turbine (shown in Column 6), the total current harmonics of the wind farm is calculated using (2.19) for two cases. The cases differ based on the sizes of the wind turbines constituting the wind farm–one with two 4.5 MW wind turbines and the other with ten 0.9 MW wind turbines. The result is presented in Columns 7 and 8. Moreover, on the last rows of Columns 7 and 8 the total voltage harmonic distortion due to the wind farm is provided. The planing level for total harmonic distortion (THD) at Column 2 is taken from IEC indicative planning level as such value is not provided in the AMP standard.

The results in Table B.2 show that harmonic emissions due to the wind farm can be beyond the absorption capacity of the system at low order even harmonics (such as the 4th, 6th and 8th) for both cases. Moreover, based on the data of harmonic emission of a couple of variable speed wind turbines, the emission limits at these harmonics seems more stringent to fulfill. Unlike the flicker case, taking small sized wind turbines does not mitigate the problem that much.

If it is not possible to find wind turbines which fulfill the harmonic limits using the simplified analysis provided above, a thorough analysis of the harmonic emission level of the system supported by measurements and simulation should be carried out to assess the possibility of connecting this capacity of wind farm. The result of the analysis may give different results as:

- the analysis in Table B.2 is done assuming harmonic transfer coefficient of 1 from HV to the MV network, it is possible for the transfer coefficient to be less than one though it can also be greater than one [36]
- not all installation in the system produce harmonic currents, hence the harmonic emission allotted to these installations is available [36]
- the general summation law can provide a conservative result as harmonics can also be generated with opposite phase and result in partial cancellation [36]

On the other hand, since the harmonic impedance is assumed to be $h \times Z$, which can be higher for

Table B.2: Calculation example of harmonic emission

h	$L_{\mathrm{hMV}(\%)}$	$G_{\mathrm{hMV+LV}}$ (%)	$E_{\mathrm{Uh},i}$ (%)	Limit, i_h (%)	Typical i_h from wind turbines	Σi_h due to	
						Two 4.5 MW WTs	Ten 0.9 MW WTs
2	2	0.5	0.16	5.2	0.58	5.2	5.2
3	5	3.0	0.93	20.8	0.61	5.5	5.5
4	1	0.4	*0.12*	**2.1**	0.34	**3.0**	**3.0**
5	6	5.0	2.19	29.3	0.92	6.8	4.3
6	0.5	0.3	*0.13*	**1.5**	0.26	**1.9**	1.2
7	5	4.0	1.72	16.5	0.72	5.3	3.3
8	0.5	0.3	0.11	**0.9**	0.19	**1.4**	0.9
9	1.5	0.8	0.36	2.7	0.21	1.5	1.0
10	0.5	0.3	*0.11*	**0.7**	0.12	**0.9**	0.6
11	3.5	3.2	1.76	10.7	0.60	3.8	1.7
12	0.5	0.5	0.26	1.4	0.12	0.7	0.3
13	3	2.6	1.45	7.5	0.42	2.6	1.2
14	0.5	0.5	0.26	1.2	0.10	0.6	0.3
15	0.5	0.4	0.22	**1.0**	0.16	**1.0**	0.5
16	0.5	0.5	0.26	1.1	0.09	0.6	0.3
17	2	1.7	0.96	3.8	0.21	1.4	0.6
18	0.5	0.5	0.26	1.0	0.07	0.5	0.2
19	1.5	1.1	0.62	2.2	0.13	0.8	0.4
20	0.5	0.5	0.26	0.9	0.07	0.4	0.2
21	0.5	0.5	0.26	0.8	0.10	0.6	0.3
22	0.5	0.5	0.26	0.8	0.06	0.4	0.2
23	1.5	1.3	0.74	2.2	0.17	1.1	0.5
24	0.5	0.5	0.26	0.7	0.13	0.8	0.4
25	1.5	1.3	0.74	2.0	0.19	1.2	0.5
THD	6.5	5.8	3.2	-	-	1.50	0.82

low order harmonic frequencies [37], the revised analysis may result in a more stringent requirement of current harmonics from the new wind farm.

Appendix C

More on effect of wind power on fault level of the system

C.1 Calculation of fault current contribution from the external grid according to IEC standard

C.1.1 Initial symmetrical short circuit current

For different fault types the initial symmetrical short circuit current I_k'' can be calculated using symmetrical components method. The equivalent source voltage, according to IEC 60909 standard, will be $cU_n/\sqrt{3}$. Where U_n is the nominal voltage of the network and c has two value, $c_{\max}$ and $c_{\min}$ which is used depending on whether the maximum or the minimum value of the short circuit current is being calculated. These $c_{\max}$ and $c_{\min}$ have different values depending on the voltage level of the network as given in Table C.1.

Table C.1: Voltage factor c

Nominal voltage U_n	$c_{\max}$	$c_{\min}$
Low voltage 100 V to 1 kV	1.05[1]	0.95
	1.1[2]	
Medium and high voltage >1kV	1.1	1

For most common cases, the highest initial short circuit current occurs for three phase fault [42], where it can be given by:

$$I_k'' = \frac{c_{\max} U_n}{\sqrt{3} Z_k} \tag{C.1}$$

Here Zk is the vector summation of the positive sequence impedance of the external grid Z_{Qt}, the transformer Z_{TK} and the cable or overhead line up to the fault point Z_L:

$$Z_k = Z_{Qt} + Z_{TK} + Z_L \tag{C.2}$$

Z_{Qt} depends on the short circuit capacity (SCC) of the external network and the nominal voltage level (U_{nQ}) [42].

$$|Z_{Qt}| = \frac{cU_{nQ}^2}{SCC} \tag{C.3}$$

Where c is chosen from Table C.1 . On the other hand for calculation of X_{Qt} and R_{Qt}, if the X/R-ratio is not known, $R_{Qt} = 0.1X_{Qt}$ can be taken for external grid with nominal voltage below 35kV. For voltage levels above 35 kV the resistance part can be neglected. Z_L is the impedance of the cable or overhead line at 20 ^{0}C. Z_{TK} is the corrected impedance of the transformer and is given by

$$Z_{TK} = K_T Z_T \tag{C.4}$$

Here Z_T is the rated impedance of the transformer and can be calculated as

$$Z_T = \frac{u_{kr}}{100\%} \cdot \frac{U_{rT}^2}{S_{rT}} \tag{C.5}$$

$$R_T = \frac{u_{Rr}}{100\%} \cdot \frac{U_{rT}^2}{S_{rT}} = \frac{P_{krT}}{3I_{rT}^2} \tag{C.6}$$

$$X_T = \sqrt{Z_T^2 - R_T^2} \tag{C.7}$$

and K_T is the correction factor for the transformer impedance. K_T is given by

$$K_T = 0.95\frac{c_{\max}}{1 + 0.6x_T} \tag{C.8}$$

Where x_T is the relative reactance of the transformer $x_T = X_T/(U_{rT}^2/S_{rT})$. Here U_{rT} and S_{rT} are the rated voltage and rated power of the transformer.

In case the fault current comes from more than on source, the initial short-circuit current at the short-circuit location F can be calculated as the phasor sum of the individual partial short-circuit currents.

C.1.2 Peak short circuit current

The peak short circuit current i_p is calculated as

$$i_p = \kappa\sqrt{2}I_k'' \tag{C.9}$$

The factor κ is the function of the X/R-ratio of the network up to the fault point as given in (C.10).

$$\kappa = 1.02 + 0.98e^{-3R/X} \tag{C.10}$$

The peak current i_p of a short circuit current fed from different sources, which are not meshed, can be calculated as the sum of the partial short circuit currents.

C.1.3 Symmetrical short circuit breaking current

For far from generator faults, which is the case for distribution systems fed from external grid, the breaking current $Ib = I_k''$. In case there is contributions from multiple sources from non-meshed sources, Ib can be calculated as the summation of the individual contributions for the fault.

C.2 Calculation examples

Consider the network shown in Fig. C.1, which depicts the schematic diagram of a network with fourteen wind turbines installed. A three phase to ground fault occurs at the substation busbar (Bus 1). The impedance data of the network along with the sizes of the wind turbines is presented in Table C.2. The capacity of the wind turbines vary from 0.225 MW to 1.5 MW and are of various generator technologies–type A, type B, and Type D–as shown in Table C.2. Here, since a simplified short circuit calculation is carried out, the loads are not of any interest. The external grid have a fault level of 160 MVA with X/R ratio of 5 and the impedance of the transformer is 8% with X/R ratio of 16.

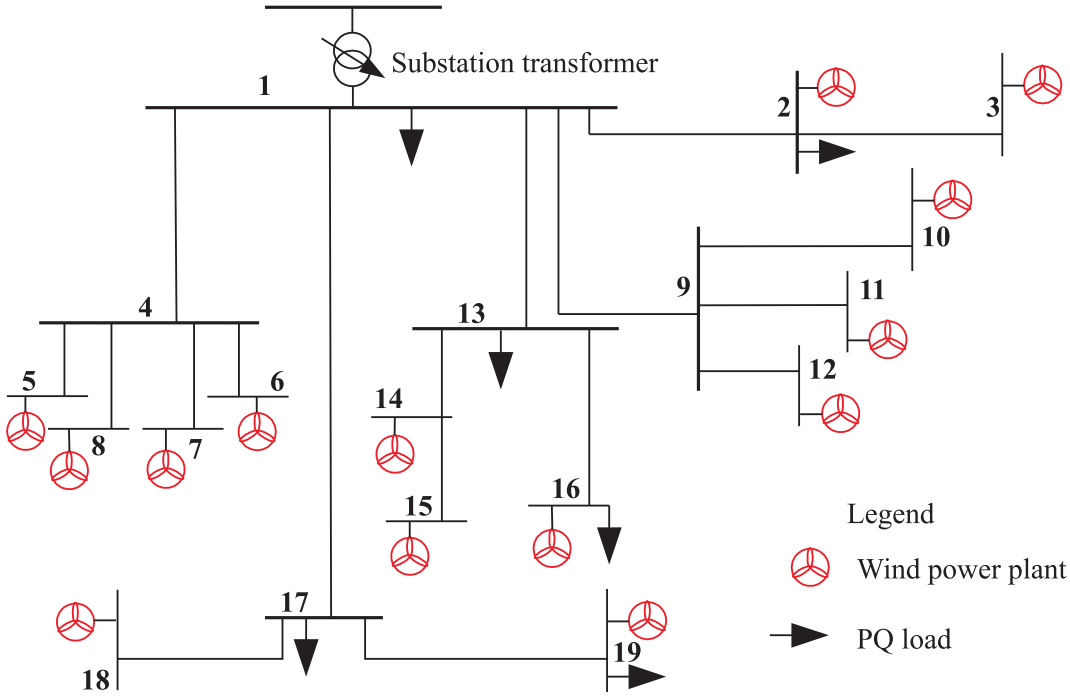

Figure C.1: A simplified representation the network of Falbygdens Energi

The task is first to calculate the short circuit current contribution of the wind turbines for a three-phase fault at the substation. Then to determine, together with the short circuit current contribution from the external grid, if the fault current would be above the design limits of the switchgear at the substation. The design limits that are of interest to us are the rated peak and short-time withstand currents. However, no information is available about the ratings of the switchgear. In this respect, the IEC specifies 1, 1.25, 1.6, 2, 2.5, 3.15, 4, 5, 6.3, 8 and their product by 10^n as standard values for short time withstand current. Thus the task is now:

Table C.2: Network data and the wind turbines in the network

Sending end bus	Receiving end bus	R (Ω)	X (Ω)	Capacity of wind power (MW)	Wind turbine type
1	2	0.697	0.217	0.8	D
2	3	0.205	0.034	0.8	D
1	4	0.289	0.196		
4	5	0.236	0.040	0.8	D
4	6	0.013	0.005	0.8	D
4	7	0.316	0.053	0.8	D
4	8	0.340	0.057	0.8	D
1	9	0.318	0.155		
9	10	3.159	0.552	1.5	D
9	11	0.173	0.035	0.95	A
9	12	0.012	0.002	0.95	A
1	13	0.339	0.247		
13	14	1.932	0.322	0.8	D
14	15	0.224	0.037	0.8	D
13	16	1.354	1.307	0.85	B
1	17	0.694	0.710		
17	18	1.306	0.933	0.225	A
17	19	1.112	1.093	0.85	B

- first, to calculate the initial symmetrical and the peak fault current in the network
- then, to check for which ratings of the switchgear these fault currents would be above the switchgear capability

C.2.1 The short circuit current contribution from the external grid

Let us start by calculating the current contribution from the external grid; for this the IEC procedure, as discussed above, is followed. From (C.1) the contribution of the external grid to the initial symmetrical fault current ($I_k^{''}$) can be calculated. Then (C.9) can used to calculate the contribution of the external grid to the peak fault current (i_p). Table C.3 shows the calculation steps along with the result.

C.2.2 The short circuit current contribution from the wind turbines

To calculate the contribution of the wind turbines to the fault, we note that there are three types of wind turbines: 3 Type A, 2 Type B, and 9 Type D wind turbines. As mentioned in Section 2.2.5, Type A and Type B behave similarly in terms of short circuit current contribution. Their short circuit current is dependent on the machine parameters and the network impedance up to the fault point. Type D wind turbines, on the other hand, behave differently; their fault current contribution is dependent on the voltage dip felt at the terminal of the wind turbine [138]. They also have a maximum short circuit current, which depends on the overcurrent capability of the converter system.

Table C.3: Fault current contribution from the external grid

Impedance of the external grid	$(C.3) \Rightarrow \lvert Z_{Qt}\rvert = \frac{1.1\cdot(11e3)^2}{160e6} \Rightarrow \lvert Z_{Qt}\rvert = 0.8319$ $R_{Qt} = \frac{\lvert Z_{Qt}\rvert}{\sqrt{\left(X_{Qt}/R_{Qt}\right)^2+1}} \Rightarrow R_{Qt} = 0.1631 \Rightarrow X_{Qt} = 0.8157$ $\Rightarrow Z_{Qt} = 0.1631 + 0.8157i\ \Omega$
Impedance of the transformer	$(C.5) \Rightarrow \lvert Z_T\rvert = \frac{8\%}{100\%}\cdot\frac{(11.5e3)^2}{10e6} \Rightarrow \lvert Z_T\rvert = 1.0580$ $R_T = \frac{\lvert Z_T\rvert}{\sqrt{\left(X_T/R_T\right)^2+1}} \Rightarrow R_T = 0.0660 \Rightarrow X_T = 16\cdot R_T \Rightarrow X_T = 1.0559$ $(C.8) \Rightarrow K_T = 0.95\frac{1.1}{1+0.6x_T}, x_T = \frac{X_T}{U_{rT}^2/S_{rT}} \Rightarrow x_T = 0.0798 \Rightarrow K_T = 0.9973$ $(C.4) \Rightarrow Z_{TK} = 0.9973\cdot(0.0660+1.0559i) \Rightarrow Z_{TK} = 0.0658 + 1.0530i\ \Omega$
Total impedance of the network up to the fault point	$(C.2) \Rightarrow Z_k = (0.1631 + 0.8157\text{i}) + (0.0658 + 1.0530\text{i})$ $\Rightarrow Z_k = 0.2289 + 1.8687i\ \Omega$
The maximum initial symmetrical short circuit current	$(C.1) \Rightarrow I_k'' = \frac{1.1\cdot 11e3}{\sqrt{3}(0.2289+1.8687i)} \Rightarrow I_k'' = 4.5115\text{e}2 - 3.6831\text{e}3i$ $\Rightarrow \left\lvert I_k''\right\rvert = 3.7107kA$
The peak short circuit current	$\frac{R}{X} = \frac{R_k}{X_k} \Rightarrow \frac{R}{X} = 0.1225,\ (C.10) \Rightarrow \kappa = 1.02 + 0.98e^{-3\cdot 0.1225} \Rightarrow \kappa = 1.6986$ $(C.9) \Rightarrow i_p = 1.6986\cdot\sqrt{2}\cdot 3.7107kA \Rightarrow i_p = 8.9138kA$

The initial short circuit calculation, by modeling the different wind turbine types according to IEC approach (see Table C.4), have resulted in fault current contribution from type D wind turbines above their converter over current capability; the overcurrent capability of the converter system is taken to be 20% higher than the rated current. Hence the calculation is done in two steps. First it is assumed that type D wind turbine will contribute their full short circuit current with an angle $56.44^0(0.985\,\text{rad})$ [138]. The angle indicates the nature of the current in terms of active and reactive current composition. The calculation of the fault current from Type A and Type B wind turbines is, then, made following the IEC procedure as shown in Table C.5. Observe that, whenever necessary, some adjustment is made in the fault current calculation to accommodate the effect of fault currents from type D wind turbines.

C. MORE ON EFFECT OF WIND POWER ON FAULT LEVEL OF THE SYSTEM

Fault current contribution from type D wind turbines:

$$I_k'' = 1.2 \times \left(8 \cdot \frac{800e3}{400\sqrt{3}} + \frac{1.5e6}{400\sqrt{3}} \right) \times \frac{400}{11e3} e^{-i0.985} \Rightarrow I_k'' = 275.09 - 414.61i$$

$$\Rightarrow I_k'' = 497.57A$$

$$i_p = \sqrt{2} I_k'' \Rightarrow i_p = 703.67A$$

Table C.4: Electrical data of the wind turbines and the associated transformer

Type A & B	225 kW wind turbine	Generator data :$P_{rG} = 225kW, U_{rG} = 400V$, 6 pole, $I_{rG} = 324A, I_{LR}/I_{rG} = 7.0, R_G/X_G = 0.15$ $\hookrightarrow$ (2.23) $\Rightarrow \lvert Z_G\rvert = 76.83\Omega$, (2.24) $\Rightarrow X_G = 75.98\,\Omega \Rightarrow R_G = 11.40\,\Omega \Rightarrow Z_G = 11.40 + 75.98i\,\Omega$ Transformer data :$11 \pm 2 \times 2.5\%/0.4kV, 50Hz, 0.315MVA, u_{kr} = 4\%,\ u_{Rr} = 1.16\%$ $\hookrightarrow$ (C.5) $\Rightarrow \lvert Z_T\rvert = 15.37\,\Omega$, (C.6) $\Rightarrow R_T = 4.46\,\Omega, \Rightarrow X_T = 14.70\,\Omega$, (C.8) $\Rightarrow K_T = 1.02$, (C.4) $\Rightarrow Z_{Tk} = 4.55 + 15.02i\,\Omega$ $\hookrightarrow Z_{\mathrm{GT}_{0.225\mathrm{MW}}} = 15.95 + 91.00i\,\Omega$
	850 kW wind turbines	Generator data :$P_{rG} = 850kW, U_{rG} = 690V$, 4 pole, $I_{rG} = 711A, I_{LR}/I_{rG} = 7.7,\ R_G/X_G = 0.1$ $\hookrightarrow$ (2.23) $\Rightarrow \lvert Z_G\rvert = 18.49\Omega$, (2.24) $\Rightarrow X_G = 18.40\,\Omega, \Rightarrow R_G = 1.84\,\Omega \Rightarrow Z_G = 1.84 + 18.40i\,\Omega$ Transformer data :$11 \pm 2 \times 2.5\%/0.69kV, 50Hz, 1MVA, u_{kr} = 6\%,\ u_{Rr} = 1.1\%$ $\hookrightarrow$ (C.5) $\Rightarrow \lvert Z_T\rvert = 7.26\,\Omega$, (C.6) $\Rightarrow R_T = 1.33\,\Omega, \Rightarrow X_T = 7.14\,\Omega$, (C.8) $\Rightarrow K_T = 1.01$, (C.4) $\Rightarrow Z_{Tk} = 1.34 + 7.20i\,\Omega$ $\hookrightarrow Z_{\mathrm{GT}_{0.850\mathrm{MW}}} = 3.18 + 25.60i\,\Omega$
	950 kW wind turbines	Generator data :$P_{rG} = 950kW, U_{rG} = 690V$, 4 pole, $I_{rG} = 795A, I_{LR}/I_{rG} = 8.0,\ R_G/X_G = 0.1$ $\hookrightarrow$ (2.23) $\Rightarrow \lvert Z_G\rvert = 15.92\Omega$, (2.24) $\Rightarrow X_G = 15.84\,\Omega, \Rightarrow R_G = 1.58\,\Omega \Rightarrow Z_G = 1.58 + 15.54i\,\Omega$ Transformer data :$11 \pm 2 \times 2.5\%/0.69kV, 50Hz, 1MVA, u_{kr} = 6\%,\ u_{Rr} = 1.1\%$ $\hookrightarrow$ (C.5) $\Rightarrow \lvert Z_T\rvert = 7.26\,\Omega$, (C.6) $\Rightarrow R_T = 1.33\,\Omega, \Rightarrow X_T = 7.14\,\Omega$, (C.8) $\Rightarrow K_T = 1.01$, (C.4) $\Rightarrow Z_{Tk} = 1.34 + 7.20i\,\Omega$ $\hookrightarrow Z_{\mathrm{GT}_{0.950\mathrm{MW}}} = 2.92 + 22.74i\,\Omega$
Type D	0.8 MW wind turbine	Generator data :$P_{rG} = 800kW, U_{rG} = 400V,\ I_{rG} = 1.15kA, I_{LR}/I_{rG} = 3.0, R_G/X_G = 0.1$ $\hookrightarrow$ (2.23) $\Rightarrow \lvert Z_G\rvert = 50.42\Omega$, (2.24) $\Rightarrow X_G = 50.17\,\Omega \Rightarrow R_G = 5.02\,\Omega \Rightarrow Z_G = 5.02 + 50.17i\,\Omega$ Transformer data :$11 \pm 2 \times 2.5\%/0.4kV, 50Hz, 0.315MVA, u_{kr} = 6\%,\ u_{Rr} = 1.1\%$ $\hookrightarrow$ (C.5) $\Rightarrow \lvert Z_T\rvert = 7.26\,\Omega$, (C.6) $\Rightarrow R_T = 1.33\,\Omega, \Rightarrow X_T = 7.14\,\Omega$, (C.8) $\Rightarrow K_T = 1.01$, (C.4) $\Rightarrow Z_{Tk} = 1.34 + 7.20i\,\Omega$ $\hookrightarrow Z_{\mathrm{GT}_{0.8\mathrm{MW}}} = 6.36 + 57.37i\,\Omega$
	1.5 MW wind turbine	Generator data :$P_{rG} = 1500kW, U_{rG} = 400V,\ I_{rG} = 2.17kA, I_{LR}/I_{rG} = 3.0, R_G/X_G = 0.1$ $\hookrightarrow$ (2.23) $\Rightarrow \lvert Z_G\rvert = 26.89\Omega$, (2.24) $\Rightarrow X_G = 26.76\,\Omega \Rightarrow R_G = 2.68\,\Omega \Rightarrow Z_G = 2.68 + 26.76i\,\Omega$ Transformer data :$11 \pm 2 \times 2.5\%/0.4kV, 50Hz, 2MVA, u_{kr} = 6\%,\ u_{Rr} = 0.8\%$ $\hookrightarrow$ (C.5) $\Rightarrow \lvert Z_T\rvert = 3.63\,\Omega$, (C.6) $\Rightarrow R_T = 0.48\,\Omega, \Rightarrow X_T = 3.60\,\Omega$, (C.8) $\Rightarrow K_T = 1.01$, (C.4) $\Rightarrow Z_{Tk} = 0.49 + 3.63i\,\Omega$ $\hookrightarrow Z_{\mathrm{GT}_{1.5\mathrm{MW}}} = 3.16 + 30.39i\,\Omega$

Table C.5: Fault current contribution from Type A & B wind turbines

	Based on IEC approach	
Fault contribution from wind turbines at buses 11 & 12	Equivalent impedance:	$Z_k = Z_{L_{1-9}} + \left(Z_{GT_{0.950MW}} + Z_{L_{9-11}}\right) // \left(Z_{GT_{0.950MW}} + Z_{L_{9-12}}\right)$ $Z_k = 1.82 + 11.53i\ \Omega$
	short circuit current:	$I_{1.5MW} = \frac{1.2 \cdot 1.5e6}{11e3\sqrt{3}} e^{-i0.985} \Rightarrow I_{1.5MW} = 52.23 - 78.73\text{i}$ $I_k'' = \frac{\frac{c_{\max} U_n}{\sqrt{3}} - Z_{L_{1-9}} \cdot I_{1.5MW}}{Z_k} \Rightarrow I_k'' = 94.41 - 588.25\text{i} \Rightarrow I_k'' = 595.77\text{A}$ $(\text{C.9}) \Rightarrow i_p = 1.37kA$
Fault contribution from wind turbine at buses 16	Equivalent impedance:	$Z_k = Z_{L_{1-13}} + Z_{L_{13-16}} + Z_{GT_{0.850MW}}$ $\Rightarrow Z_k = 4.87 + 27.15\text{i}\ \Omega$
	short circuit current:	$I_{0.8MW} = \frac{1.2 \cdot 800e3}{11e3\sqrt{3}} e^{-i0.985} \Rightarrow I_{0.80MW} = 27.85 - 41.99\text{i}$ $I_k'' = \frac{\frac{c_{\max} U_n}{\sqrt{3}} - 2 \cdot Z_{L_{1-13}} \cdot I_{0.8MW}}{Z_k} \Rightarrow I_k'' = 45.00 - 247.74\text{iA} \Rightarrow I_k'' = 251.79\text{A}$ $(\text{C.9}) \Rightarrow i_p = 566.95A$
Fault contribution from wind turbines at buses 18 & 19	Equivalent impedance:	$Z_k = Z_{L_{1-17}} + \left(Z_{GT_{0.225MW}} + Z_{L_{17-18}}\right) // \left(Z_{GT_{0.85MW}} + Z_{L_{17-19}}\right)$ $Z_k = 4.15 + 21.40\text{i}\ \Omega$
	Short circuit current:	$I_k'' = \frac{c_{\max} U_n}{\sqrt{3} Z_k} \Rightarrow I_k'' = 60.95 - 314.65\text{iA}$ $\Rightarrow I_k'' = 320.50\text{A}$ $(\text{C.9}) \Rightarrow i_p = 710.58A$

C.2.3 Total fault current and its effect on the protection system

The total initial short circuit current is given by

$$\left|I_k''\right| \cong |451 - 3683i + 275.09 - 414.61i + 94.41 - 588.25i + 45 - 247.74i + 60.95 - 314.65i|$$
$$\Rightarrow \left|I_k''\right| = 5.33kA$$

Moreover, according to IEC standard [42], the total peak short-circuit current i_p fed from sources

which are not meshed can be determined by algebraically adding the partial short circuit currents:

$$i_p = \sum_{\mathrm{i}} i_{p\mathrm{i}}$$

$$i_p = 8914 + 704 + 1370 + 567 + 711$$

$$i_p = 12.27kA$$

Now due to the introduction of wind power the fault current has increased from $I_k^{''} = 3.71\ kA,\ i_p = 8.91\ kA$ to $I_k^{''} = 5.33\ kA,\ i_p = 12.27\ kA$.

Let us assume that the switchgear is designed considering a fault current contribution from the external grid only. This means to with stand a fault current of 3.71kA, from standard values, it is enough to have a switchgear with 4kA short time withstand current. Clearly, the introduction of wind power could have jeopardized the reliability of the switchgear. But the typical short time withstand current ratings of a switchgear these days are 25 kA, 31.5 kA and 40 kA; i.e, such a low rated switchgear at HV/MV station is very unlikely.

However the analysis clearly shows that the fault current contribution from wind turbines can have a considerable impact on short circuit current handling of a switchgear depending on the wind turbine type which is installed in a given distribution system. The effect also depends on the fault current contribution from the external grid and the margin left in the rating of the switchgear to accommodate additional fault current from other sources. In this case the fault current contribution from the external grid is not that significant. Moreover the majority of wind turbines in the grid are of Type D, which has very low short circuit current contribution. But in case the fault current contribution from the external grid is high and the wind turbines in the distribution system are composed of type A, B, or/and C then it is most likely for the fault current handling capacity of the distribution network to be jeopardized.

It is also good to note that the impedance of the external grid up to the fault point is considerably low compared to the impedance of the wind turbines (including their step up transformer). This means additional impedance added to the external grid is more effective in reducing the fault current than those added to the impedance of the wind turbines. Consequently, the fault current at the substation is more likely to be the highest compared to other buses in the network.